

THEORETICAL AND EXPERIMENTAL INVESTIGATION ON CENTRIFUGAL  
FANS WITH A SPECIAL INTEREST ON FAN NOISE

A THESIS SUBMITTED TO  
THE GRADUATE SCHOOL OF NATURAL AND APPLIED SCIENCES  
OF  
MIDDLE EAST TECHNICAL UNIVERSITY

BY

SONGÜL BAYRAKTAR

IN PARTIAL FULLFILMENT OF THE REQUIREMENTS  
FOR  
THE DEGREE OF DOCTOR OF PHILOSOPHY  
IN  
MECHANICAL ENGINEERING

DECEMBER, 2006

Approval of the Graduate School of Natural and Applied Sciences

---

Prof. Dr. Canan ÖZGEN  
Director

I certify that this thesis satisfies all the requirements as a thesis for the degree of Doctor of Philosophy.

---

Prof. Dr. S. Kemal İDER  
Head of Department

This to certify that we have read this thesis and that in our opinion it is fully adequate, in scope and quality, as a thesis for the degree of Doctor of Philosophy.

---

Prof.Dr. Mehmet ÇALIŞKAN  
Co-Supervisor

---

Prof. Dr. O. Cahit ERALP  
Supervisor

Examining Committee Members

Prof. Dr. Kahraman ALBAYRAK (Chairman)(METU, ME) \_\_\_\_\_

Prof. Dr. O. Cahit ERALP (METU, ME) \_\_\_\_\_

Prof. Dr. Mehmet ÇALIŞKAN (METU, ME) \_\_\_\_\_

Prof. Dr. Nafiz ALEMDAROĞLU (METU, AE) \_\_\_\_\_

Prof. Dr. Ali DURMAZ (Gazi Unv.) \_\_\_\_\_

**I hereby declare that all information in this document has been obtained and presented in accordance with academic rules and ethical conduct. I also declare that, as required by these rules and conduct, I have fully cited and referenced all material and results that are not original to this work.**

Name, Last Name : Songül Bayraktar

Signature :

## **ABSTRACT**

### **THEORETICAL AND EXPERIMENTAL INVESTIGATION ON CENTRIFUGAL FANS WITH A SPECIAL INTEREST ON FAN NOISE**

Bayraktar, Songül

Ph.D., Department of Mechanical Engineering

Supervisor : Prof. Dr. O. Cahit Eralp

Co-Supervisor : Prof. Dr. Mehmet Çalışkan

December, 2006, 123 pages

In this study, the effects of design parameters on the fan noise level are investigated both theoretically and experimentally. For the theoretical study, a computational aero- acoustic method is used to predict the flow induced noise of a fan. This method involves the coupling of a flow solver and a wave equation solver. Unsteady flow analysis is performed with URANS using FLUENT. Then the time dependent data are processed with LMS Sysnoise to compute the acoustic radiation. Experimental studies are performed to verify the theoretical results and additionally to investigate the effects of different design alternatives on noise level of the fan. The sound pressure and intensity level measurements are performed in the full anechoic room of Arçelik A.Ş. Research and Development Laboratories. The validation experiments indicate that there is a good agreement between numerical and experimental results. The experimental study with different fan designs gives information about the noise reduction possibilities.

Keywords: Computational Fluid Dynamics, Computational Aero-acoustics, Aero-acoustic Analogy, Centrifugal Fan, and Boundary Element Method

## ÖZ

### SANTRİFUJ FAN GÜRÜLTÜSÜ İLE İLGİLİ TEORİK VE DENEYSEL ÇALIŞMALAR

Bayraktar, Songül

Doktora, Makina Mühendisliği Bölümü

Tez Yöneticisi : Prof. Dr. O. Cahit Eralp

Ortak Tez Yöneticisi : Prof. Dr. Mehmet Çalışkan

Aralık, 2006, 123 sayfa

Bu çalışmada, fan tasarım parametrelerinin fan gürültüsü üzerindeki etkisi teorik ve deneysel olarak araştırılmıştır. Teorik çalışmada, hava akışı kaynaklı gürültüleri tahmin etmek için hesaplamalı aero-akustik metodu kullanılmıştır. Bu metod akış çözücü ile dalga denklemi çözücüsünün ortak kullanımından oluşmaktadır. Durağan olmayan akışın analizi URANS metoduyla FLUENT kullanılarak yapılmıştır. Daha sonra zamana bağlı veriler LMS Sysnoise programına aktarılarak akustik yayılım çözülmüştür. Teorik çalışmaların doğrulaması ve değişik tasarım alternatiflerinin fan gürültüsü üzerindeki etkisi deneysel olarak çalışılmıştır. Ses basıncı ve ses şiddeti ölçümleri Arçelik A.Ş. Ar-Ge tam yansız ses odasında yapılmıştır. Doğrulama deneyleri sayısal simulasyon ile deneysel verilerin uyumlu olduğunu göstermektedir. Fan tasarımında yapılan değişikliklerin ses yayılımı üzerindeki etkisinin incelendiği deneysel çalışmalar sonucunda fanın gürültü seviyesini azaltacak bilgiler edinilmiştir.

Anahtar Kelimeler: Hesaplamalı Akışkan Dinamiği, Hesaplamalı Akış Akustiği, Aeroakustik Analoji, Santrifüj Fan, Sınır Eleman Yöntemi

To My Family

## ACKNOWLEDGMENTS

The author wishes to express her deepest gratitude to her supervisor Prof. Dr. Cahit Eralp for his guidance, advice, criticism and encouragements throughout the research. The author would like to thank to her co-supervisor Prof. Dr. Mehmet Çalışkan for his supports during the study.

The author would also like to express her deepest thanks to Prof. Dr. Nafiz Alemdarođlu. It was impossible to finish this study without his invaluable supports and contributions.

The author wishes to thank to thesis examining committee member of Prof. Dr. Kahraman Albayrak for his kind comments.

The author wishes to thank to Mr. Şemsettin Eksert and Mr. Salih Arslantaş, the Directors of Arçelik A.Ş, for their heartfelt and financial supports during the study.

The author wishes to express her sincere thanks to Mr. Atilla Uz, the Manager of Product Development Department of Arçelik Dishwasher Plant, for his invaluable helps and encouragements.

Furthermore, the author would like to thank to Mr. Mehmet Çavuş, a design engineer, for his helpful contributions.

Finally, the author expresses her thanks to her family and her friends for their patience during the long period of the study.

## TABLE OF CONTENTS

|  |      |
|--|------|
| PLAGIARISM.....                        | iii  |
| ABSTRACT.....                          | iv   |
| ÖZ.....                                | v    |
| DEDICATION.....                        | vi   |
| ACKNOWLEDGEMENTS.....                  | vii  |
| TABLE OF CONTENTS.....                 | viii |
| LIST OF TABLES.....                    | xi   |
| LIST OF FIGURES.....                   | xii  |
| LIST OF SYMBOLS AND ABBREVIATIONS..... | xvii |

### CHAPTER

|  |    |
|--|----|
| 1. INTRODUCTION.....   | 1  |
| 1.1 General.....   | 1  |
| 1.2 Scope, Objectives and Achievements.....                                      | 2  |
| 1.3 Outline of the Thesis.....   | 3  |
| 2. LITERATURE SURVEY.....  | 4  |
| 2.1 Experimental Studies.....  | 4  |
| 2.1.1 Effect of Design Parameters and Flow Characteristics on<br>Fan Noise ..... | 4  |
| 2.1.2 Acoustical Characteristics of Fan Noise.....                               | 7  |
| 2.1.3 Fan Noise Modelling.....   | 10 |
| 2.2 Theoretical Approach.....  | 14 |
| 2.2.1 Flow Computation.....  | 15 |
| 2.2.2 Acoustic Computation.....  | 16 |
| 2.2.2.1 Aeoaoustic Analogy (AAA).....  | 17 |
| 2.2.2.1.1 Volume integral methods.....   | 17 |
| 2.2.2.1.2 Surface integral methods.....  | 18 |



|  |    |
|--|----|
| 2.2.2.2 Broadband Noise Source Model.....                    | 19 |
| 2.2.2.3 Computational Aeroacoustics (CAA).....               | 20 |
| 2.3 Noise Measurement Standards.....                         | 22 |
| 3. THE THEORY OF FLOW ACOUSTICS .....                        | 25 |
| 3.1 Basic Principles And Terminology.....                    | 25 |
| 3.1.1 Classical Acoustics .....                              | 25 |
| 3.1.2 Aeroacoustics.....                                     | 26 |
| 3.2 Aeroacoustic Analogies.....                              | 28 |
| 3.2.1 Lighthill’s Acoustic Analogy.....                      | 29 |
| 3.2.2 The Formulation of Ffowcs Williams and Hawkings.....   | 32 |
| 3.2.3 The Porous Ffowcs Williams and Hawkings Formulation... | 34 |
| 3.3. The Boundary Element Method.....                        | 36 |
| 3.3.1 Acoustic Boundary Integral Equation.....               | 36 |
| 3.3.1.1 Exterior Problems.....                               | 36 |
| 3.3.1.2 Interior Problems.....                               | 38 |
| 3.3.1.3. Numerical Solution.....                             | 38 |
| 4. NUMERICAL ANALYSIS .....                                  | 37 |
| 4.1 The Approach for the Numerical Analysis .....            | 37 |
| 4.1.1 The Analysis Cases .....                               | 42 |
| 4.1.2 The Turbulence Model .....                             | 44 |
| 4.2 Numerical Analysis .....                                 | 46 |
| 4.2.1 Discretization of the Flow Field .....                 | 46 |
| 4.2.1.1 Case-A and Case-B .....                              | 47 |
| 4.2.1.2 Case-C .....   | 50 |
| 4.2.2 Transient Flow Solution Procedure .....                | 51 |
| 4.3 Aeroacoustic Analysis.....                               | 53 |
| 4.3.1 Acoustical Modal Analysis .....                        | 54 |
| 4.3.2 Multi-Domain Boundary Element Method (MDBEM) .....     | 56 |
| 5. EXPERIMENTAL METHODOLOGY.....                             | 58 |
| 5.1 Introduction .....                                       | 58 |
| 5.2 Test Facilities.....                                     | 58 |

|   |     |
|---|-----|
| 5.3 Sound Power Level Measurements.....                               | 59  |
| 5.3.1 Measurement Instruments.....                                    | 62  |
| 5.3.2 Analyzer Settings.....  | 62  |
| 5.3.3 Measurement Methodology.....                                    | 62  |
| 5.4 Sound Intensity Measurements.....                                 | 63  |
| 5.4.1 Instruments.....  | 63  |
| 5.4.2 Measurement Grid and Alternative Fans.....                      | 65  |
| 6. RESULTS OF THEROTICAL AND EXPERIMENTAL STUDIES.....                | 69  |
| 6.1 The Results of Flow Field Solution .....                          | 69  |
| 6.1.1 Velocity Contours of Case-a and Case-B .....                    | 69  |
| 6.1.2 Pressure Contours of Case-a and Case-B .....                    | 74  |
| 6.1.3 Velocity and Pressure Contours for Case-C .....                 | 77  |
| 6.2 The Results of Acoustical Analysis .....                          | 79  |
| 6.2.1 Cavity Excitation Modes .....                                   | 80  |
| 6.2.2 The Source Strength Distributions of Case-A .....               | 83  |
| 6.2.3 The Source Strength Distributions of Case-C .....               | 86  |
| 6.3 Experimental Investigations for Noise Reduction .....             | 92  |
| 7. DISCUSSION, CONCLUSIONS AND RECOMMENDATIONS OF<br>FUTURE WORK..... | 104 |
| 7.1 Summary .....   | 104 |
| 7.2 Discussion .....  | 105 |
| 7.3 Conclusions .....   | 113 |
| 7.4 Recommendations for Future Work .....                             | 115 |
| REFERENCES.....   | 117 |
| CURRICULUM VITAE.....   | 123 |

## LIST OF TABLES

### TABLES

|  |    |
|--|----|
| Table 2.1 Values of the tip speed exponent found by various investigators... | 13 |
| Table 3.1 - Noise Source Characterization .....                              | 28 |
| Table 6.1 The fan models used for the experimental study.....                | 92 |
| Table 6.2 Peak Levels of the alternative cases.....                          | 95 |

## LIST OF FIGURES

### FIGURES

|   |    |
|---|----|
| Figure 2.1 Fan Noise Classification proposed by Neise.....  | 10 |
| Figure 2.2 – Different noise prediction approaches.....   | 15 |
| Figure 3.1 Directivity patterns for an acoustic monopole (a), dipole (b),<br>and quadrupole (c) ..... | 27 |
| Figure.3.2 - Aeroacoustic Analogies.....  | 29 |
| Figure 3.3- Model for FfowcsW. and Hawkings Equation.....   | 32 |
| Figure 3.4 Exterior Problem Domain.....   | 37 |
| Figure 3.5 Interior Problem Domain .....  | 38 |
| Figure 4.1 Steps of Sound Prediction Approach .....   | 41 |
| Figure 4.2 Numerical Solution Steps followed for the noise prediction .....                           | 42 |
| Figure 4.3 Original Impeller .....  | 43 |
| Figure 4.4 Impeller without splitter .....  | 43 |
| Figure 4.5 Volute with channel .....  | 43 |
| Figure 4.6 Volute without channel .....   | 43 |
| Figure 4.7 Volute with inlet modification .....   | 43 |
| Figure 4.8 Volute coated with bitumen .....   | 43 |
| Figure 4.9 Spectrum of the fan noise (measured at 0.5 m away from the fan<br>exit).....               | 46 |
| Figure 4.10 Hex mesh of a blade.....  | 47 |
| Figure 4.11 Hex mesh of a splitter.....   | 48 |
| Figure 4.12 The mesh of Blade Spacings.....   | 48 |
| Figure 4.13 The mesh at blade tips.....   | 49 |
| Figure 4.14 The Mesh of the Rotating Region (without top part and blades)                             | 49 |
| Figure 4.15 The mesh of the volute with channel.....  | 50 |
| Figure 4.16 Blade Mesh for Case-C.....  | 51 |
| Figure 4.17 Boundary Element meshes prepared with IDEAS Simulation<br>Software.....                   | 53 |

|   |    |
|---|----|
| Figure 4.18 Numerical model used to obtain cavity excitation modes (ISO 3744 -1996).....                                      | 55 |
| Figure 4.19 Numerical experiment set-up for cavity excitation modes investigation.....  | 55 |
| Figure 4.20 Dipole sound sources on the surfaces of the fan casing (the light green cells).....                               | 56 |
| Figure 4.21 MBEM analysis set-up.....   | 57 |
| Figure 5.1 The sound pressure measurement set-up in Anechoic Room of Arçelik A.Ş .....  | 59 |
| Figure 5.2 Fan motor noise suppressing box.....   | 60 |
| Figure 5.3 Sketch for the microphone positions – Top View.....  | 61 |
| Figure 5.4 Sketch for the microphone positions – Front View.....  | 61 |
| Figure 5.5 Sound Intensity Measurement Platform.....  | 64 |
| Figure 5.6 Original Impeller .....  | 66 |
| Figure 5.7 Splitters eliminated.....  | 66 |
| Figure 5.8 Volute with Channel.....   | 66 |
| Figure 5.9 Channel Eliminated.....  | 66 |
| Figure 5.10 Inlet Modified .....  | 66 |
| Figure 5.11 Bitumen Coated .....  | 66 |
| Figure 5.12 Velocity measurement points at fan exit.....  | 67 |
| Figure 5.13 Velocity Distributions along the fan exit in Cases A, B, C, D, E  | 68 |
| Figure 6.1 The section of the fan for which the pressure and velocity contours are presented .....                            | 69 |
| Figure 6.2 Velocity contours of the fan (a) with channel, (b) without channel (section corresponds to %30 of the height)..... | 70 |
| Figure 6.3 (a) Velocity contours of the fan with channel (at the casing surface).....   | 71 |
| Figure 6.3 (b) Velocity contours of the fan without channel (at the casing surface).....                                      | 72 |
| Figure 6.4 Velocity distributions along (0-X) section after the spiral.....   | 72 |

|   |    |
|---|----|
| Figure 6.5 Velocity distributions at the fan exit (a) with channel, (b) without channel.....                                | 73 |
| Figure 6.6 Velocity distributions at the fan exit.....  | 73 |
| Figure 6.7 The pressure contours of (a) casing with channel, (b) casing without channel (at the mid height of the fan)..... | 75 |
| Figure 6.8 Pressure distributions along (0-X) section (between tongue and the end point of channel).....                    | 75 |
| Figure 6.9 Pressure change at the tongue region.....  | 76 |
| Figure 6.10 Velocity vectors showing the recirculation zone.....  | 76 |
| Figure 6.11 Velocity contours of the Case-C (at mid-height of the blades)...  | 77 |
| Figure 6.12 Vorticity levels of the flow region for the Case-C.....   | 78 |
| Figure 6.13 Pressure Contours for the Case-C.....   | 78 |
| Figure 6.14 The blade distributions of Case-A.....  | 80 |
| Figure 6.15 Sound Pressures at 885 Hz when the casing cavity is excited with monopole source.....                           | 81 |
| Figure 6.16 Sound Pressures at 900 Hz when the casing cavity is excited with monopole source.....                           | 81 |
| Figure 6.17 Sound Pressures at 910 Hz when the casing cavity is excited with monopole source.....                           | 82 |
| Figure 6.18 Sound Pressures at 915 Hz when the casing cavity is excited with monopole source.....                           | 82 |
| Figure 6.19 Spectrum of the fan sound pressures for Case-A (measured at fan inlet).....                                     | 83 |
| Figure 6.20 Case-A: The pressure distributions of sound at 1073 Hz .....  | 84 |
| Figure 6.21 Numerical sound directivity map for Case-A at 1073 Hz   | 85 |
| Figure 6.22 Experimental sound pressure levels at the surfaces 0.5m away from the fan surfaces .....                        | 85 |
| Figure 6.23 Sound directivity map at 912 Hz for the Case-C.....   | 86 |
| Figure 6.24 Experimental sound pressure levels (dB) for Case C at the surfaces 0.5m away from the fan surfaces .....        | 87 |

|   |     |
|---|-----|
| Figure 6.25 Sound directivity map at 770 Hz - 1 <sup>st</sup> harmonic of BPF.....  | 88  |
| Figure 6.26 Experimental Sound Pressure Spectrum at 0.5 m away from the inlet.....  | 89  |
| Figure 6.27 Experimental Sound Pressure Spectrum at 0.5 m away from the outlet.....   | 89  |
| Figure 6.28 Experimental Sound Pressure Spectrum at 0.5 m away from the left side.....  | 90  |
| Figure 6.29 Experimental Sound Pressure Spectrum at 0.5 m away from the right side.....   | 90  |
| Figure 6.30 (a) Sound intensity maps for the inlet surface – Numerical Results.....   | 91  |
| Figure 6.30 (b) Sound intensity maps for the inlet surface - Experimental Results.....  | 91  |
| Figure 6.31 The orientation of the measurement surfaces for intensity mapping.....  | 92  |
| Figure 6.32 A-weighted Sound Pressure Spectrum measured at the center of top surface for (a) original design, (b) channel eliminated, (c) splitters eliminated, (d) inlet modified..... | 94  |
| Figure 6.32 – cont. – A-weighted Sound Pressure Spectrum measured at the center of top surface for (e) bitumen-coated design .....  | 95  |
| Figure 6.33 A-weighted Sound Pressure Levels in 1/3 Octave Band for the alternative cases (in the range of 100 – 5000 Hz) .....   | 96  |
| Figure 6.34 Intensity Map for the FRONT (Exit) Surfaces (100-5000 Hz)...  | 98  |
| Figure 6.35 Intensity Map for the TOP (Inlet) Surfaces (100-5000 Hz).....   | 98  |
| Figure 6.36 Intensity Map for the LEFT Surfaces (100-5000 Hz).....  | 99  |
| Figure 6.37 Intensity Map for the RIGHT Surfaces (100-5000 Hz).....   | 99  |
| Figure 6.38 Intensity Map for the BACK Surfaces (100-5000 Hz) .....   | 100 |
| Figure 6.39 Intensity Map for the FRONT (Fan Exit) Surfaces at the Peak Frequency Values.....   | 101 |
| Figure 6.40 Intensity Map for the TOP (Fan Inlet) Surfaces at the Peak Frequency Values.....  | 101 |

|  |     |
|--|-----|
| Figure 6.41 Intensity Map for the LEFT Surfaces at the Peak Frequency  |     |
| Values.....  | 102 |
| Figure 6.42 Intensity Map for the RIGHT Surfaces at the Peak Frequency |     |
| Values.....  | 102 |
| Figure 6.43 Intensity Map for the BACK Surfaces at the Peak Frequency  |     |
| Values.....  | 103 |
| Figure 7.1 The steps of Aero-acoustic Analysis .....                   | 106 |
| Figure 7.1 - cont. - The steps of Aero-acoustic Analysis .....         | 107 |
| Figure 7.2 The steps of Cavity Excitation Modes Analysis .....         | 108 |



## LIST OF SYMBOLS AND ABBREVIATIONS

### SYMBOLS

|            |  |
|------------|--|
| $p_0$      | : Reference sound pressure of $2 \times 10^{-5}$ Pa = 20 $\mu$ Pa                                |
| $p$        | : sound pressure, in $\text{N/m}^2 = \text{Pa}$  |
| $f$        | : frequency, in Hz   |
| $\rho$     | : density of air, in $\text{kg/m}^3$   |
| $c$        | : speed of sound, in m/s   |
| $v$        | : sound velocity, in m/s   |
| $\omega$   | : angular frequency = $2\pi \cdot f$   |
| $\xi$      | : particle displacement (particle amplitude), in m   |
| $Z$        | : acoustic impedance (characteristic impedance) = $c \cdot \rho$ , in $\text{Pa}\cdot\text{s/m}$ |
| $a$        | : particle acceleration, in $\text{m/s}^2$   |
| $E$ or $w$ | : sound energy density, in $\text{J/m}^3$  |
| $P_c$      | : sound power or acoustic power, in W  |
| $A$        | : area, in $\text{m}^2$  |

### ABBREVIATIONS

|       |  |
|-------|--|
| CAD   | : Computer Aided Design                            |
| CFD   | : Computational Fluid Dynamics                     |
| RANS  | : Reynolds Average Navier Stokes Equation          |
| URANS | : Unsteady Reynolds Average Navier Stokes Equation |
| LES   | : Large Eddy Simulation                            |
| DNS   | : Direct Numeric Simulation                        |
| AAA   | : Aeroacoustics                                    |
| FW-H  | : Ffowcs Williams and Hawking Equation             |
| CAA   | : Computational Aeroacoustics                      |
| EN    | : European Norm                                    |
| SPL   | : Sound Power Level                                |
| BEM   | : Boundary Element Method                          |

MDBEM : Multi Domain Boundary Element Method  
RD : Research and Development  
dBA : A-weighted Sound Pressure Level  
B&K : Brüel and Kjaer

## **CHAPTER 1**

### **INTRODUCTION**

#### **1.1 General**

Fans are important machines for cooling, drying and circulating the flow. In the household appliance market, compactness and low-noise requirement are keys as purchase requirements. Fan is one of the major noise sources in appliances. Therefore, the high efficiency and low-noise fan is seriously needed. For this reason, it is desired to develop a methodology that guides the fan designer in the conceptual design stage by predicting its noise characteristics.

Today, there is still no systematic methodology that can be implemented for the design of a low noise fan. There have been some attempts to develop mathematical models for the prediction of aerodynamic noise. Some acceptable correlations with experimental data have been achieved for particular situations, but no universal theory has yet emerged. In fact, most of the studies performed are on axial-fans, compressors and turbofan engine, but only a few studies has been done on centrifugal fans because of its complicated flow region and scattering effect of the casing.

The noise of a fan consists of vibration noise and flow-induced noise. In the case of a small fan that is used in household appliances, the flow-induced noise is dominant. The flow-induced noise is a branch of aero-acoustics, which is concerned with sound generated by aerodynamic forces or motions originated in the flow.

The sound generated from the fans has both tonal and broadband characteristics. Tones are produced as a result of the regular cyclic motion of the fan blade with respect to a stationary observer, and by interaction with adjacent structures. The

broadband component arises from random fluctuations in pressure over a wide range of frequencies, and is associated with turbulent flow in the inlet stream, in the boundary layer's, and in the wake behind the blades.

Many researchers concluded that the dominant acoustic source of the fan is dipole type. This means that the sound is generated from the fluctuations of forces on the blade, induced by interactions between the flow passing through the impeller and structures of the casing. So if the unsteady force on the blades can be calculated accurately, the tonal sound can be predicted with a good accuracy. Analysis of unsteady flow is then essential to understand and analyze the flow noise in fans.

## **1.2 Scope, Objectives and Achievements**

In this study, a computational aeroacoustic method is used to investigate the noise characteristics of a centrifugal fan. Two commercial softwares FLUENT and LMS SYSNOISE are employed for this purpose. The numerical computations are performed in two steps. First, the turbulent flow is computed with URANS. Second, the time dependent flow data is exported to the aeroacoustic modal where the wave equation is solved and the noise propagation is computed by LMS SYSNOISE. Both tonal noise radiation representing Blade Passing Frequency and its harmonics, and the excitation at the structural resonance frequencies are investigated. The sound pressure and intensity levels are predicted at near and far field. The validation of the numerical results is checked with sound power (and pressure) levels measurements.

The flow field is analyzed with Fluent CFD package to obtain force variations, and the acoustic pressures are calculated using an acoustic analogy. Noise caused by the unsteady pressure fluctuations at the impeller blades are predicted by using the force (or pressure) information calculated from the flow field. In order to do this, forces acting on elements of the impeller blades are calculated, and using this result, FfowcsWilliam-Hawkings' acoustic analogy based on the Lighthill's equation is performed numerically in time domain. The validation of the developed model is checked with sound pressure and intensity levels measurements.

Additionally, the effect of geometrical changes on the designed fan is investigated experimentally. For this purpose, impeller, volute and fan inlet designs are modified. Fan is coated with bitumen and its noise isolation property is investigated.

### **1.3 Outline of the Thesis**

Contents of this study are presented in seven chapters. Chapter 1 is Introduction. In this chapter the necessity of investigation on fan noise and the scope of this study are explained. Chapter 2 gives a brief summary of the previous research work relevant to this fan noise investigation study. Chapter 3 introduces the theory of flow acoustics. Turbulence model used in Computational Fluid Dynamics and Boundary Element Method applied for the structure effect on sound propagation are given in this chapter. Chapter 4 is devoted to the numerical analysis methods used for the modeling of flow field and acoustical field. Experimental studies performed to verify the theoretical approach and to investigate the effect of some geometrical changes on the fan noise characteristics are explained in Chapter 5. Chapter 6 presents the results and comparisons of numerical and experimental studies. Discussions and conclusions of the thesis and possible future research subjects based on the current study are given in Chapter 7.

## **CHAPTER 2**

### **LITERATURE SURVEY**

Methods for predicting sound power level of rotating blades have encompassed the range of empirical, semi-theoretical and theoretical approaches since sixties. The experimental studies have focused on the parameters affecting the sound generation and development of experimental correlations. Theoretical approach needs the solution of flow field first. The success of this method depends on the computational power. Therefore, it has shown great growth in parallel to the developments in computer technology in recent years.

Many researchers have studied on fan noise reduction methods and the numerical methods to predict the flow and acoustic fields of an axial fan. The numerical prediction methods for the centrifugal fan are still a hot topic. In order to calculate the radiated acoustic field of a centrifugal fan, the modification of the generated noise by the casing should be considered.

In this chapter, previous works related to low-speed centrifugal fans will be reviewed. The relevant studies about axial fans will be cited where appropriate.

#### **2.1 Experimental Studies**

##### **2.1.1 Effect of Design Parameters and Flow Characteristics on Fan Noise**

Many investigations were carried on the impeller design parameters and flow properties related to the noise generated by the fan.

Tyler and Sofrin [1] first introduced the concept of applying linear infinite duct, spinning mode analysis, to the prediction of ducted fan engine noise. In this research, simple propagation and radiation models were applied to single radial modes incident on the duct inlet. Reflections and inflow effects were ignored. They studied the role of blade and vane number in noise generation. They showed that, for a fan rotating with a subsonic tip speed, it is straightforward to suppress the fundamental blade passing frequency (first harmonic) by choosing a sufficiently high number of stator vanes. Then, all acoustic duct modes become cut-off and do not propagate along the duct.

Bommes [2] presented a mathematical model based on dimensional analysis of the sound power level generated by any type of aerodynamic noise source. The model was applied to evaluate the effect of blade design on acoustical performances of centrifugal fans. The geometry of the various blade shapes was used to calculate the theoretical acceleration of the airflow through the channels between the blades. Then, large negative accelerations were used as indication of flow separations, which was considered as a major effect on noise generation.

Fehse and Neise [3] proved that the low frequency noise of centrifugal fans is generated by flow separations in the impeller and/or the casing. Experiments were made with 5 industrially manufactured test impellers having different geometries and specific speed values in the range of  $n_q=80-100$ . All impellers were run in the same casing and operated in a ducted inlet/free outlet installation.

Konieczny and Bolton [4] identified the influence of several impeller and housing design elements on the broadband random noise produced by centrifugal blowers having forward curved impellers by measuring the sound power produced by each member of a family of blowers. The design parameters considered were; impeller type, axial and radial inlet clearances, scroll development angle and length, and cut-off clearance.

Boltezar [5] investigated the influence of irregular blade spacing of car alternator radial fans on the total sound pressure level and the noise spectrum. Blades were modelled as dipole sources. Author showed that alterations in blade spacing do not significantly alter the total sound power level. However, the sound energy at the blade passage frequency of a fan with uneven blade spacing is spread over several prominent tones thus, allowing for a reduction of the siren effect.

Sentek [6] studied on the influence of geometrical parameters on the sound power level of centrifugal fans. The noise generated by the fan was interpreted as a dipole on the basis of several tests done by Neise, 1976. They fixed the impeller aspect ratio and changed inlet and outlet blade angles. A substitution of the mean value of the gas exhaust absolute velocity at the impeller outlet for the impeller tip speed allows a generalized relationship between the sound power or its level and geometrical parameters of the fan.

Trunzo et al. [7] gives the generation of noise in low speed turbomachinery as a function of blade geometry and upstream flow characteristics which are inlet turbulence, centerbody and annulus wall boundary layer turbulence, mean flow distortions and turbulence caused by vortices and wakes of upstream struts. The noise spectrum was characterized as broadband and pure tone. The reason of the broadband sound was explained as the random velocity fluctuations in wall and blade boundary and free stream. The pure tone was indicated as the result of elongated turbulent eddies present in the free stream, and mean velocity defects in wakes and boundary layers. They investigated the relative importance of two noise sources in the overall noise generation; which are long eddies present in the free stream and the wall boundary layer, and disturbances caused by upstream struts.

There are some other experimental studies correlating internal flow, noise and aerodynamic performance to the geometrical parameters of centrifugal fans [8-13]. The most comprehensive experimental investigation was performed by Morinushi [12].



Morinushi investigated the effect of width to inner diameter ratio of the impeller, axial clearance between the fan inlet nozzle and the impeller shroud plate, blade setting angle, blade pitch to chord ratio and expansion angle of the scroll, on noise generation and aerodynamic performance of forward curved centrifugal fan having an outer diameter of 0.18 m. As a result of investigation, the following were found as the most suitable values for low noise: the impeller width to diameter ratio between 0.6 and 0.8, axial clearance in the range of 3 – 10 %, blade setting angle 26°. The pitch to chord ratio has two optimal regions depending on the flow and the scroll angle also affects the noise levels.

### **2.1.2 Acoustical Characteristics of Fan Noise**

Many researchers demonstrated that the fans are dipole in nature. The idea was first proposed by Cremer [14] and measurement methods that can realize this idea have been developed by Terao and Sekine [15]. Abom and Boden [16] illustrated that low frequency aero-acoustical characteristics of an induct axial fan is dipole source located at the fan blades. It was also shown that for predictions of in-duct sound fields it is possible to assume an equivalent ideal dipole instead of the actual source. Baade [17] has indicated that the noise at the blade passing frequency is primarily a dipole source by measuring noise from a ducted axial fan over a range of speeds and with a range of duct lengths. Margett [18] demonstrated that the axial fan in ducted inlet/ducted outlet configuration generates predominantly a dipole noise. The phasing of the inlet and outlet noise were 180 degrees apart, regardless of whether the fan was generating tonal or broadband noise for frequencies from direct current to just a few Hertz below the first higher mode cut-on frequency. Clark and Ribner [19] validated the Curle theory by demonstrating a direct relationship between the fluctuating lift on an airfoil and the resulting far field acoustic pressure. Hersh et al. [20] confirmed that small airfoils exhibit dipole directivity. Chanaud [21] claimed that the centrifugal fan noise has dipole characteristics by conducting experiments for a fan having forward curved blades. Wright [22, 23] found that the fluctuating forces on rotating blades, i.e., rotating acoustic dipoles, are the principal sources for discrete- frequency noise.

Mudridge [24] modelled the acoustic radiation from low speed fans as an array of dipoles whose strengths are related to the unsteady surface pressures and shear stresses and obtained a good agreement between its model and measurements.

The noise in a centrifugal fan is dominated by tones at the blade passage frequency and its higher harmonics. This is a consequence of the strong interactions between the flow discharged from the impeller and the cut-off in the casing [25]. In addition to the discrete tones, the broadband component arises from random fluctuations in pressure over a wide range of frequencies, and is associated with turbulent flow in the inlet stream, in boundary layer, and wake behind the blade [25].

Measured noise signals are considered as composition of two components; one from an original fan noise and the others from a modified part of the fan noise. The latter means diffracted and/or scattered noise due to a fan case and a duct of the fan system in the noise propagation. The former also includes the effect of fan supporter, fan shroud etc. in the fan system in regarding of noise generation.

Longhouse [26,27] classified the noise mechanism of low tip speed axial flow fans as either rotational or non-rotational. The dominant rotational noise mechanism was defined as blade fluctuating forces that are caused by interactions with inflow distortions, unsteady flow, turbulence, and nearby stationary objects. These mechanisms of noise are defined as tonal and related to the motor or blade passage frequency. The non-rotational noise mechanisms are defined as random and generally broadband with peaks occurring in the spectrum. The fan blade vortex shedding and the blade tip clearance vortex interactions are stated as the dominant mechanism of non-rotational noise. The resulting spectrum was given as depending on the flow velocity relative to the blades, the Strouhal number, tip clearance and aerodynamic loading.

Neise [29] divided the aerodynamic sound from centrifugal fans into two: the harmonic part and the broadband noise. He stated that the harmonic part is caused by

the interaction between mean airflow leaving the impeller and the fan casing. The main source region is volute cut-off where the mean velocity profile with respect to the circumferential direction exposes sharp minima and maxima due to the blade wakes. This non –uniformity of the velocity profile produces strong pressure fluctuations at the cut-off that result in an effective sound radiation at the BPF and its harmonics.

The noise reduction studies have mostly concentrated on the reduction of the rotor-stator interaction at the scroll cut-off. These studies aim to reduce the noise generated at the blade passing frequency. Increasing the cut-off distance decreases the strength of the tone, but adversely affects the performance of the blower. Alternative methods for reducing the BPF noise include: streamlined cut-off geometry [2,13], a spatial modulation of blade spacing, inclined blades relative to the cut-off [51], and mechanical and electro-acoustical resonators located at the cut-off region [52]. While it is widely recognized that these effects depend on the specific fan application, increasing the fan cut-off normally attenuates the discrete tonal component by softening the impact of the dipole sources as well as a corresponding decrease in fan performance.

Reduction of broadband noise has been generally less successful than reduction of pure tone levels such as at the BPF. This difficulty is due to the added complexity of broadband noise mechanism that extends over the complete frequency range. There are studies on housing effects on centrifugal blower noise [53] and techniques relating to various housing treatment such as an acoustically lined scroll [54].

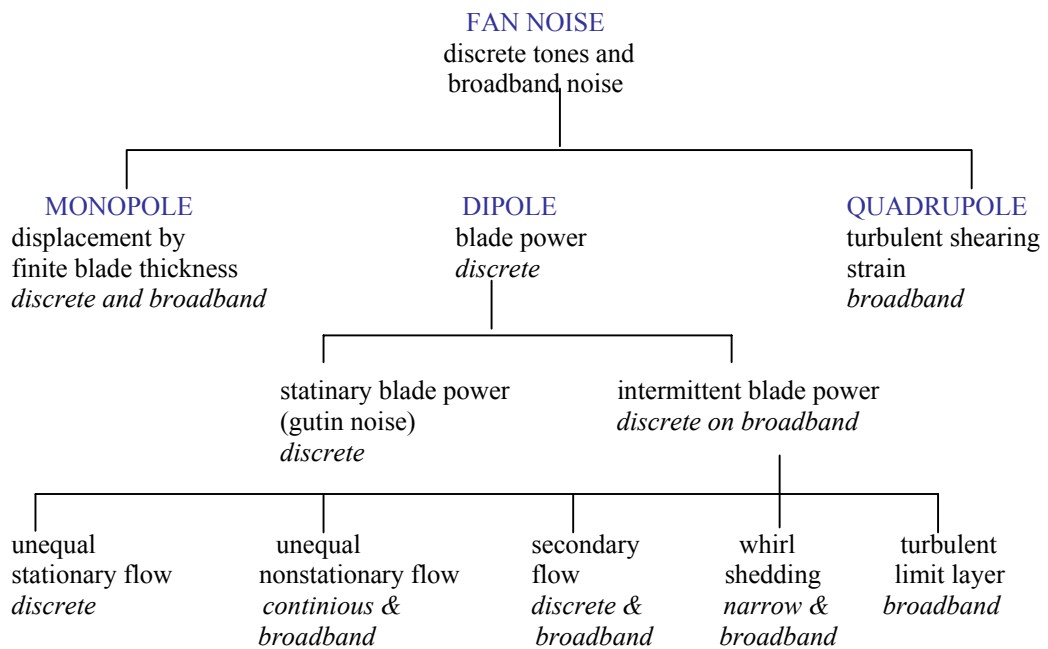


Figure 2.1 Fan Noise Classification proposed by Neise [49]

### 2.1.3 Fan Noise Modelling

The characteristics of aerodynamic sound have been studied using acoustic similarity law through numerical and experimental methods [30–33]. Wright [34] has developed a method for estimation of wideband sound power levels of low-pressure axial flow fans. The resulting algorithms are used to relate the fan performance specifications to fan diameter, rotational speed and specific diameter of the fan. Madison assumed aerodynamic flow through the rotor is similar for all members of the series and that the effects of viscosity can be neglected. Then total sound power is found to be proportional to the fifth power of (mean) flow speed  $U$  and to the second power of the diameter  $D$  :  $W \sim D^2U^5$ .

Maling [35] proposed a simple equation by the dimensional analysis using Buckingham PI theorem for broadband noise of a centrifugal blower with forward curved blades. In Maling study measurements were performed in anechoic discharge duct. The influence of Reynolds number was neglected and only broadband noise was considered. Then total sound power is found to be proportional to the 5.67 power of (mean) flow speed  $U$  and to the 0.33 power of the diameter:  $W \sim D^{0.33}U^{5.67}$ .

The  $U^5$  dependence of fan noise law in the proposed relations neither agrees with the  $U^4$  dependence of free-field monopole radiation, nor with the  $U^6$  dependence of the dipole, nor with the  $U^8$  dependence of the quadrupole.

Chanaud made tests with 4 uncased forward curved impellers in an anechoic room. The rotors were not precisely similar. Influence of Reynold's number is neglected. Overall broadband sound measurement confirmed Madison's  $U^5$  law. However, when frequencies below 100 Hz were excluded, the tip speed exponent became slightly greater than 6. The difference was supposed to be caused by the microphone being in the near field of the rotor.

The problem in application of acoustic similarity law is that it is difficult to divide the original noise source from the measured signals. It is generally accepted that the measured spectrum of signal is the combination of flow and geometry functions. Sound measurements concerned with similarity over a wide range of impeller sizes were made by Weidemann [36]. Weidemann investigated the noise prediction model by testing uncased 6 backward curved centrifugal rotors under free field condition. He divided the noise into sound generation and sound radiation parameters.

The generation of sound was expressed as a function of Mach number, Reynold's number and Strohoul number as:  $Ma^\alpha Re^\beta F(St)$  where  $F(St)$  represents the spectral distribution of the sound generated

The sound radiation characteristics were described as a function of Helmholtz number as  $G(He)$  which can be considered as an acoustic frequency response function. This function is purely geometric.

Weidemann proposed the following relation:

Noise=(sound generation components)(sound radiation components)

$$K = (Ma^{\alpha} Re^{\beta} F(St)(G(He)))$$

Table 2.1 shows the margin of tip speed exponents measured by various investigators.

Neise [31] verifies experimentally the similarity law for the fan as formulated by Weidemann. He applied Weidemann's result to the analysis of noise at BPF (blade passing frequency) and its higher harmonics for centrifugal fans. Neise also applied it to the broadband noise in 1982. Neise, measured the sound power level of two dimensionally similar fans within anechoic discharge ducts. Only the discrete frequency sound was considered, and the flow coefficient,  $\phi$ , was kept constant.

Other empirical formula widely used is the total sound power level which is a function of mass flow  $Q$ , and pressure difference in the system with some constants. The constants are different for different fan system geometries, which are obtained from measurement data. Once, the constants are obtained, the total SPL can be predicted for several operating conditions in the ranges of parameters, which is very useful in engineering point of view. The constants are related to the geometry function and the others are related to spectral distribution function of the sound source generated, roughly [35].

Table 2.1 Values of the tip speed exponent found by various investigators [31]

| <b>Authors</b>      | <b>Tip Speed Exp.</b> | <b>Sound type considered</b>                                      | <b>Fan type and measuring method</b>  | <b>Tip Sped range covered (m/s)</b> |
|---------------------|-----------------------|---|---|-------------------------------------|
| Howes and Real 1958 | 3-7<br>5-6            | Outlet overall noise<br>Inlet overall noise                       | Centrifugal impellers, both forward and backward curved blades, anechoic discharge duct         | 13-33 forward<br>25-56 backward     |
| Huebner 1963        | 5.5 – 6.5             | Overall broadband noise   | Freely rotating centrifugal rotors of various shape, free field conditions                      | 20-100                              |
| Maling, 1963        | 4 – 5.7               | Overall broadband noise   | Centrifugal blower, forward curved blades, anechoic discharge duct                              | 8-13                                |
| Chanaud 1965        | 6<br>5<br>6.4         | Discrete freq.sound<br>Overall broadband<br>Broadband over 100 Hz | Uncased centrifugal rotor, forward curved blades, wedge placed near rotor, free field condition | 9-30                                |
| Leidel 1969         | 5.2-6.4               | BPF, distance between impeller and cut-off was varied             | Centrifugal impeller, backward curved blades, anechoic discharge duct                           | 21-42                               |
| Weidemann 1971      | 5.6<br>5.2            | Discrete freq.sound<br>Overall broadband                          | Uncased centrifugal rotor with rectangular wedge, backward curved blades, free field conditions | 30-60                               |
| Agnon 1973          | 4.6                   | Discrete freq.sound   | Centrifugal impeller, backward curved blades, volute casing, free field condition               | 30-60                               |
| Yeow 1974           | 4<br>>4               | Outlet<br>Inlet overall broadband                                 | Centrifugal impeller, both forward curved and radial blades, anechoic discharge duct            | 16-34                               |

Fukano and Takamatsu [42] investigated the turbulent noise experimentally in detail and derived theoretical formulae for estimating the sound power generated by low-pressure axial flow fans. The parameters included in this formulae are rotational speed, outer diameter of impeller, number of blades, blade chord length and blade thickness. Authors suggested that thinning the blade thickness at the trailing edge and sweeping the fan blades can reduce the sound pressure level although it cannot be reduced by cambering the fan blade.

Thus the sound radiation from fans has been regarded as resulting from a distribution of monopoles, dipoles, and quadrupoles located inside the fan. The tip speed exponent depends not only on this sound generation mechanism but also on the impedance of the fan itself together with its acoustic load. Therefore it is concluded that there is no hope of finding a universal value for the tip speed exponent and the generation of fan noise is not understood well enough to predict tip speed exponents for arbitrary configurations.

## **2.2 Theoretical Approach**

The earliest theoretical study of the noise generated by rotating machinery was the work of Gutin [28], who analyzed the sound produced by a two-bladed propeller. He discovered that the forces exerted by the propeller on the surrounding air generate the sound. On the other hand, the nature of the sound produced by centrifugal fans, with their large number of blades, bears very little resemblance to Gutin's model.

Hybrid methods are used for the simulation of aero-acoustic noise. Since it is not possible to solve the transient Navier-Stokes Equations from the location of sound generation up to the observer position. All hybrid methods subdivide the aero-acoustic problem into two parts, sound generation and sound propagation. In general,



computational, aero-acoustic methods need the transient aerodynamic flow in the region where the sound is generated as an input.

Figure 2.1 shows the main computational approaches that may be used when evaluating the sound field generated by turbulent flows.

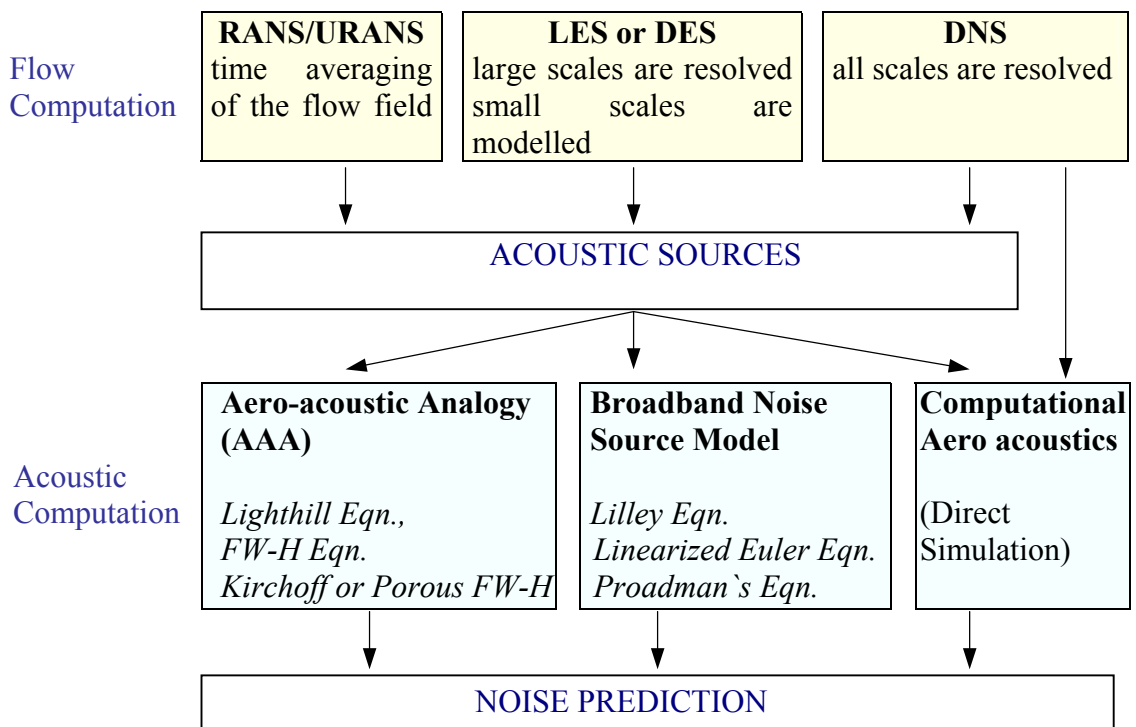


Figure 2.2 – Different noise prediction approaches

### 2.2.1 Flow Computation

In order to understand the aero-acoustic source of a centrifugal fan, the detailed information of the flow field is necessary. The Computational Fluid Dynamics

methods for the calculation of the flow field can be subdivided into three main categories, depending on the approach to simulating turbulence:

**Reynolds Averaging Navies Stokes Equations (RANS/Unsteady RANS) equations:** The turbulent fluctuations are needed by any computational aero-acoustic procedure. Therefore a method was developed to reconstruct the time dependent turbulent flow field based on the averaged properties from the RANS calculation. This approach models the whole range of turbulent scales present.

**LES or DES (Large Eddy Simulation or Detached Eddy Simulation):** The LES technique solves the largest turbulence length scale motions of the flow while modelling only the small scale motions. It can be regarded as a kind of compromise between RANS and DNS (Direct Numerical Simulation). The computational mesh needs to be finer compared with RANS methods, but not as fine as for a DNS. To avoid the very fine near-wall mesh requirements of the LES method, the hybrid detached eddy simulation method was developed. The DES approach creates two separate regions inside the flow domain: one that is based on the pure LES formulation and another that is close to the wall where the modelling is dominated by a RANS-based approach.

**DNS (Direct Numerical Simulation):** The most accurate approach to turbulence simulation is to solve the Navier-Stokes equations without averaging or approximation. All of the motions contained in the flow are resolved. To capture all of the kinetic energy dissipation the computational grid needs to be very fine and the time steps must be small enough that the small-scale motion can be resolved in a time accurate manner.

### **2.2.2 Acoustic Computation**

There mainly three computational approaches for predicting noise level of a system as it is summarized in Figure 2.2: Aero-acoustic Analogy, Broadband Noise Source Models and Computational Acoustics.

## 2.2.2.1 Aero-acoustic Analogy (AAA)

### 2.2.2.1.1 *Volume integral methods*

Most of the recent progress in aerodynamic sound generation by rotating blades is based on the traditional acoustic analogy developed by Ffowcs –Williams and Hawkings [55] and Lighthill [56]. In the acoustic analogy, the governing Navier-Stokes equations are rearranged to be in wave-type form. Lighthill's work is concerned with the estimation of sound radiated from a fluctuating flow with special reference to the sound field of a turbulent jet. In the acoustic analogy of Lighthill, the sound radiation from a turbulent flow within a volume is described as the solution of the non-homogeneous wave equation for the acoustic pressure at a field point away from the source. The forcing function for the wave equation, serves as a source term having the form of a double divergence of a stress tensor, indicates a quadrupole source distribution. The solution to this partial differential equation is in the form of a double derivative of a volume integral over the turbulent shear stress tensor in the flow region and represents the generation of sound due to volume sources. The essence of the solution lies in the nature of the sources that may be regarded as a field of quadrupoles whose strength per unit volume is the stress tensor. Lighthill's Analogy, therefore, equates the sound of real turbulence to that induced by a quadrupole distribution in a medium. Curle [57] extended Lighthill's theory by including a solid boundary into the source region. Therefore, he included additional terms in the solution developed by Lighthill to account for the fluctuating forces acting on the fluid by the boundary. FfowcsWilliams and Hawkings [55] showed that when the sources of sound are in motion, the sound power increases with the reciprocal of  $(1-M)$  for Mach numbers less than unity. This implies that the level of sound from a moving source is greater than for a stationary source.

The difficulty in this method is that when acoustic sources (i.e., quadrupoles) are present in the flow field, volume integration is needed. This volume integration of the quadrupole source term is difficult to compute and is usually neglected in most acoustic analogy codes.

### ***2.2.2.1.2 Surface integral methods***

The Kirchhoff method and Porous FW-H equation are the most widely used methods. Kirchhoff's integral formulation has been used extensively for the prediction of acoustic radiation in terms of quantities on boundary surfaces (the Kirchhoff control surface coincides with the body). Kirchhoff's method has also been used for the computation of acoustic scattering from rigid bodies using a boundary element technique with the Galerkin method.

Porous FW-H equation was generated for the difficulties of original FW-H equations. The usual practice is to assume that the FW-H integration surface corresponds to a solid body and is impenetrable. However, if the surface is assumed to be porous, the porous surface can be used as a control surface in a similar fashion as the Kirchhoff method. Thus, the pressure signal in the far field can be found based on quantities on the control surface provided by a CFD code.

Kirchhoff's and porous FW-H methods consist of the calculation of the nonlinear near and mid-field numerically with the far-field solutions found from a Kirchhoff/Porous FW-H formulation evaluated on a control surface  $S$  surrounding the nonlinear-field. The surface  $S$  is assumed to include all the nonlinear flow effects and noise sources. The separation of the problem into linear and nonlinear regions allows the use of the most appropriate numerical methodology for each. The advantage of these methods is that the surface integrals and the first derivatives can be evaluated more easily than the volume integrals and the second derivatives needed for the evaluation of the quadrupole terms when the traditional acoustic analogy is used.

The porous FW-H equation method is a new idea and there are few applications in the literature. The method is equivalent to Kirchhoff's method and has the same advantages. In comparison, it is more robust with the choice of control surface and does not require normal derivatives. Since the method also requires a surface

integral, it is very easy to modify existing Kirchhoff/solid surface FW-H codes. The method requires larger memory, because more quantities on the control surface are needed. However, considering the robustness, the porous FW-H is the recommend method [61].

The use of both methods has increased substantially over the last 10 years, because of the development of reliable CFD methods that can be used for the evaluation of the near-field. The methods can be used to study various acoustic problems, such as propeller noise, high-speed compressibility noise, blade-vortex interactions, jet noise, ducted fan noise, etc. The methods are becoming more popular and have been coupled with production codes, such as Overflow, Fluent and Star-CD.

#### **2.2.2.2 Broadband Noise Source Models**

In many practical applications involving turbulent flows, noise does not have any distinct tones, and the sound energy is continuously distributed over a broad range of frequencies. In those situations involving broadband noise, statistical turbulence quantities readily computable from RANS equations can be utilized in conjunction with semi-empirical correlations and Lighthill's acoustic analogy to shed some light on the source of broadband noise. Literature offers several source models that enable to quantify the local contribution (per unit surface area or volume) to the total acoustic power generated by the flow. They are: Proudman's formula, source terms in the linearized Euler equations and source terms in Lilley's equation.

These equations can be employed to extract useful diagnostics on the noise source to determine which portion of the flow is primarily responsible for the noise generation. However, these source models do not predict the sound at receivers.

Unlike the direct method (CAA) and the integral methods, the broadband-noise-source models do not require transient solutions to any governing fluid dynamics equations. All the source models need are what typical RANS models would provide, such as the mean velocity field, turbulent kinetic energy ( $k$ ) and the dissipation rate

( $\epsilon$ ). Therefore, the use of broadband-source models requires the least computational resources.

The Proudman's formula gives an approximate measure of the local contribution to total acoustic power per unit volume in a given turbulence field. However proper caution should be taken when interpreting the results in view of the assumptions made in the derivation, such as high Reynolds number, small Mach number, isotropy of turbulence, and zero mean motion.

Linearized Euler Equations (LEE) have been used in order to extend the CFD solutions to the far field. Basically LEE can be used if the viscous effects can be neglected. The LEE equations employ a division of the flow field into a time-averaged flow and a time-dependent disturbance that is assumed to be small. The hybrid approach consists of the near-field evaluation using an accurate CFD code (e.g. LES) and the extension of the solution to the mid-field using LEE. Considerable CPU savings can be realized, since the LEE calculations are much cheaper than the CFD calculations.

Lilley's equation is a third-order wave equation that can be derived by combining the conservation of mass and momentum of compressible fluids. The self-noise and shear- noise can be obtained separately.

### **2.2.2.3 Computational Aero Acoustics (CAA)**

The growth of computer technology in the recent years made possible to predict the aerodynamic sound sources and the propagation of the generated sound, by starting from the unsteady flow governing equations. This powerful tool for analyzing noise generation and propagation is known as Computational Aero-Acoustics (CAA). The compressible Navier-Stokes equations have been rearranged exactly to yield the acoustic wave with a source term involving the acoustic pressure fluctuation, the mass flow rate, the external forces acting on the fluid and Lighthill stress tensor containing momentum flux, thermal and viscous terms. This equation expresses a

linear wave problem in a medium at rest with equivalent acoustic sources derived from the unsteady flow phenomena [37].

Some researchers have developed their own codes based on the above methods. Dunn, Tweed and Farassat [39] used Boundary Integral Equation Method (BIEM) for predicting ducted fan engine noise. The BIEM is based on the equations of linearized acoustics with uniform inflow and predicts the sound scattered by an infinitesimally thin, finite-length cylindrical duct that has been irradiated by some simple source process. Brentner and Farassat [58] investigated the aerodynamically generated sound of helicopter rotors, giving also an overview of the theoretical background in the field, starting with the Ffowcs Williams-Hawkings equation and its integral formulations. In Ref.[41], Farassat has shown the solutions of two linear wave equations, Kirchoff Method and FW-H equations, which are the two major approaches used in the discrete frequency noise prediction for rotating blade machinery in the time domain.

Wu, Su [40] developed a semi-empirical formula for predicting the noise spectra of axial flow fans in a free field. For derivation they assumed that the sound radiation from an axial fan in free field is primarily due to the fluctuating pressure exerted on the fan blade surface. Kiya studied the separated flow field of a centrifugal impeller by the discrete vortex method (DVM) [43]. Lowson [44] derived the formula for predicting the acoustic field generated by the moving point force from the wave equation. By applying this equation to each blade element, the acoustic pressure generated by the impeller can be predicted. But Lowson's equation can be applied only in the free field. The effects of the solid boundaries cannot be considered with this method. The scattering effect of acoustic is calculated by the boundary element method (BEM) in Ref.[45-48]. It is reported that the Kirchhoff-Helmholtz BEM is developed to calculate the solid boundary to take into account the scattering effect of the solid boundaries such as casing and duct. Rumsey et al. [38] used Navier-Stokes computer code to predict one of the ducted fan engine acoustic modes that result from rotor-wake/ stator-blade interaction. In the study to find the far field noise two acoustic codes were used. Near-field propagation was computed by using

Eversman's wave envelope code, which is based on a finite-element model. Propagation to the far field was accomplished by using the results of the wave envelope code as input.

### **2.3 Noise Measurement Standards**

There are international standards describing sound power measurement methods. The selection of the method is made according to the required accuracy from the measurement results. The measurement system is selected considering the information that can be obtained, the required degree of precision, the frequency range of interest, the bandwidth of the noise source, the volume of the noise source machinery and the measurement field. *"ISO 3740-2000: Acoustics - Determination of sound power levels of noise sources - Guidelines for the use of basic standards"* is used for determining the required measurement method.

Generally, the measurement approaches may be classified as Precision, Engineering and Survey Methods.

**The Precision Methods** can be applied in laboratory conditions. Acoustics Laboratories provides the highest accuracy levels. However these laboratory facilities are expensive and can only be used for the machinery having very small volumes compared to the room sizes. The type of the rooms to be used is decided considering the characteristics of the noise radiated.

A reverberation room or reverberation chamber is an acoustically designed room for uniform distribution of acoustic energy. It is used to determine the sound power of a source and also to find the absorption coefficient of a material. It is constructed to reflect sound as much as possible, thus it is the acoustic opposite of an anechoic room.



An anechoic chamber is a room that is isolated from external sound or electromagnetic radiation sources, sometimes using sound proofing, and prevents the reflection of wave phenomena (reverberation). In rooms such as these, the only sounds which exist are emitted directly from their source, and not reflected from another part of the chamber. Anechoic chambers are widely used for measuring the acoustic properties of acoustic instruments, measuring the transfer functions of acoustic devices, testing microphones, performing psychoacoustics experiments and for hearing aid test chambers.

Semi-anechoic rooms or chambers have conducting floors that do not have absorber installed. The size can be anything from small to large. The small ones for testing smaller motors, tool machinery or any other items intended for standing on the floor. The larger ones are for testing tool machinery, small cars and motorcycles, refrigerators and many other things. 75% of all testing in anechoic chambers is done in semi-anechoic chambers also called Open Field Rooms.

**The Engineering Method** is used when the noise source is placed over a reflecting plane and outside of the building or in a very large room. Measurement is performed while the machinery is working in its normal environment. “*EN ISO 3744 Acoustics - Determination of sound power levels of noise sources using sound pressure - Engineering method in an essentially free field over a reflecting plane*” is used as the measurement standard. The accuracy of the measurements is in engineering level.

**Survey Method** is used when the noise source is placed over a reflecting plane and inside of the building or in a very large room. There is no restrictions about the size of the machinery. Measurement is performed while the machinery is working in its normal environment. “*EN ISO 3746 Acoustics - Determination of sound power levels of noise sources using sound pressure - Survey method using an enveloping measurement surface over a reflecting plane*” is applied as the standard. The

accuracy of the measurements is in survey level. This method is suitable for industrial applications.

## CHAPTER 3

### THE THEORY OF FLOW ACOUSTICS

#### 3.1 Basic Principles And Terminology

##### 3.1.1 Classical Acoustics

Sound is the sensation produced by a pressure disturbance that propagates through a fluid at the acoustic velocity. A sound wave is characterized by its speed, wavelength and amplitude. The speed of sound depends on the medium through which the sound travels and also depends on temperature. Sound propagation is nondispersive, i.e., speed of sound does not change with the frequency. The wavelength,  $\lambda$  of a sound wave is related to the speed of sound  $c$  and its frequency  $f$  by  $\lambda = c/f$ . Sound pressure level (SPL) is calculated in decibels as:

$$L_p = 20 \log \left( \frac{p}{p_0} \right) \text{ dB} \quad (3.1)$$

Here  $p$  is taken as the rms value of the acoustic pressure at a particular point in the field.  $p_0$ , the reference sound pressure, is 20  $\mu\text{Pa}$  in air.

The homogeneous wave equation for propagation of sound waves in air can be written as follows.

$$\frac{\partial^2 \rho'}{\partial t^2} - c_0^2 \frac{\partial^2 \rho'}{\partial x_i^2} = 0 \quad (3.2)$$

The sound field is characterized as near field or far field according to the distance between sound source and receiver. In the study of diffraction, the near field is that

part of the radiated field that is within a small number of wavelengths of the diffracting edge. The far field is beyond the near field.

### 3.1.2 Aero Acoustics

Aero acoustics is the study of aerodynamic sound, generated when a fluid flow interacts with a solid surface or with another flow. Aerodynamically generated sound is governed by a nonlinear process. When acoustic sources ( $Q$ ) are specified in the Equation (3.2), the equation becomes nonhomogeneous wave equation. Equation 3.3 gives the nonhomogeneous wave equation in the order of  $2^n$ .

$$\frac{\partial^2 \rho'}{\partial t^2} - c_0^2 \frac{\partial^2 \rho'}{\partial x_i^2} = \frac{\partial^n Q_{ij\dots}}{\partial x_i \partial x_j \dots} \quad (3.3)$$

which is usually solved by the Green's function technique. The solution with Green's function of generalized wave equation is given in Equation 3.4.

$$4\pi c_0^2 \rho'(\vec{x}, t) = \frac{\partial^n}{\partial x_i \partial x_j \dots} \int_{-\infty}^{\infty} Q_{ij\dots} \frac{d\vec{y}}{r} \quad (3.4)$$

where  $r$  shows the distance from the center of the source.

All acoustic sources are characterized by specific radiating properties according to the efficiency of the energy conversion from kinetic energy in the source mechanism into acoustic energy. The sound produced by a monopole like acoustic source is associated with the displacement of the fluid due to the acceleration of the moving surface. The acoustic waves generated by a monopole are propagating equally in all directions (Fig. 3.1 (a)).

The sound produced by a dipole like source is due to the distribution of the forces (fluctuating loading) on the surface. The directivity pattern of a dipole shows two lobes and it has maxima along  $0^\circ$  and  $180^\circ$  directions as it is presented in Fig. 3.1 (b). No sound radiation is found along the  $90^\circ$  and  $270^\circ$  directions. As practical examples, those acoustic forces are found in the cases when fluctuating forces act on blades (propellers or fans). A quadrupole acoustic source consists of two identical dipoles which are opposite in phase. In the case of the lateral quadrupole, the dipole axes do not lie along the same line. A lateral quadrupole like acoustic source is found in all turbulent flows (jets, mixing layers) and is associated with the noise generated by shear-layer and entropy. In this case there are four directions (four lobes) where sound is radiated and four directions where no sound is radiated, as shown in Fig.3.1 (c). [59]. Table 3.1 summarizes the characteristic properties of three types of aero acoustic sources.

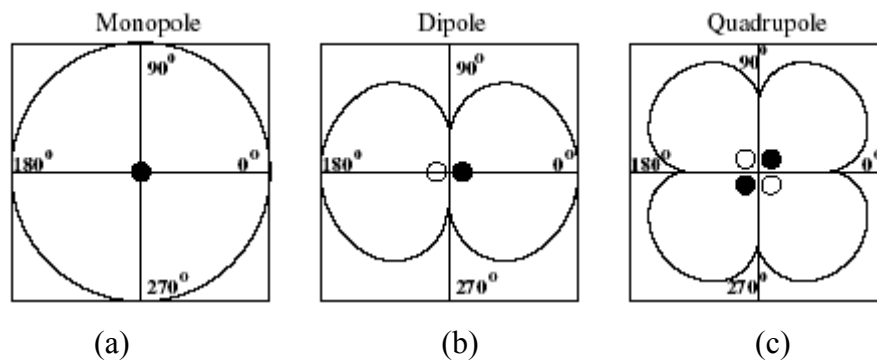


Figure 3.1 Directivity patterns for an acoustic monopole (a), dipole (b), and quadrupole (c)

Table 3.1 - Noise Source Characterization ( Ref. [60] )

| Source Type | Time Variation   | Strenght  | Place excitation | Acoustic Power |
|-------------|------------------|---|------------------|----------------|
| Monopole    | Mass             | $\partial u_n / \partial t$                     | boundary         | $\sim U^4$     |
| Dipole      | Pressure         | $\partial p / \partial t$                       | boundary         | $\sim U^6$     |
| Quadrupole  | Lighthill Stress | $\partial^2 T_{ij} / \partial x_i \partial x_j$ | internal         | $\sim U^8$     |

### 3.2 Aero Acoustic Analogies

The approach suggested by acoustic analogy is to consider equivalent classical acoustic sources radiating as if the medium were unbounded and uniformly at rest. The primary work of Lighthill, performed in the fifties to tackle the problem of jet noise, is the starting point of the theories generally referred to for the investigation of the aerodynamic noise. This work was next extended by FfowcsWilliams and Hawkings at the end of sixties for application to rotating machines.

The real problem of the noise radiated by a rotor/and or a highly disturbed flow was replaced by the problem of the classical acoustic radiation in a medium at rest with equivalent acoustic sources. Therefore, the difficulty of deriving exact equations was then avoided and replaced by the question of defining equivalent sources, which is a task of aerodynamic nature [42, 43, 44]. The general outline of the acoustic analogy in Ref. [45] is given in Figure 3.2.

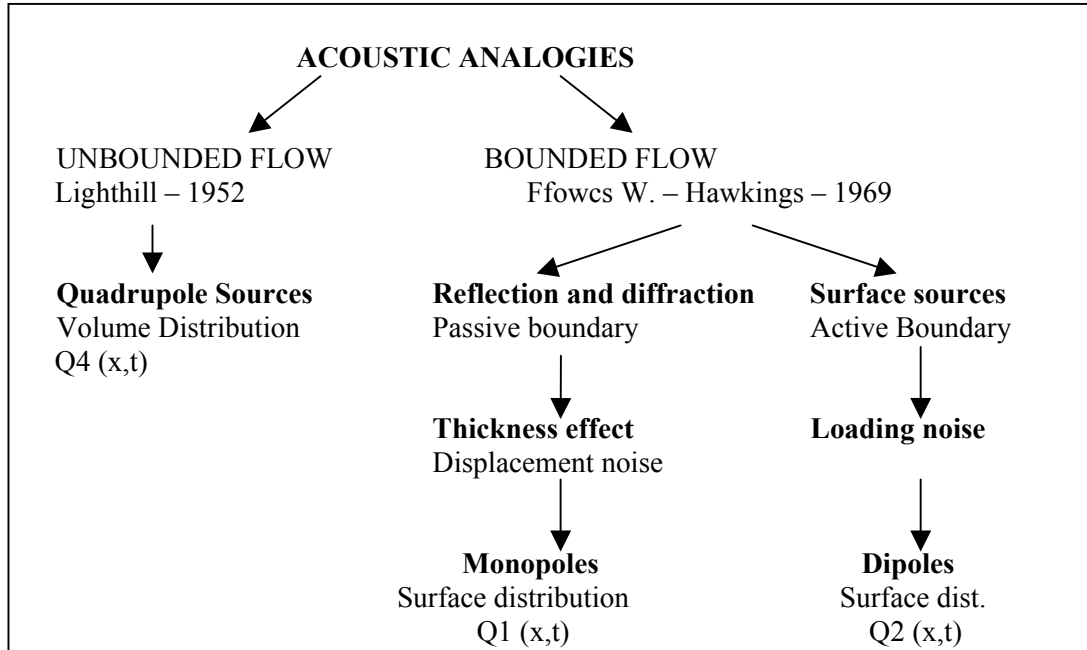


Figure.3.2 - Aero-Acoustic Analogies

### 3.2.1 Lighthill's Acoustic Analogy

Lighthill's acoustic analogy was the first attempt to describe the radiation of the sound generated by a turbulent flow. The analogy is based on the hypothesis that the part of the flow field that is the source for acoustics is distinct, so that the acoustic waves do not interfere with the flow. The governing equations for a compressible fluid motion are the conservation laws of mass, momentum, and energy:

$$\frac{\partial \rho}{\partial t} + \frac{\partial(\rho u_i)}{\partial x_i} = 0 \quad (3.5)$$

$$\frac{\partial(\rho u_i)}{\partial t} + \frac{\partial(\rho u_i u_j)}{\partial x_j} = \frac{\partial}{\partial x_j} (-p \delta_{ij} + \sigma_{ij}) \quad (3.6)$$

$$\frac{\partial(\rho h)}{\partial t} + \frac{\partial(\rho u_j h)}{\partial x_j} = \frac{\partial p}{\partial t} + \frac{\partial}{\partial x_j} \left( \frac{\mu}{Pr} \frac{\partial h}{\partial x_j} \right) \quad (3.7)$$

where  $\rho$ ,  $u_i$ ,  $p$ ,  $h$  are the density, velocity, pressure, and the mixture enthalpy per unit mass, respectively.  $\delta_{ij}$  is the Kronecker delta function,  $\mu$  represents the molecular viscosity and  $Pr$  is Prandtl number. The viscous stress tensor ( $\sigma_{ij}$ ) is defined as:

$$\sigma_{ij} = \mu \left[ \frac{\partial u_i}{\partial x_j} + \frac{\partial u_j}{\partial x_i} - \frac{2}{3} \left( \frac{\partial u_k}{\partial x_k} \right) \delta_{ij} \right] \quad (3.8)$$

The equation of state:

$$p = \rho R_{gas} T \quad (3.9)$$

where  $R_{gas}$  is the gas constant and  $T$  represents the temperature.

The basic idea of Lighthill was to reformulate the general equations of gas dynamics, in order to derive a wave equation for acoustic fluctuation with a source term on the right-hand side. No special assumption was made nor linearization was introduced. Then subtracting the space derivative of the momentum equation, Eqn. (3.6), from the time derivative of the continuity equation, Eqn. (3.5), gives Eqn. (3.10).

$$\frac{\partial^2 \rho}{\partial t^2} - \frac{\partial^2}{\partial x_i \partial x_j} (\rho u_i u_j) = \frac{\partial^2}{\partial x_i \partial x_j} (p \delta_{ij} - \sigma_{ij}) \quad (3.10)$$

The equation (3.10) remains true if the same quantity is added on both sides. Add the term  $-c_0^2 \partial^2 \rho / \partial x_j^2$ ,  $c_0$  being the characteristic speed of sound of the undisturbed gas (precisely the speed of sound in the medium surrounding the flow region in the applications; this is different from the local speed of sound  $c^2$  in the flow). Then, forming a wave operator on the left-hand side and removing all other terms on the right-hand side leads to:



$$\frac{\partial^2 \rho}{\partial t^2} - c_0^2 \frac{\partial^2 \rho}{\partial x_i^2} = \frac{\partial^2}{\partial x_i \partial x_j} [\rho u_i u_j + (P - c_0^2 \rho) \delta_{ij} - \sigma_{ij}] \quad (3.11)$$

This result is the well-known Lighthill's equation. When applied to a true problem of acoustics, it reduces to the homogeneous wave equation at large distances from the flow, since all terms on the right-hand side vanish (according to the reasonable assumptions related to the propagation of acoustic waves). Neglecting the contribution of the viscous stresses to the total acoustic source term and introducing the decomposition of flow variables as given in Eqn. (3.12), Lighthill's acoustic analogy formulated in terms of acoustic density fluctuations can be obtained as in Eqn. (3.13).

$$\mathbf{u}_i = \mathbf{u}_{0i} + \mathbf{u}'_i \quad p_i = p_{0i} + p'_i \quad \rho_i = \rho_{0i} + \rho'_i \quad (3.12)$$

$$\frac{\partial^2 \rho'}{\partial t^2} - c_0^2 \frac{\partial^2 \rho'}{\partial x_i \partial x_i} = \frac{\partial^2 T_{ij}}{\partial x_i \partial x_j} \quad (3.13)$$

Equation (3.13) describes a distributed source of sound, where the acoustic source term can be seen as negligible outside the flow where only generated sound waves are present. The nonhomogeneity in Eqn. (3.13) is given by the "forcing term" (total acoustic source term) on the right-hand side, which is responsible for the generation of sound and is a second order spatial derivative (quadrupole) of the Lighthill stress tensor ( $T_{ij}$ ):

$$T_{ij} = \rho u_i u_j + [(p - p_0) - c_0^2 (\rho - \rho_0)] \delta_{ij} \quad (3.14)$$

Eqn. (3.13) and (3.14) are valid for any flow field which has no external forces. Beside the sound source, the propagation of sound waves with flow ( $\rho u_i u_j$ ), the propagation of sound waves with heat transfer ( $p - c_0^2 \rho$ ) can be calculated with Lighthill's equation. Since the dominant term is the propagation with flow,  $T_{ij} = \rho u_i u_j$  can be used for practical applications. This reduction includes the error in the order of  $M^2$  since ( $p' \approx \rho c_0^2 \approx M^2$ ). Especially for the flow with low Mach number, Lighthill stress tensor is in the order of square of mean velocity ( $T_{ij} \sim u^2$ ).

### 3.2.2 The Formulation of FfowcsWilliams and Hawkings

In Lighthill's equation the sound generated aerodynamically was considered with no solid bodies in the source region.

FfowcsWilliams and Hawkings extended the aero-acoustic analogy to bounded flows. To represent the real medium with flow and obstacles in a convenient way, FW- H defined an equivalent medium where the rigid bodies are replaced by mathematical surfaces as in Figure 3.3.

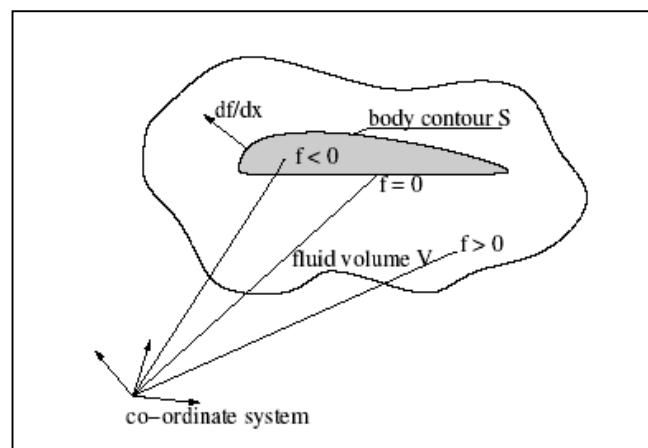


Figure 3.3- Model for FfowcsWilliams and Hawkings Equation

The inner volume of the surfaces is assumed to contain the ambient fluid at rest. In order to preserve both the kinematics of the flow and the boundary condition of no-cross flow on the surfaces, continuity must be imposed at the surface location.

Mass and momentum equations are written as:

$$\frac{\partial \rho}{\partial t} + \frac{\partial}{\partial x_i} (\rho u_i) = \rho_0 u_{s_i} \delta(f) \frac{\partial f}{\partial x_i} \quad (3.15)$$

$$\frac{\partial}{\partial t} (\rho u_i) + \frac{\partial}{\partial x_i} (\rho u_i u_j - \tau_{ij}) + \frac{\partial p}{\partial x_j} = p_{ij} \delta(f) \frac{\partial f}{\partial x_i} \quad (3.16)$$

In this equations  $\rho$ ,  $u_i$  are respectively the density and total velocity components of the flow,  $\rho_0$  is the mean density,  $u_{s_i}$  is the velocity field of a point on the surfaces,  $\delta$  means the Dirac delta function,  $p_{ij} = p' \delta_{ij} - \tau_{ij}$  is the viscous stress tensor ( $p$  being the static pressure and  $f(\vec{x}, t) = 0$  is an equation defining the kinematics of the surface. If the normal unit vector on the surfaces is  $\vec{n}$  the boundary condition of no cross-flow is simply:  $\vec{u}(\vec{x}, t) \cdot \vec{n}(\vec{x}, t) = u_s(\vec{x}, t) \cdot \vec{n}(\vec{x}, t) = u_s(\vec{x}, t) = 0$ .

A formal procedure can be used to derive an equation for the density fluctuation  $\rho' = \rho - \rho_0$  in the following way from Equation (3.15) and (3.16):

$$\frac{\partial^2 \rho'}{\partial t^2} - c_0^2 \frac{\partial^2 \rho'}{\partial x_i^2} = \frac{\partial^2 T_{ij}}{\partial x_i \partial x_j} - \frac{\partial}{\partial x_i} (p_{ij} \delta(f) \frac{\partial f}{\partial x_j}) + \frac{\partial}{\partial t} \left( \rho_0 v_i \delta(f) \frac{\partial f}{\partial x_i} \right) \quad (3.17)$$

The statement of the Eqn. (3.17) follows:

- a volume distribution  $\partial^2 T_{ij} / \partial x_i \partial x_j$  in the outer region of the surfaces, due to the flow. This term represents the quadrupole sources.

- a surface distribution  $\partial / \partial x_i (p_{ij} \delta (f) \partial f / \partial x_j )$  due to the interaction of the flow with the moving bodies. This term is called as “loading noise” and it represents the aerodynamic forces acting on the surface in the flow field. Therefore, it is an acoustic dipole.
- a surface distribution  $\partial / \partial t (\rho_0 v_i \delta (f) \partial f / \partial x_i )$  due to the kinematics of the bodies. It represents the acoustic contribution of the displacement of the fluid due to acceleration of the surface. It is called as “thickness noise” and is a monopole.

The Lighthill’s acoustic source term is zero inside the surface and exists just outside of the moving surface. The Dirac delta function ensures the existence of the second and third acoustic source terms only on the moving surface.

### 3.2.3 The Porous FfowcsWilliams and Hawkings Formulation

The contribution of the volume integrals in the original FW-H Equation becomes small when the flow is low subsonic and the source surface encloses the source region. Therefore the acoustic field can be considered as:

$$p'(\vec{x}, t) = p'_T(\vec{x}, t) + p'_L(\vec{x}, t) \quad (3.18)$$

The solution of FW-H with free-space Green function ( $\delta(\mathbf{g})/4\pi r$ ) can be written for a moving control surface as follows [63]:

$$4\pi p'_T(\vec{x}, t) = \int_{f=0} \left[ \frac{\rho_0 (\dot{U}_n + U_{\dot{n}})}{r(1 - M_r)^2} \right] dS + \int_{f=0} \left[ \frac{\rho_0 U_n \{ r \dot{M}_r + c(M_r - M^2) \}}{r^2 (1 - M_r)^3} \right] dS \quad (3.19)$$

$$\begin{aligned}
4\pi p'_L(\vec{x}, t) = & \frac{1}{c} \int_{f=0} \left[ \frac{\dot{L}_r}{r(1-M_r)^2} \right] dS + \int_{f=0} \left[ \frac{L_r - L_M}{r^2(1-M_r)^2} \right] dS \\
& + \frac{1}{c} \int_{f=0} \left[ \frac{L_r \{ r\dot{M}_r + c(M_r - M^2) \}}{r^2(1-M_r)^3} \right] dS
\end{aligned} \tag{3.20}$$

where the new variables  $U_i$  and  $L_i$  are defined as [62] .

$$U_i = v_i + \frac{\rho}{\rho_0} (u_i - v_i) \tag{3.21}$$

$$L_i = P_{ij} \hat{n}_j + \rho u_i (u_n - v_n) \tag{3.22}$$

where subscript  $o$  implies ambient conditions, superscript  $'$  implies disturbances (e.g.  $\rho = \rho' + \rho_0$ ),  $\rho$  is the density,  $u$  is the fluid velocity,  $v$  is the velocity of the control surface, and  $P_{ij}$  is the compressive stress tensor with the constant  $p_o \delta_{ij}$  subtracted.

When the integration surface coincides with an impenetrable wall, the two  $p'_T(\mathbf{x}, t)$  and  $p'_L(\mathbf{x}, t)$ , are often referred to as thickness and loading terms, respectively, in light of their physical meanings. The square brackets in the Equations denote that the kernels of the integrals are computed at the corresponding retarded times,  $\tau$ , defined as follows, given the observer time,  $t$ , and the distance to the observer,  $r$ ,

$$\tau = t - \frac{r}{c} \qquad L_r = \vec{L} \cdot \hat{\mathbf{r}} = L_i r_i \qquad U_n = \vec{L} \cdot \vec{n} = U_i n_i \tag{3.23}$$

where  $\vec{r}$  and  $\vec{n}$  denote the unit vectors in the radiation and wall-normal directions, respectively.

### 3.3. The Boundary Element Method

The Boundary Element Method (BEM) is a numerical analysis technique used to obtain solutions to the partial differential equations of a variety of physical problems with well-defined boundary conditions. The differential equation, which is defined over the entire problem domain, is transformed into a surface integral equation over the surfaces that enclosed entirely the problem domain. The surface integral equation can then be solved by discretizing the surfaces into smaller regions (boundary elements). Therefore, BEM is an integral equation technique.

The solution of the problem is found by superposing singular solutions distributed over the entire boundary of the problem. The singular source located at one point of the boundary exerts influence on each and every point on the boundary of the problem. When this influence of a single source for a discretized boundary is summed over all the boundary segments, it fills the entire row of the final algebraic matrix equation [65,67,68].

#### 3.3.1 Acoustic Boundary Integral Equation

For steady state, constant frequency motion, the acoustic wave equation reduces to the Helmholtz equation where  $p$  is the acoustic pressure and  $k = \omega/c$  is the wave number.

$$\nabla^2 p + k^2 p = j\rho\omega s_d(\vec{r}) \quad (3.24)$$

##### 3.3.1.1 Exterior Problems

In this class of problems, the problem domain  $V$  is the exterior region.  $V$  is considered enclosed in between the surface  $S$  and an imaginary surface  $A$  that is at a

sufficiently large distance from the acoustic sources and the surface  $S$  such that the boundary condition on  $A$  satisfies Sommerfeld's acoustic radiation condition. In other words, the integral over  $A$  vanishes as the distance approaches infinity.

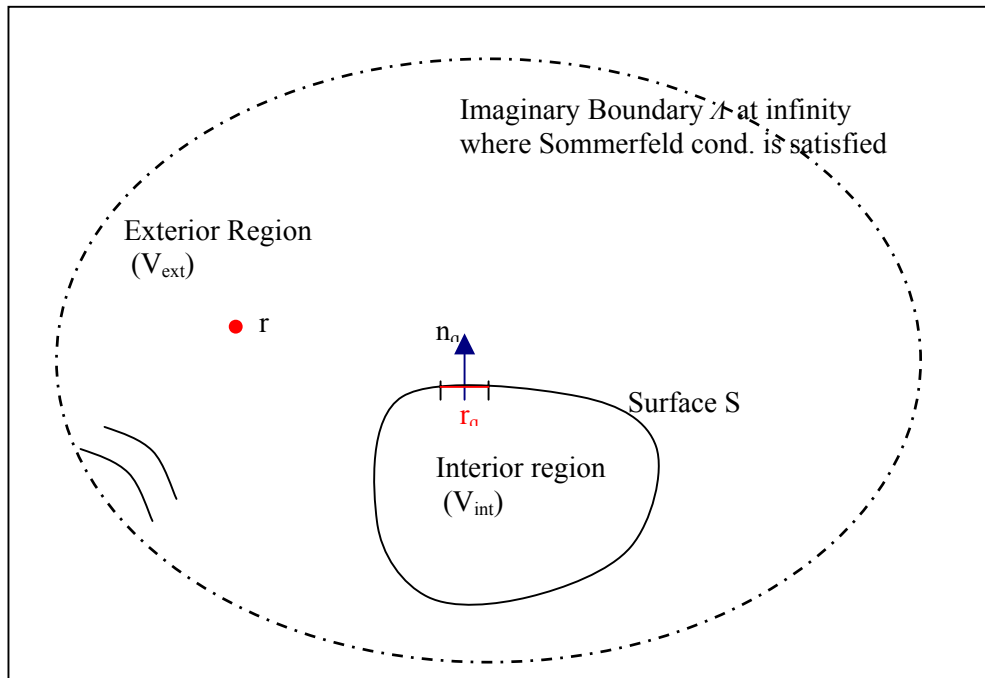


Figure 3.4 Exterior Problem Domain

The integral equation for the total wave, i.e, scattered and incident waves

$$\int_S \left[ p(r_q) \frac{\partial G(r|r_q)}{\partial n_q} - \frac{\partial p(r_q)}{\partial n_q} G(r|r_q) \right] dS = \begin{cases} p(r) - p_i(r), & r \in V_{\text{ext}} \\ \frac{1}{2} p(r) - p_i(r), & r \in S \\ -p_i(r), & r \in V_{\text{int}} \end{cases} \quad (3.25)$$

where term on left-hand side are dipole and monopole source distributions, respectively.

### 3.3.1.2 Interior Problems

In an interior problem, the problem domain  $V$  is the region  $V_{\text{int}}$  inside the enclosing surface  $S$ . Since it is a finite region, there is no need to construct the imaginary surface  $\Lambda$  at infinity.

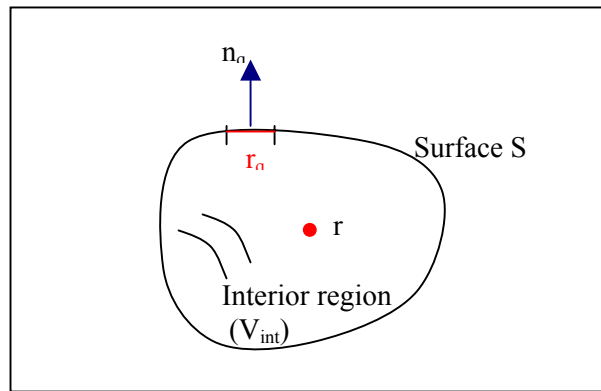


Figure 3.5 Interior Problem Domain

$$\int_S \left[ p(r_q) \frac{\partial G(r|r_q)}{\partial n_q} - \frac{\partial p(r_q)}{\partial n_q} G(r|r_q) \right] dS = \begin{cases} -(p(r) - p_i(r)), & r \in V_{\text{int}} \\ -\left(\frac{1}{2} p(r) - p_i(r)\right), & r \in S \\ p_i(r), & r \in V_{\text{ext}} \end{cases} \quad (3.26)$$

### 3.3.1.3 Numerical Solution

The solution is obtained by discretising the Helmholtz integral equation, using a shape function  $[N]$  to interpolate the pressure and its derivative in each boundary element:



$$\varepsilon p(\mathbf{r}) - p_i(\mathbf{r}) = \sum_{i=1}^N \int_{S_i} \frac{\partial G(\mathbf{r}|\mathbf{r}_{q_i})}{\partial \mathbf{n}_{q_i}} [\mathbf{N}] dS \{p(\mathbf{r}_{q_i})\} - \sum_{i=1}^N \int_{S_i} G(\mathbf{r}|\mathbf{r}_{q_i}) [\mathbf{N}] dS \left\{ \frac{\partial p(\mathbf{r}_{q_i})}{\partial \mathbf{n}_{q_i}} \right\} \quad (3.27)$$

For aero acoustic analogy (distributed dipoles boundary condition), the Eqn. (3.27) reduces to,

$$\varepsilon p(\mathbf{r}) - p_i(\mathbf{r}) = \sum_{i=1}^N \int_{S_i} \frac{\partial G(\mathbf{r}|\mathbf{r}_{q_i})}{\partial \mathbf{n}_{q_i}} [\mathbf{N}] dS \{p(\mathbf{r}_{q_i})\} \quad (3.28)$$

## CHAPTER 4

### NUMERICAL ANALYSIS

#### 4.1 The Approach for the Numerical Analysis

The sound prediction approach is based on Aero-acoustic Analysis. FfowcsWilliams-Hawkings equation (Equation 3.17) can be re-written as Equation 4.1.

$$\left( \frac{1}{a_0^2} \frac{\partial^2}{\partial t^2} - \nabla^2 \right) p' = \frac{\partial m_s}{\partial t} + \frac{\partial f_s}{\partial x_i} + \frac{\partial^2 T_{ij}}{\partial x_i \partial x_j} \quad (4.1)$$

There are three terms on the right hand side of the Equation 4.1. First term represents the monopoles (thickness noise), which are due to the displacement of the fluid particles. Second term stands for the dipoles (loading noise) that are resulted from the unsteady pressure loading of the surfaces. Third term represents the quadrupoles (jet noise) that are due to the time-dependent stresses including viscosity and turbulence.

In this relation left hand side is obtained from the flow field solution. On the right hand side monopoles and quadrupoles are neglected considering that the fan is compact, fan speed is small and the dominant noise is dipoles for fans. Therefore, Equation 4.1 is solved for the dipole sources only.

The dipoles obtained from Equation 4.1 are defined as discrete noise sources on the nodes of acoustic mesh (boundary element mesh). Then Boundary Element Method is utilized for the solution of inhomogeneous wave equations and calculation of acoustic pressures at the receiver point.

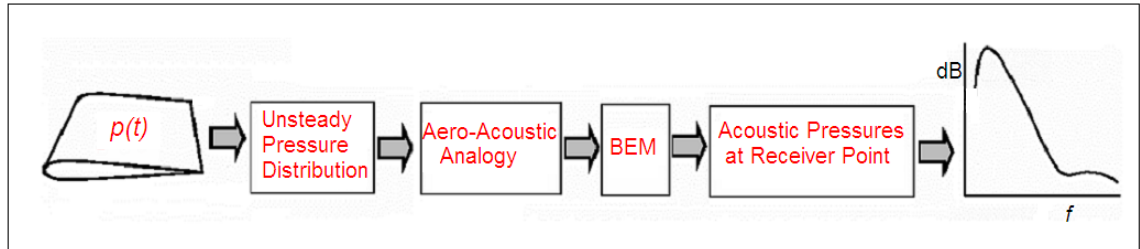


Figure 4.1 Steps of Sound Prediction Approach

Based on the approach given in Figure 4.1, first 3D model of the fan is prepared by using I-DEAS Simulation Software. For the Aero-acoustic Analysis, this model is transferred to Gambit where flow field is discretized. Fluent is utilized for the solution of flow field. Dipoles are calculated with the help of Aero-acoustic Analogy. These dipoles are introduced as discrete noise sources on the nodes of the Boundary Element Mesh that is prepared by using I-DEAS. D-BEM Interior and D-BEM Exterior methods of LMS Sysnoise are used to solve the acoustic field and finally, acoustic pressures at receiver points are predicted.

The cavity itself creates excitation modes and generates noise. This effect is investigated with a numerical experiment by using a monopole noise source for the excitation of resonance frequencies of the cavity. LMS Sysnoise is utilized for the task.

Numerical solution steps are summarized in Figure 4.2.

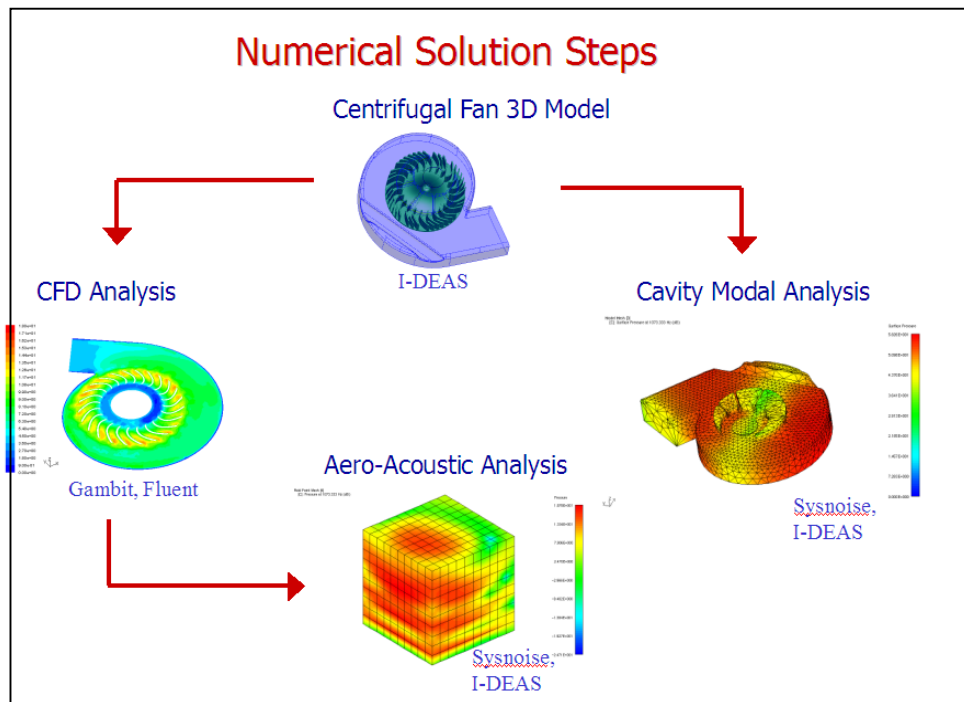


Figure 4.2 Numerical Solution Steps followed for the noise prediction

#### 4.1.1 The Analysis Cases

Five different fan configurations are used in this research study. These are :

**Case A:** The impeller with splitter (Figure 4.3), the volute with channel (Figure 4.5).

**Case B:** The impeller with splitter (Figure 4.3), the volute without channel (Figure 4.6).

**Case C:** The impeller without splitter (Figure 4.4), the volute with channel (Figure 4.5).

**Case D:** The impeller with splitter (Figure 4.3), the volute with channel but the ribs on the volute inlet are eliminated (Figure 4.7).

**Case E:** The impeller with splitter (Figure 4.3), the volute with channel but the volute is coated with bitumen (Figure 4.8).

Cases A, B and C are investigated theoretically and experimentally; Cases D and E are investigated only experimentally. In this section, the numerical analysis performed for Cases A, B and C are explained. Experimental studies are given in Chapter 5.

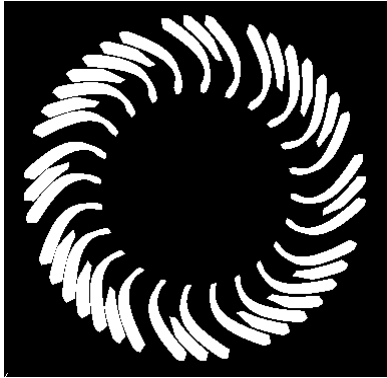


Figure 4.3 Original Impeller

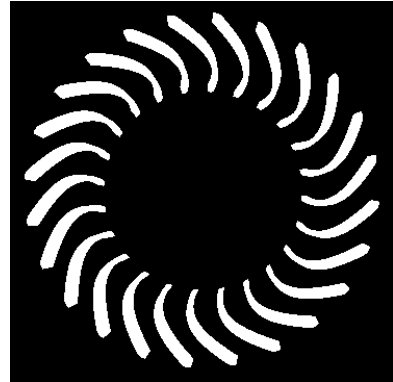


Figure 4.4 Impeller without splitter



Figure 4.5 Volute with channel



Figure 4.6 Volute without channel



Figure 4.7 Volute with inlet modification



Figure 4.8 Volute coated with bitumen

#### 4.1.2 The Turbulence Model

The sound generated from the fans has both tonal and broadband characteristics. The tonal noise is the discrete contribution due to the interaction of the transient flow with the blades. This noise happens at blade passing frequency (BPF) and this is, from an acoustical point of view, the most annoying noise. The broadband component arises from random fluctuations in pressure over a wide range of frequencies, and is associated with turbulent flow in the inlet stream, in boundary layer, and wake behind the blade.

The need for URANS, LES or DES kind of flow simulation approaches for the fan noise depends on what really generates the noise.

URANS solution makes sense in providing adequate noise prediction for a reasonable level of CPU and short times. This type of eddy viscosity model will predict the broadband noise poorly but is able to resolve the dominant tonal frequencies.

In order to capture the broadband noise in detail, a filtering turbulence model such as LES or DES will be necessary, because they capture the fluctuations in a better way. These models require a much finer mesh to allow the larger turbulent eddies being resolved and only the small eddies to be filtered. Broadband noise contains only a tiny fraction of energy of the primary flow, so the magnitude of acoustic pressure is very small compared to the hydrodynamic pressure. Hence very small transient variations need to be captured, and this requires adequate spatial and temporal resolution. Consequently, to achieve an accurate simulation of the broadband noise from the fan, a very fine mesh would be required with a high-end turbulence model. This would take a substantial amount of time and computing power. For example, considering 3 revolutions to achieve steady state, a further 1 revolution to obtain data and estimating 15 seconds per time step, the fan model which is subject of this study requires the following computer power and time in order to complete flow field computations adequately.

URANS:

4 million cells for mesh size

with 8 processors it takes 6 days per rotation

total elapsed time for CPU runs needs approximately 1 month

LES or DES:

40 million cells for mesh size for suitable accuracy in noise prediction

with 8 processors it needs *10 months* for the solution

The fan has 24 blades and 16 splitters. The splitters are unevenly distributed so that the BPF cannot be computed exactly. Assuming only 24 blades and then considering 40 evenly distributed blades, two values for the BPF can be computed. It can be predicted that the exact value will be between these two levels.

Blade Passing Frequency 1 =  $24 * 1925 \text{ rpm} / 60\text{s} = 770 \text{ Hz}$

Blade Passing Frequency 2 =  $40 * 1925 \text{ rpm} / 60\text{s} = 1283 \text{ Hz}$

The fan to be analyzed in this study has 1925 rpm revolution speed. At this high speed, the tonal noise is expected to dominate. The Sound Pressure Spectrum of the fan that is given in Figure 4.1 supports this information. The peak pressure value in Figure 4.9 is near 1000 Hz that may correspond to the tonal noise of the fan. The pressure levels are lower at the broadband. The signature of the spectrum implies that the tonal noise is dominant. Therefore URANS analysis is decided to be suitable for this system.

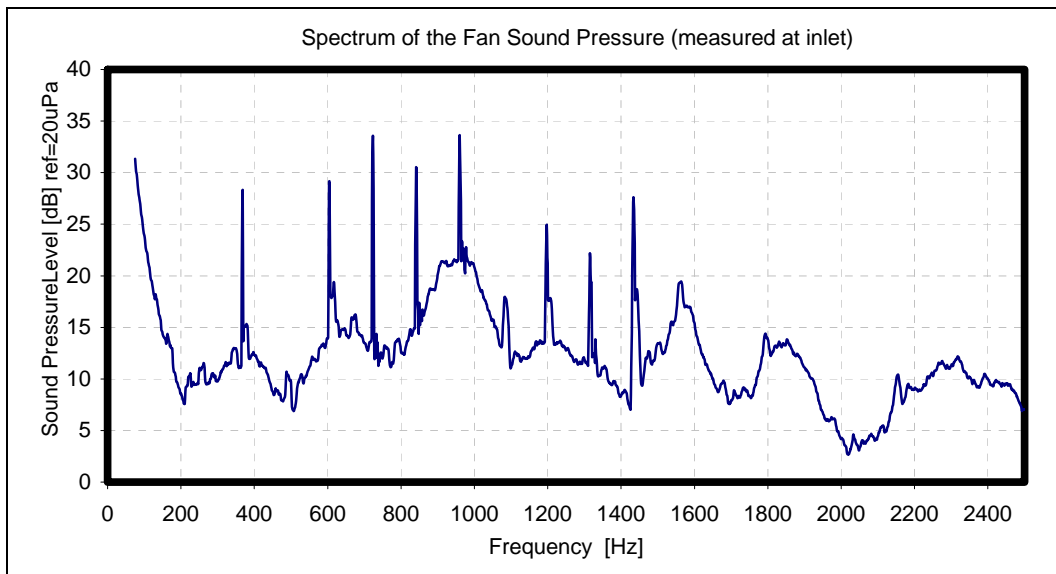


Figure 4.9 Spectrum of the fan noise for the original design (measured at 0.5 m away from the fan exit)

## 4.2 Numerical Analysis

Numerical analysis study starts with the discretization of flow field into small control volumes. Then flow field is solved with a finite volume method by means of a flow solver. The flow is taken as 3D and unsteady. Incompressible flow assumption is made since the fan rotates at 1925 rpm and, tip Mach number  $< 0.15$ .

### 4.2.1 Discretization of the Flow Field

GAMBIT is used for developing the unstructured mesh for the fans. The Case-A (original design) and Case-B are meshed with very fine elements. Prismatic elements (hex type) are used as much as possible. However the fan without splitters (Case-C) is meshed with respectively coarser and tetrahedral elements. The reason for this difference is the computational power and time requirement increase with the increase in number of grids.



#### ***4.2.1.1 Case-A and Case-B***

The grid of these simulations consists of 3.1 million cell volumes. The blades, splitters and the rotating region are prepared with hex mesh to increase the accuracy. The remaining volumes are filled with tetra meshes. Boundary layer meshes are applied near walls.

Figure 4.10 - Figure 4.15 shows the computational domain for the simulation.

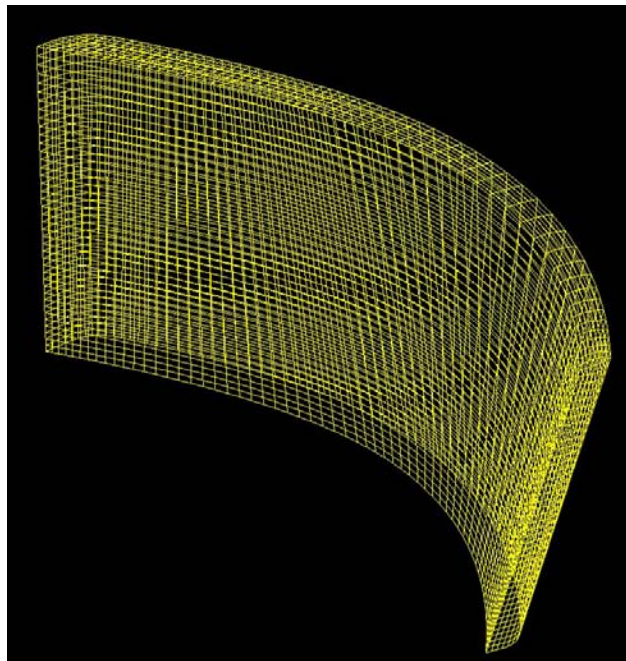


Figure 4.10 Hex mesh of a blade

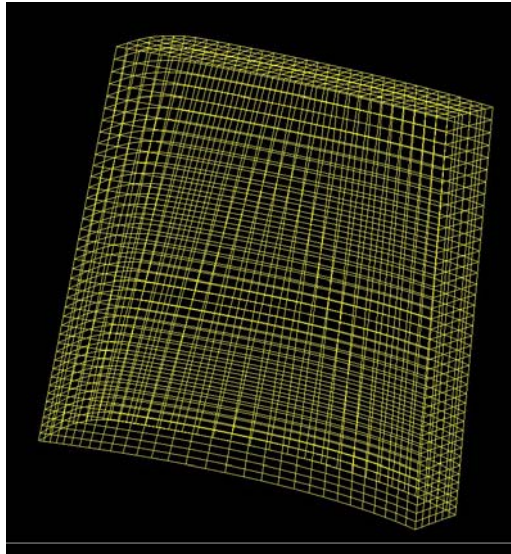


Figure 4.11 Hex mesh of a splitter

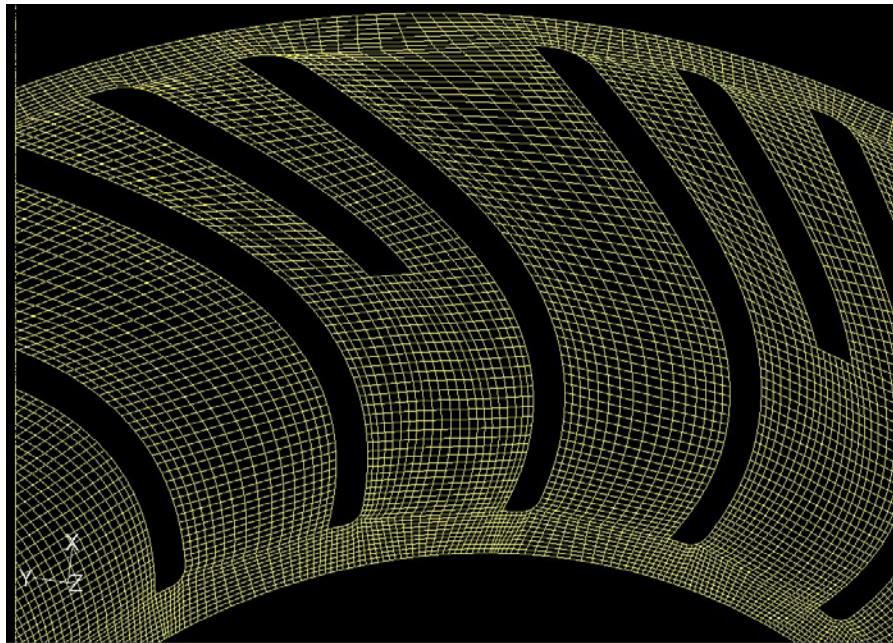


Figure 4.12 The mesh of Blade Spacings

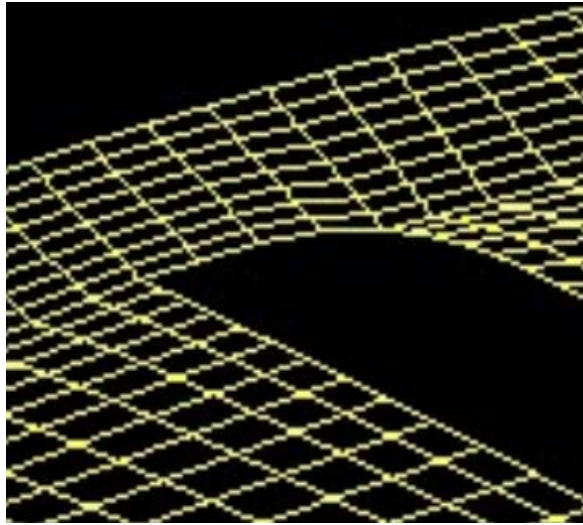


Figure 4.13 The mesh at the blade tips

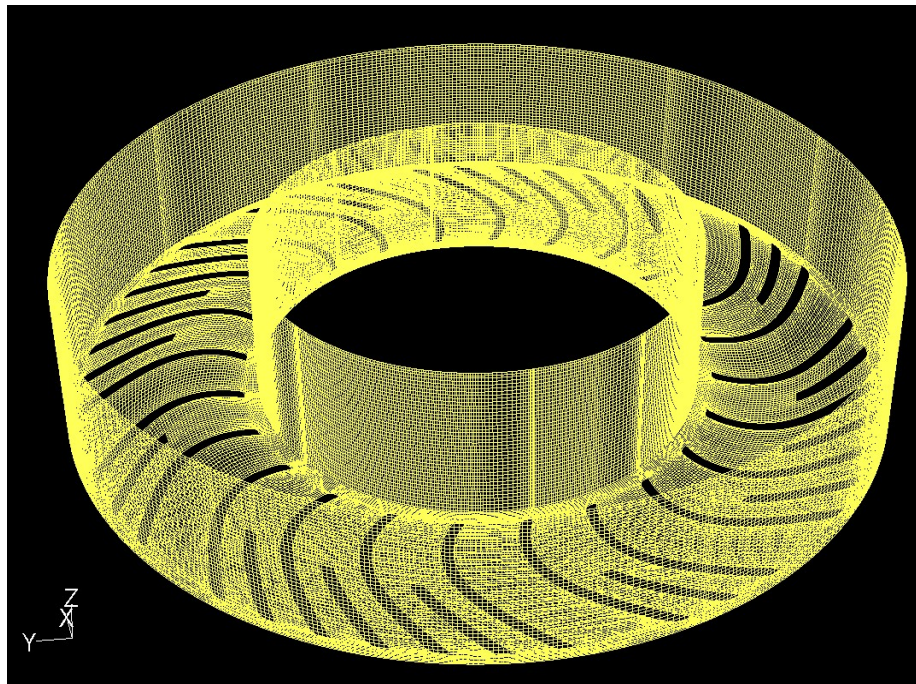


Figure 4.14 The Mesh of the Rotating Region (without top part and blades)

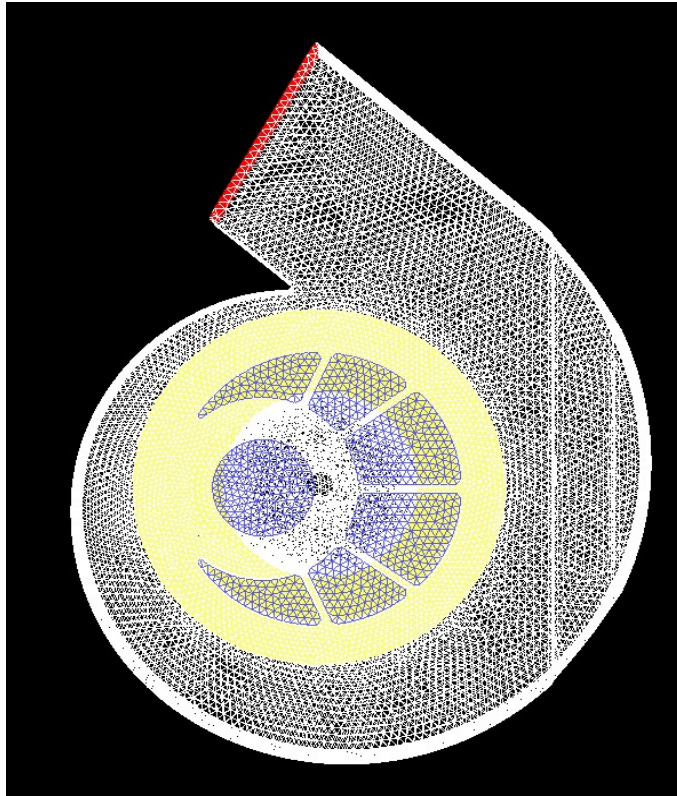


Figure 4.15 The mesh of the volute with channel

#### ***4.2.1.2 Case-C***

In this case impeller has 24 long blades only. These blades are meshed with tetrahedral elements. Considering the computing time, the sizes of the elements are increased to decrease the total number of control volumes where the computation is carried out. Total number of control volumes is 1.5 million in this case.

Figure 4.16 represents the mesh of a blade. The volute is again meshed with tetrahedral elements like Case A and Case B, given in Figure 4.15, but coarser grids are created.

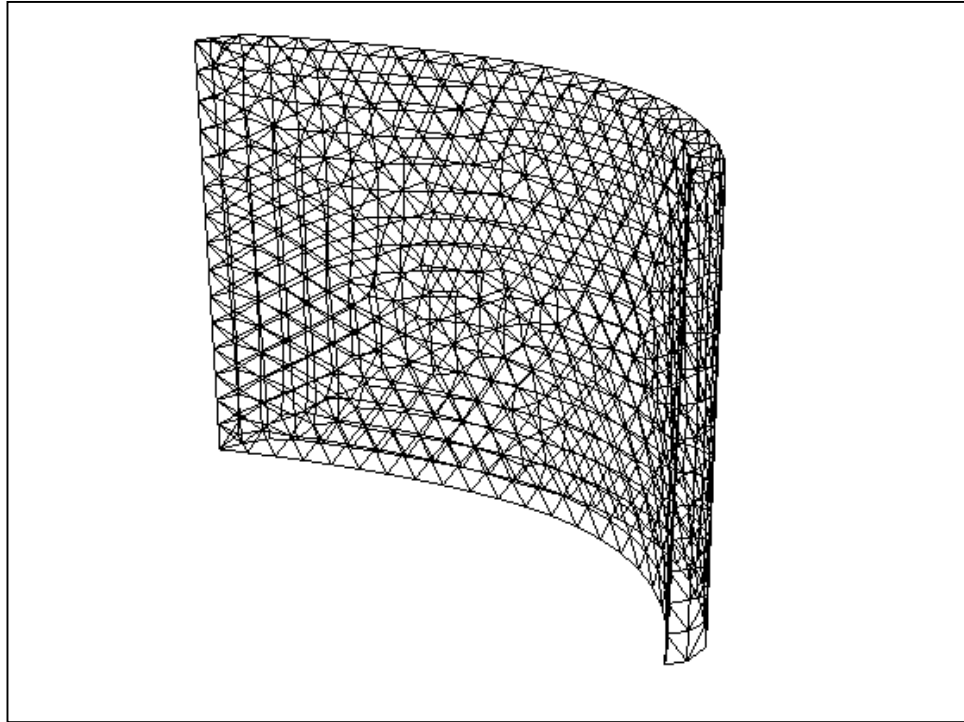


Figure 4.16 Blade Mesh for Case-C

#### **4.2.2 Transient Flow Solution Procedure**

Flow field is solved in FLUENT that uses finite volume method. Flow is taken as 3D, viscous and incompressible. There are three alternative solvers in FLUENT. Segregated-Implicit, Coupled- Implicit and Coupled-Explicit. In this study, the solver is selected as segregated – implicit which solves the conservation equations in sequence and needs less memory source. Time dependent terms are second order implicit. Second order upwind discretization is used for convective terms. FLUENT uses pressure velocity coupling in order to be sure that the computed pressure field satisfies the solution. SIMPLE, SIMPLEC and PISO are the available schemes for this coupling [64]. Among them PISO algorithm is preferred since it is the recommended scheme for the time dependent analysis.

Spalart Allmaras and URANS are preferred for the turbulence modeling. To simulate the relative motion of rotating impeller and stationary casing the sliding mesh approach is used. The result of a steady Multiple Rotating Frames of reference (MRF) simulation is employed as an initial guess for sliding mesh simulation to reduce the convergence time.

The boundary conditions are defined as total pressure at the inlet and static pressure at the outlet, which are equal to 101325 Pa. The volume immediately adjacent to the blades are defined as rotating with them at 1925 rpm, and the rest of the flow region is taken as static. Wall boundary condition is defined for the casing wall. No-slip conditions are imposed on all static and rotating surfaces.

The CFD simulation is carried out in two parts. First, a steady-state RANS calculation is performed, This is then used as an initial guess for the unsteady RANS and DES solutions. By providing a representative initial field, the computation time to reach a statistically stationary flow field solution is reduced. The time step is taken as  $8.3e-05$  s that corresponds approximately to a rotation of 1 degree.

A complete revolution of fan is performed at 72 hours of CPU time with 8 processors for the Case-A and Case-B. As for the Case-C, it is 20 hours. After 4 complete revolutions, the statistically steady-state condition is reached and then further 1 revolution is made for data sampling. The time varying forces on a single blade in the CFD model over this last rotation of the fan are used to construct the fan sources for the acoustical analysis.

### 4.3 Aero Acoustic Analysis

The time varying force on the fluid boundary generates dipole like sound. In particular, the tonal free-field sound radiation can be derived analytically from the force harmonics. Time-dependent pressure and velocity data, which is obtained from CFD solution, are used to calculate the acoustic source terms of Eqn. (3.11).

The vibroacoustic solver LMS Sysnoise is employed for the aero acoustic analysis. LMS Sysnoise is capable of solving wave equation in interior and exterior domains with Boundary Element Method (BEM) and Finite Element Method [65].

Figure 4.17 shows the aero acoustic grid on which the wave equation is discretized. Boundary Element meshes used in the aero acoustic analysis are generated in IDEAS Simulation Software. This surface grid is coarser than the CFD grid.

The limit in deciding the acoustic mesh spacing is the acoustic wavelength at the highest frequency of interest. The rule of thumb is that for linear boundary elements, the largest element length may be equal to one-sixth of the wavelength to capture the geometry influence. For second order elements, one-third of a wavelength may be used as the criterion [64]. In the analysis six elements per wavelength is used.

Since the flow is subsonic, and blade thickness and lengths are very small, only dipole sources are significant. Monopole and quadrupole sources are neglected. Only dipole sources are computed with LMS Sysnoise aero acoustic module. The pure transient flow data (local surface pressure vs. time) is transformed into the frequency domain by FFT (Fast Fourier Transform) algorithm and the corresponding dipole source strengths are calculated.

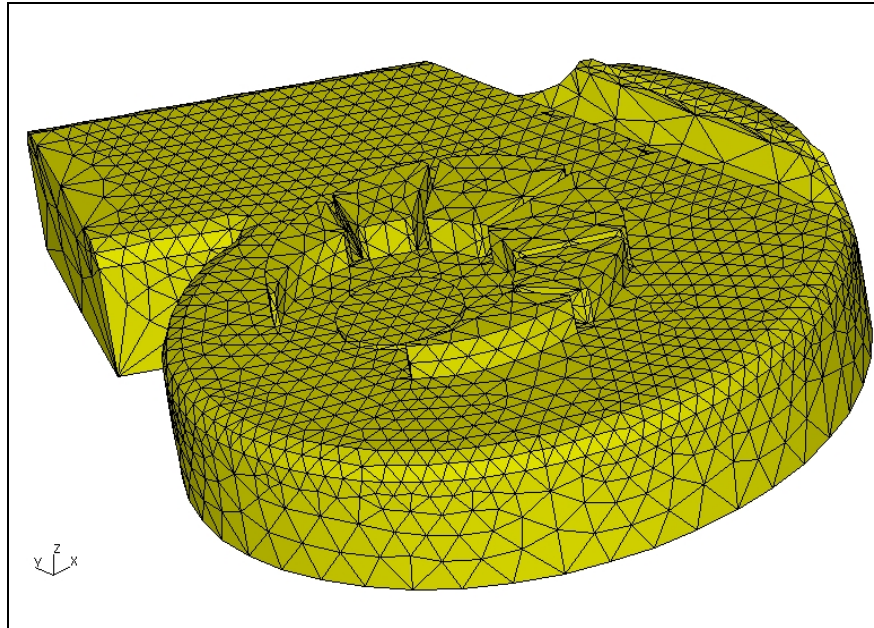


Figure 4.17 – Boundary Element grids prepared with IDEAS Simulation Software

### 4.3.1 Acoustical Modal Analysis

An acoustical modal analysis is performed in order to investigate the cavity acoustic resonance frequency of the fan casing. For this study, a multi domain BEM model is set-up and the natural frequencies of the duct cavity are excited by a discrete monopole source. The strength of the source specified arbitrarily. In this numerical experiment, the measurement sphere is selected in accordance with ISO 3744-1996 [69].

Figure 4.18 shows the fan-enclosing sphere used to obtain cavity excitation modes. In this numerical experiment, the grids on the sphere represents the sound pressure measurement points. As a sound generator, monopole sound source is placed inside the fan. This configuration is shown in Figure 4.19.



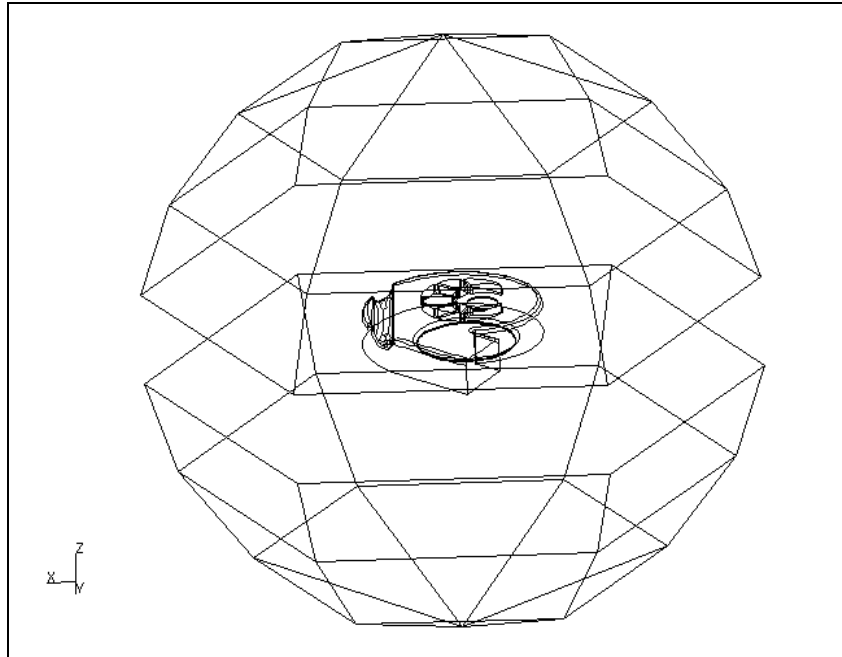


Figure 4.18 Numerical model used to obtain cavity excitation modes (ISO 3744 - 1996)

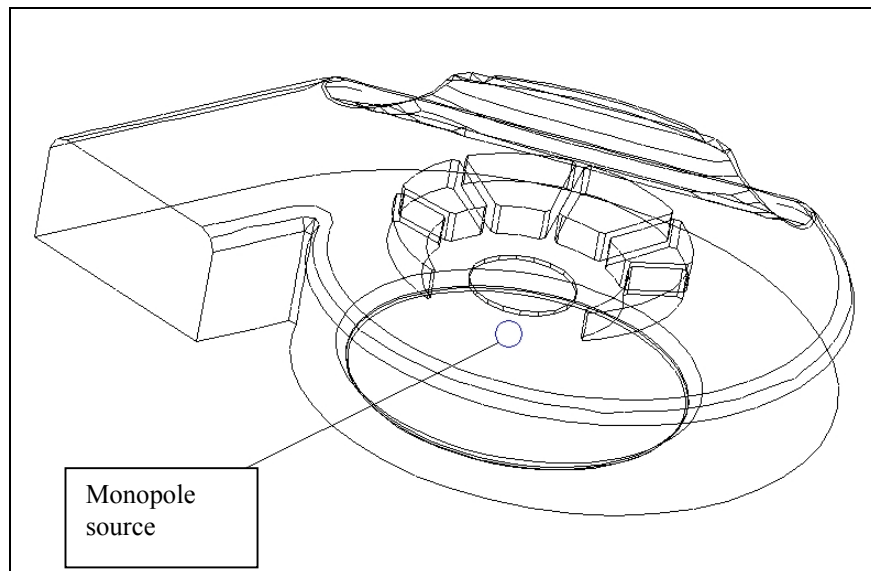


Figure 4.19 Numerical experiment set-up for cavity excitation modes investigation

### 4.3.2 Multi-Domain Boundary Element Method (MDBEM)

The Multi-Domain BEM consists of Direct BEM interior and Direct BEM exterior methods. This analysis is performed to model the interior and exterior domains simultaneously. The interior and exterior models are coupled at the inlet and exit of the fan casing through the fluid – fluid coupling.

The inlet and exit are defined taken as ambient pressure boundary conditions. The scroll surface is given as wall boundary condition. The stationary dipole sources on the scroll surface are defined as discrete sound sources on the nodes of the acoustic grid as it is shown in Figure 4.20.

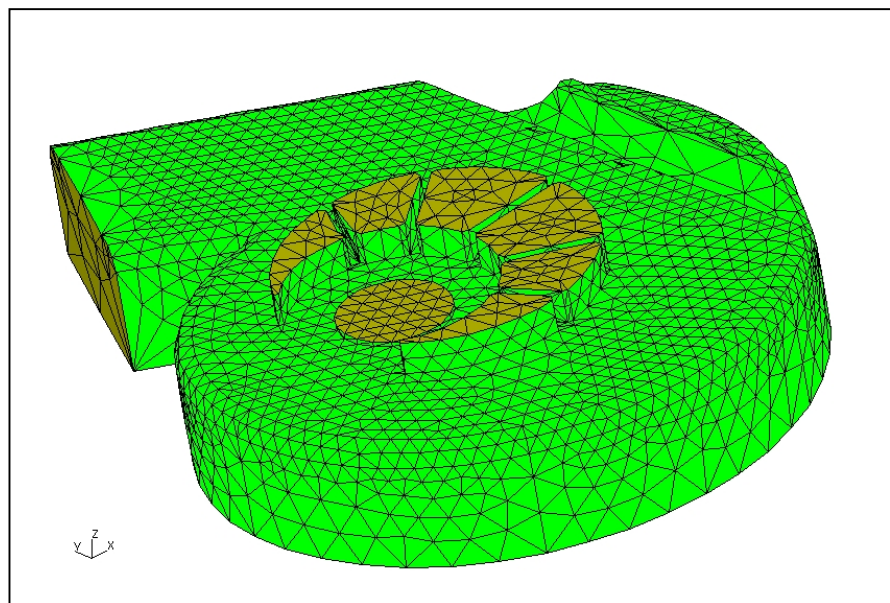


Figure 4.20 Dipole sound sources on the surfaces of the fan casing

The sound pressures at receiver locations are evaluated on the surfaces of a prism. The numerical set-up is established in accordance with the laboratory experiment set-up. The fan is located 0.8 m above from the reflected surface. The measurement walls are 0.5 m away from the fan surfaces. Each edge is divided to 10 grids for the sound pressure calculations. Figure 4.21 depicts the numerical simulation set-up used for the multi domain BEM analysis.

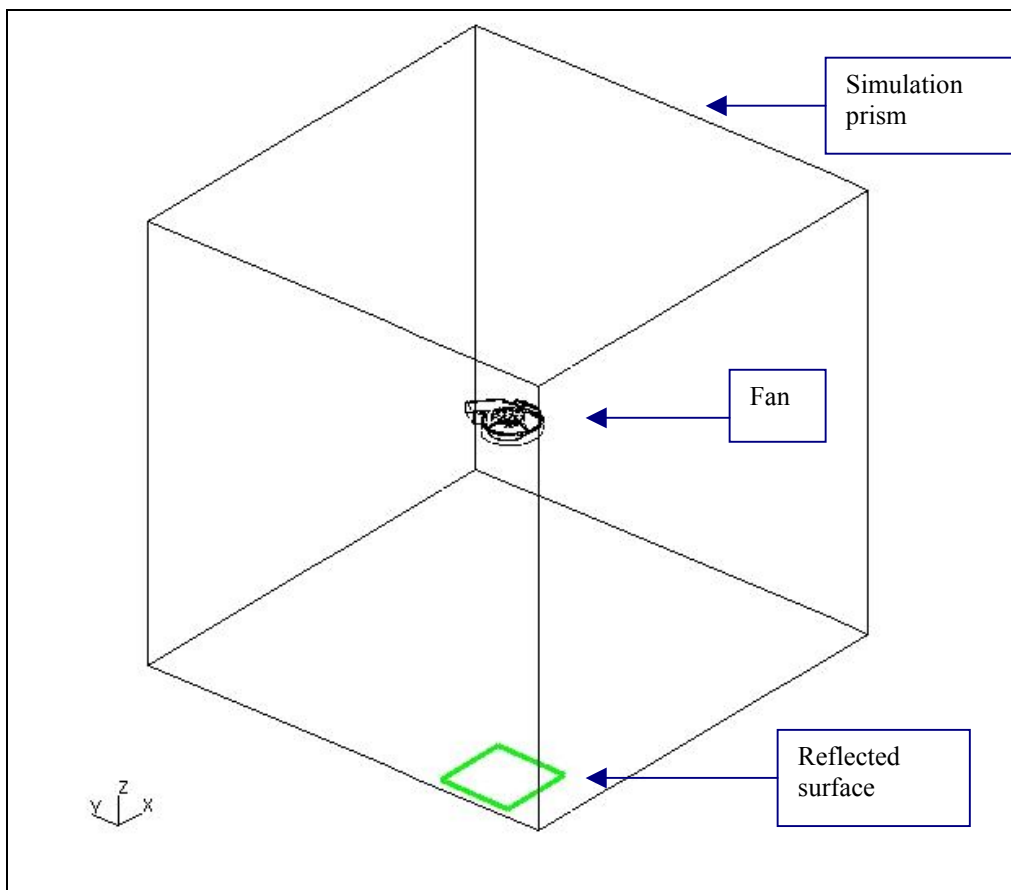


Figure 4.21 Multi Domain BEM analysis set-up

## CHAPTER 5

### EXPERIMENTAL METHODOLOGY

#### 5.1 Introduction

The experimental studies are performed in two groups. The first group of experiments is carried out for validation purposes. The numerical results are controlled with the experiments. For this purpose sound pressure and intensity measurements are performed. Cases A, B and C are analyzed.

The second group of experiments is carried out to investigate the effect of geometrical modifications on the fan noise characteristics. The possible ways of noise reduction alternatives are searched for the designed fan. A-weighted sound pressure level spectrum and sound intensity measurements are performed. Cases A, B, C, D and E are analyzed.

#### 5.2 Test Facilities

The acoustic measurements are performed in the Anechoic Room of Arçelik A.Ş. Research and Development Center and Semi-anechoic room of Arçelik A.Ş. Dishwasher Plant.

Anechoic Room of RD Center:

8.6 x 8.6 x 9.0 m

63 Hz Cut-off Frequency

Established according to ISO 3745 [69]

Dishwasher Plant Semi-Anechoic Room with reflected bottom and back wall:

3.5 x 3.5 x 3.0 m

125 Hz Cut-off Frequency

Established according to ISO 3745 [69]

### 5.3 Sound Pressure Level Measurements

The sound pressure levels at different microphone positions in the acoustic far field around the fan are measured in narrow band spectrum. Figure 5.1 shows the measurement set-up.

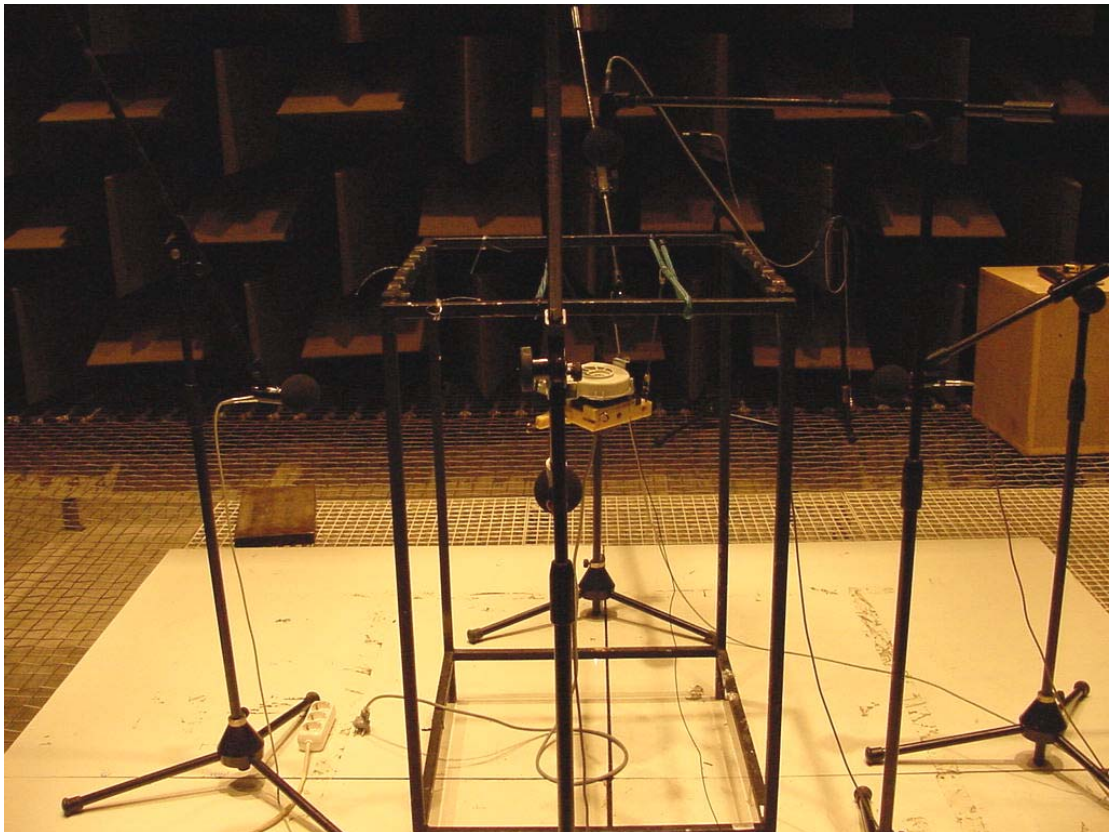


Figure 5.1 The sound pressure measurement set-up in Anechoic Room of Arçelik A.Ş.

The motor is placed in a box. The inside of the box is covered with rubber cushion for suppressing the noise coming from the motor. The box is also designed to check the fan orientation before the experiment. The fan is always adjusted to horizontal position with respect to the ground so that the experimental errors due to the fan orientations are eliminated. There are three hinges around the box. These hinges are used to hang the fan so that any contacts with the hard surfaces are eliminated and the fan becomes free from the vibrations due to the motor. Figure 5.2 shows the fan with the motor box.



Figure 5.2 Fan motor noise suppressing box

Five microphones are placed around the fan surfaces for sound pressure measurements. The center of the small circular opening at the fan inlet is accepted as the reference point. Microphone 1, 2 and 3 are used to collect the sound pressure data around the volute. These microphones are placed 0.5 m away from the reference point. Microphone 4 is placed 0.5 m away from the center of the fan outlet. Microphone 5 is put 0.5 m away from the reference point at inlet side. The fan is hanged such that the reference point is 0.8 m above the reflective ground. Figure 5.3 and Figure 5.4 show the measurement surfaces and microphone positions.

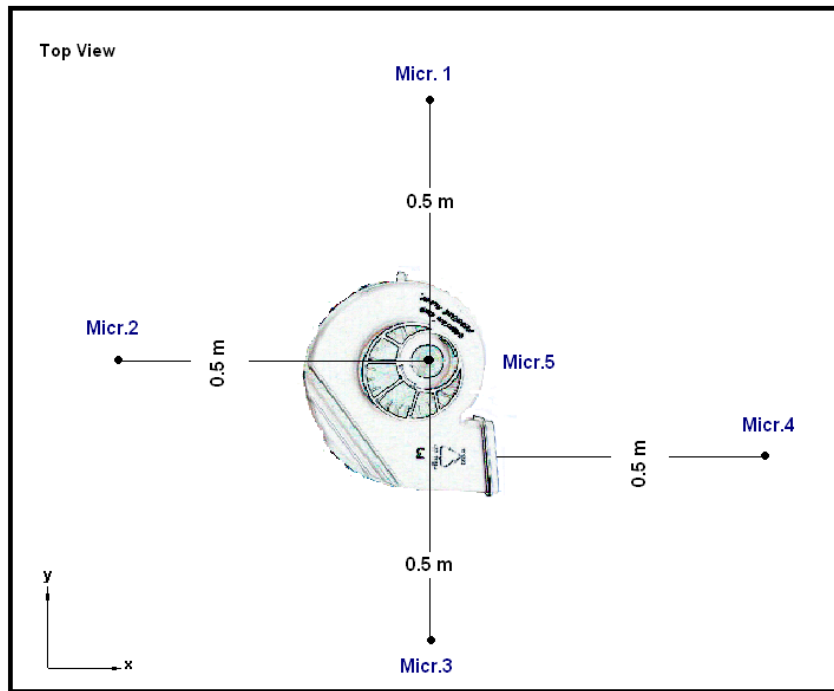


Figure 5.3 Sketch for the microphone positions – Top View

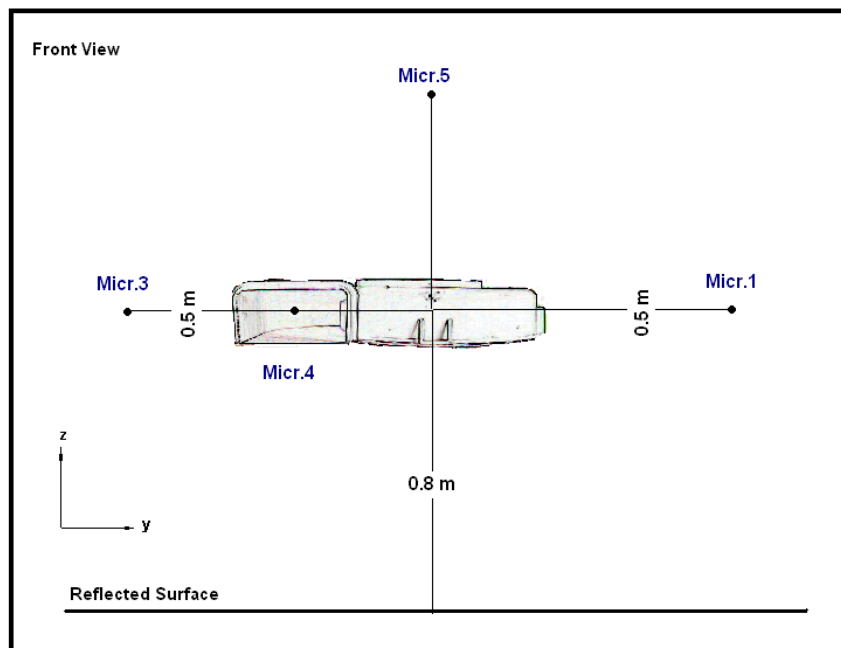


Figure 5.4 Sketch for the microphone positions – Front View

### **5.3.1 Measurement Instruments**

Measurements are performed with B&K PULSE multi-channel data acquisition system. The microphone is B&K type 4188 with diameter 1/2 inch. Data are collected in the frequency range of 100 – 5000 Hz.

### **5.3.2 Analyzer Settings**

The analyzer is prepared for the measurement as following the below steps

1. Select 1/3 octave band
2. Define the data acquisition channels
3. Set A-weighted filter
4. Adjust the average measurement duration
5. Select linear averaging. Use 16 records for spectral averaging.
6. Input reference sound pressure (20  $\mu$ Pa).
7. Select the frequency range of interest as 0 – 2500 Hz.
8. Select dynamic measurement range (Auto range)
9. Select sampling frequency as 1 Hz.
10. Select window type as hanning window.
11. Press Start button

### **5.3.3 Measurement Methodology**

Before starting the measurement set-up is prepared as follows:

- 1) Place the platform with motor carrying box in acoustic room
- 2) Check for the position and the balance
- 3) Place the fan on the platform
- 4) Check for the position and balance
- 5) Place the microphones according to the specified coordinates
- 6) Plug in the microphones to PULSE Analyzer
- 7) Plug in the current sensor to PULSE Analyzer
- 8) Make an acoustical calibration



- 9) Run the fan for 20 min to eliminate the heating effects (to reach steady state conditions)
- 10) Shut down the doors of the room
- 11) Start measurements
- 12) Plot
  - Sound Power Level Spectrum at 1/3 Octave frequency (dBA-Hz)
  - Total Sound Pressure Level (dBA)

## **5.4 Sound Intensity Measurements**

The sound intensity is mainly used for location and rating of noise sources. The sound intensity vector describes the amount and direction of flow of acoustic energy at a given point [66].

### **5.4.1 Instruments**

Measurements are performed in the anechoic room of Arçelik RD Center. The following set of equipment are utilized for the measurements:

Analyzer : B&K 2144  
Program : B&K NSL  
Microphone : B&K 4181  
Calibrator : B&K 4228

Figure 5.5 shows the set-up and measurement platform. The single microphone is moved around the fan. The microphone positions are adjusted with the five-axis robot arm.



Figure 5.5 Sound Intensity Measurement Platform

#### 5.4.2 Measurement Grid and Alternative Fans

Sound reduction alternatives are searched with the intensity measurements. The measurement prism having 700 mm x 700 mm x 700 mm dimensions is used for the intensity maps. There is 70 mm spacing between each data point. 5 surfaces, except the bottom surface, are scanned with the intensity probe. Totally 500 data records are taken for an intensity map of each cases.

Five different cases are examined by mapping:

**Original design (Case A):** The original fan modal is examined for the verification of the numerical analysis results. Case A is the fan configuration where the impeller has splitters and the volute has channel.

**Channel eliminated (Case B):** The impeller has splitters but the semi –cylindrical channel on the fan casing is removed. The effect of this channel on the fan noise is investigated and the results are compared with the original design.

**Splitters eliminated (Case C):** The short blades are removed from the impeller but the channel on the volute exists. The contribution of unevenly distributed splitters to the BPF and its harmonics are investigated.

**Inlet modified (Case D):** The ribs at the inlet are cut. The effect of the inlet design on the fan noise is investigated. Splitters are not removed.

**Bitumen coated (Case E):** The fan volute is coated with the viscoelastic material. The effect of this isolation on the fan noise level is searched. Splitters are not removed.

Figure 5.6 – 5.11 show these alternatives.

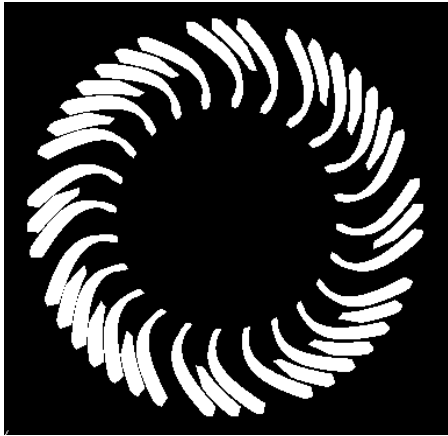


Figure 5.6 Original Impeller

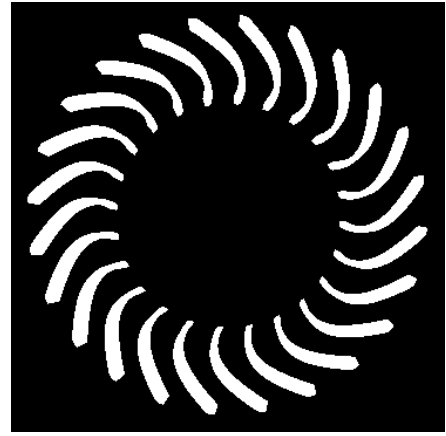


Figure 5.7 Splitters eliminated



Figure 5.8 Volute with channel



Figure 5.9 Channel Eliminated



Figure 5.10 Inlet Modified



Figure 5.11 Bitumen Coated

The fan operating point for each case is checked before the sound intensity measurements. Measurement is performed with DANTEC Hotwire anemometer (type 54N60). Figure 5.12 shows the location of data points that are adjusted as 8 mm apart from each other.

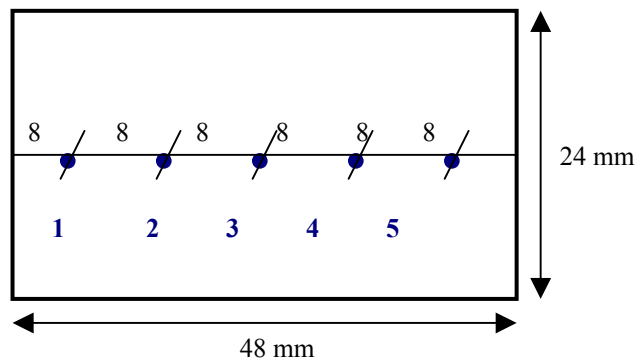


Figure 5.12 Velocity measurement points at fan exit

Figure 5.13 shows the velocity distribution at the exit of the fans. As it can be seen from Figure 5.13, all alternatives are run nearly at the same operating point. Only the splitters eliminated case has slightly higher velocity in all measurement points.

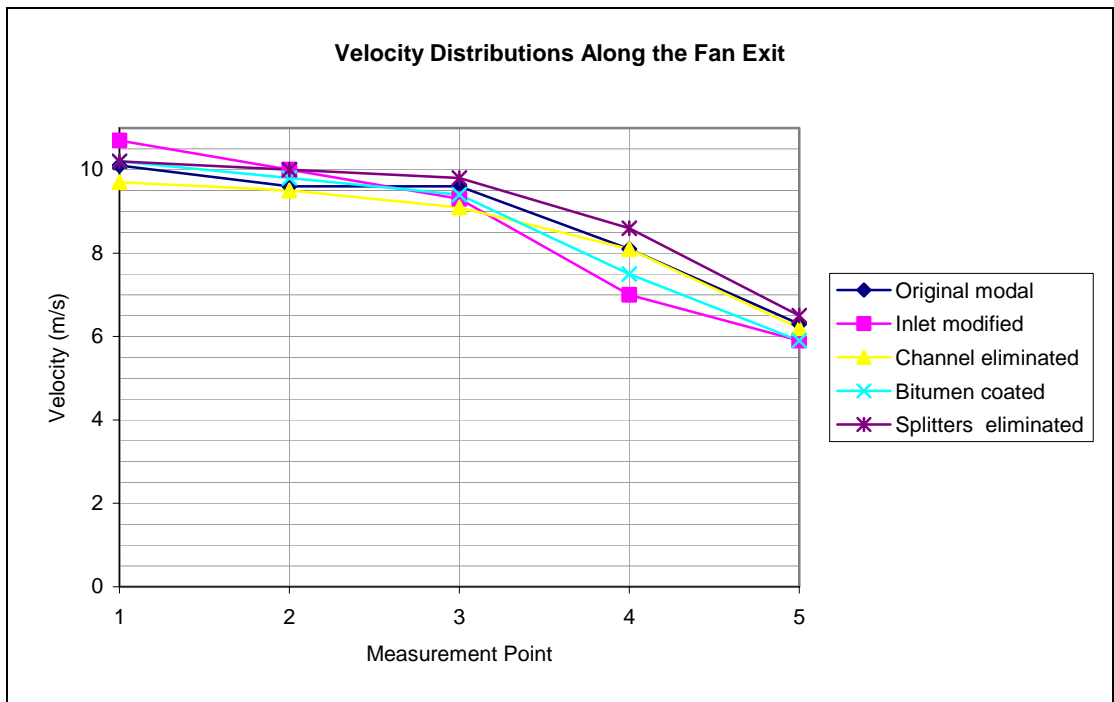


Figure 5.13 Velocity Distributions along the fan exit in Cases A, B, C, D, E

## CHAPTER 6

### RESULTS OF THEORETICAL AND EXPERIMENTAL STUDIES

#### 6.1 The Results of Flow Field Solution

The numerical simulation is carried out until a statistically steady condition is reached. This is controlled by the differences between the values of successive computations of x, y, z velocities, continuity equation, mass flow rate at the fan exit and the lift force acting on a blade.

In the first phase, the effect of volute channel on the flow field is investigated. For this reason, the design alternatives Case-A and Case-B (as mentioned in Chapter 4, page 41) are compared. Case-A is the fan having splitters on the impeller and channel on the volute. The volute of Case-B has no channel. The pressure and velocity contours are shown at the mid-height of the blades, which corresponds to 30% of the total height as it is shown in Figure 6.1.

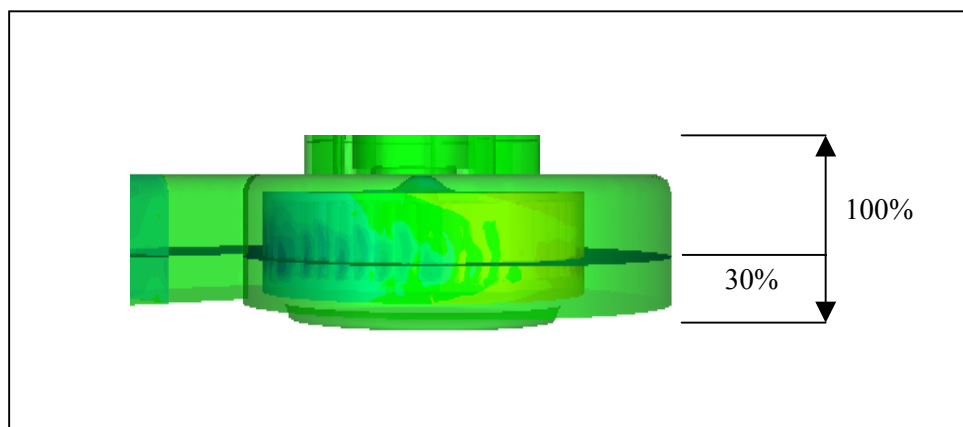


Figure 6.1 The section of the fan for which the pressure and velocity contours are presented

### 6.1.1 Velocity Contours of Case-A and Case-B

Figure 6.2 (a) and (b) give comparison of the velocity contours of the fan with channel (Case-A) and without channel (Case-B) on the volute respectively. In the first case the flow pattern is not smooth and the velocities are lower in the channel section. However, the velocity contours at the fan exit section are similar.

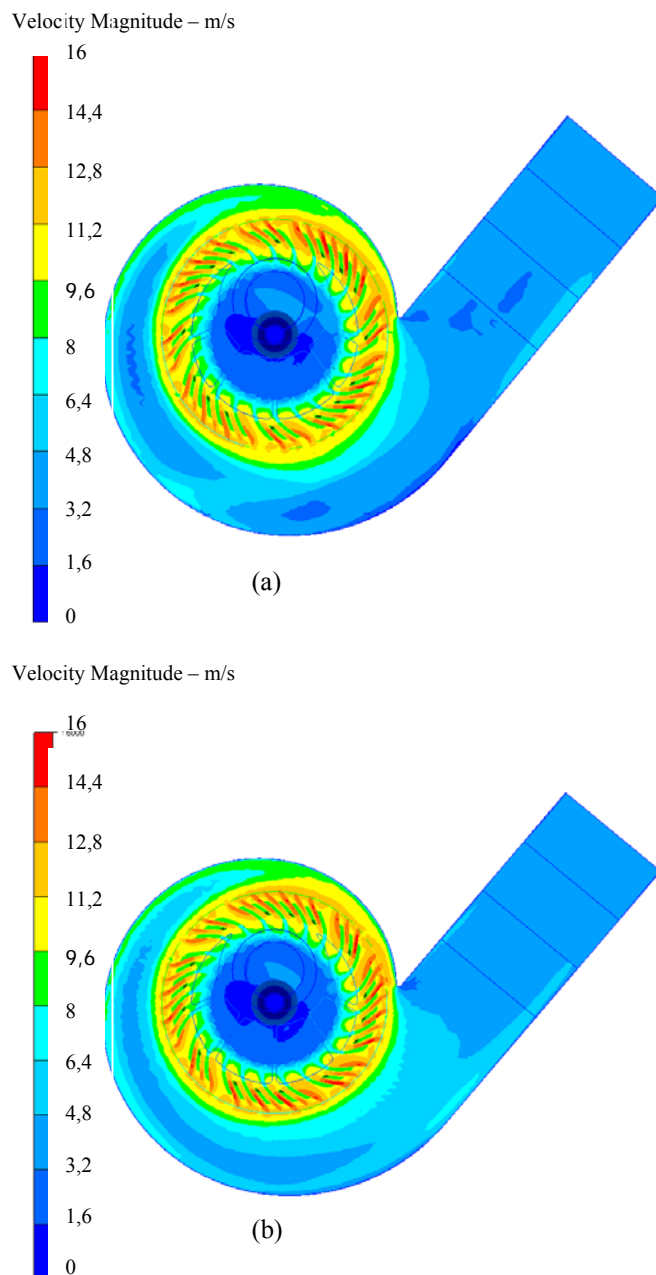


Figure 6.2 Velocity contours of the fan (a) with channel, (b) without channel (section corresponds to %30 of the height)



The effect of the channel is more clear at the surface of the casing. Figure 6.3 (a) and (b) present the velocity contours at the surface. Figure 6.4 gives the graphical representation of the velocity magnitudes along (0-X) section for both cases. It is obvious that the channel disturbs the flow. It causes higher velocities between the channel and the impeller since the flow region becomes narrower. In addition, it creates some dead regions between channel and casing wall, and just after the channel. The mass flow rate of the casing with channel and without channel are 5,34 l/s and 5,39 l/s respectively. That means channel decreases the flowrate by 1%.

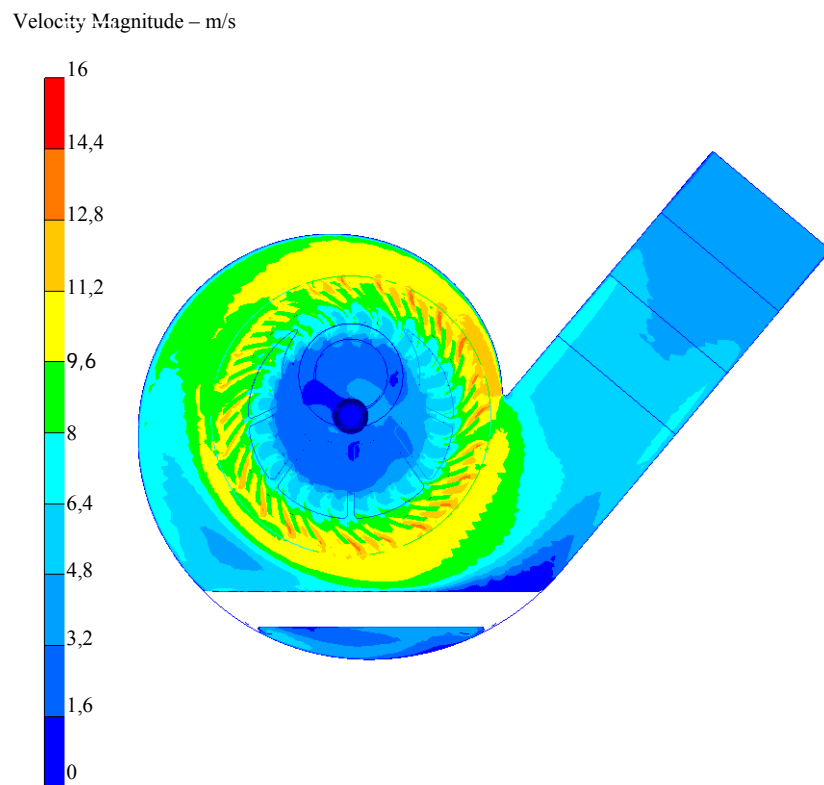


Figure 6.3 (a) Velocity contours of the fan with channel (at the casing surface)

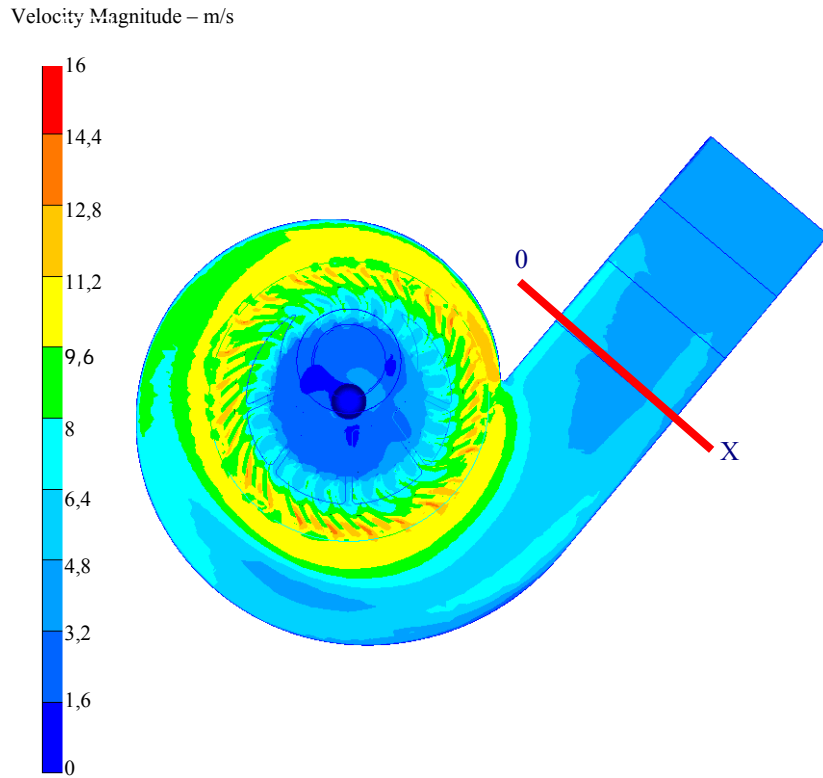


Figure 6.3 (b) Velocity contours of the fan without channel (at the casing surface)

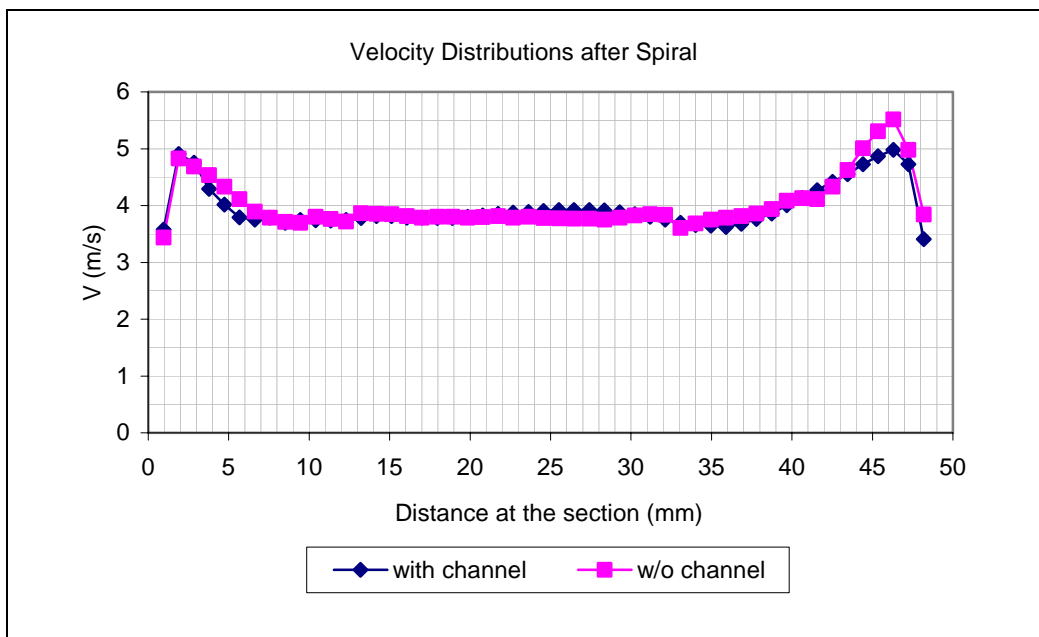


Figure 6.4 Velocity distributions along (0-X) section after the spiral

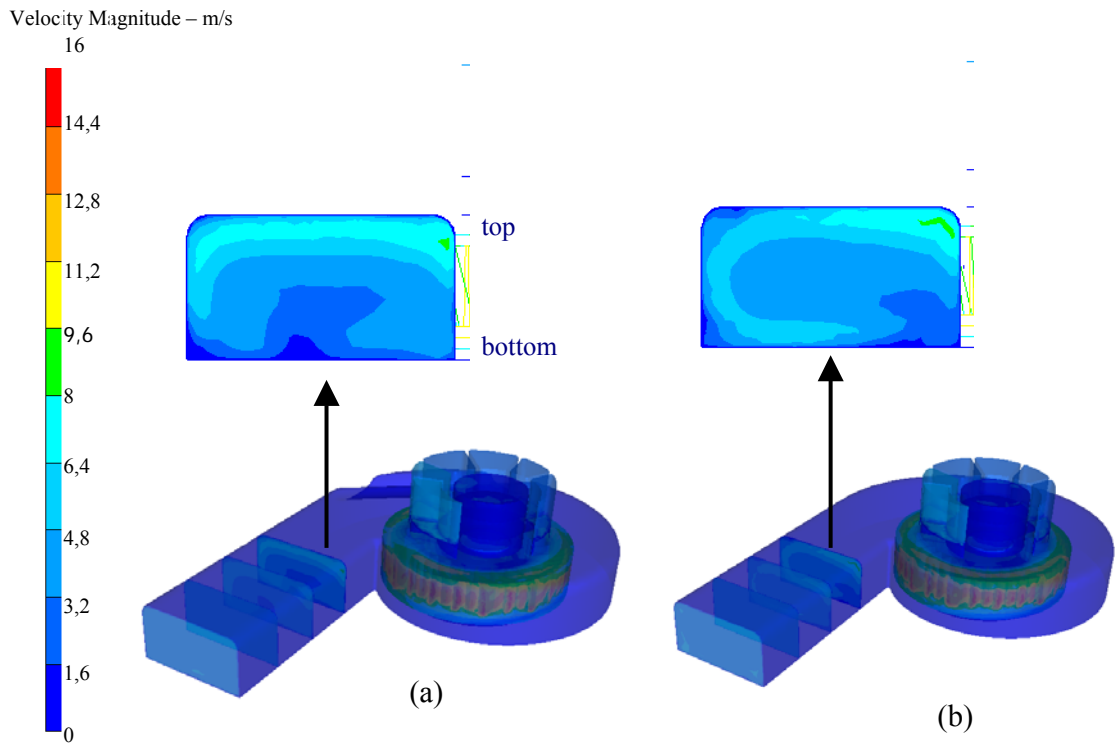


Figure 6.5 Velocity distributions at the fan exit (a) with channel, (b) without channel

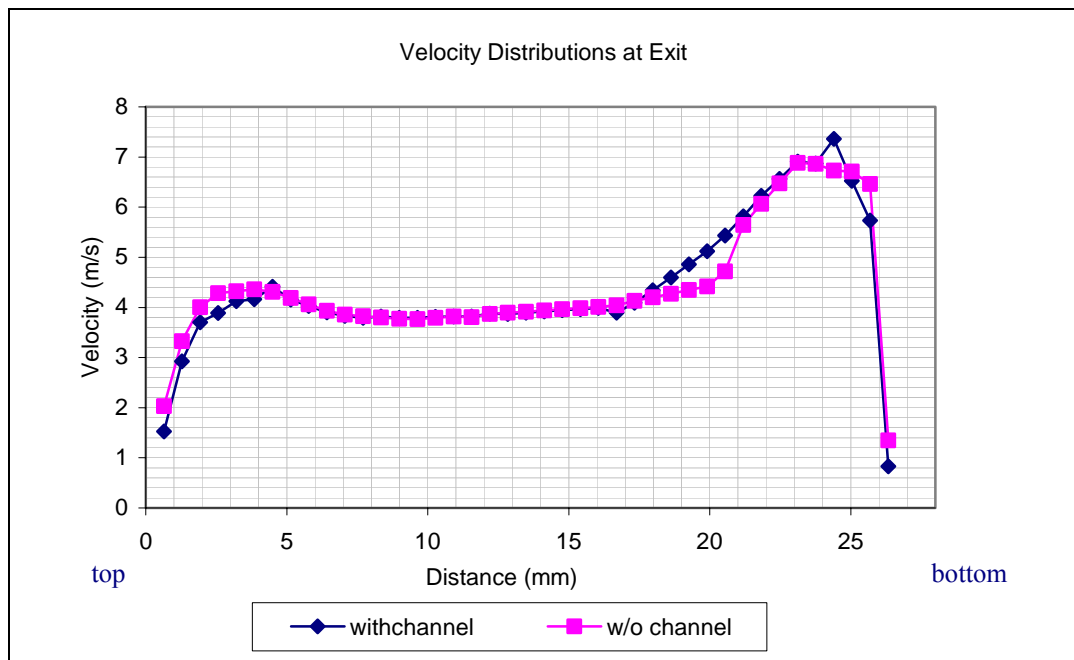


Figure 6.6 Velocity distributions at the fan exit

Figure 6.5 and Figure 6.6 show the velocity distribution from bottom to the top of the exit section. The local velocity magnitudes are higher with the existence of the channel. This may be resulted from relatively narrow cross section due to the channel.

### **6.1.2 Pressure Contours of Case-A and Case-B**

The pressure contours at the mid section of the fan for these with and without channel conditions are given in Figure 6.7 (a) and (b) respectively. There is a low-pressure region in the first case due the effect of the channel.

The comparison of the pressure distributions on the section connecting tongue to the end of the channel is given in Figure 6.8, which presents that the channel has no effect on the pressure from this section onwards.

There is a sudden change in pressure at the tongue region, which is represented in Figure 6.9. Because of tongue blockage, some of the fluid is recirculated in the volute through the inlet of the fan. The velocity vectors explaining this condition shown in Figure 6.10.

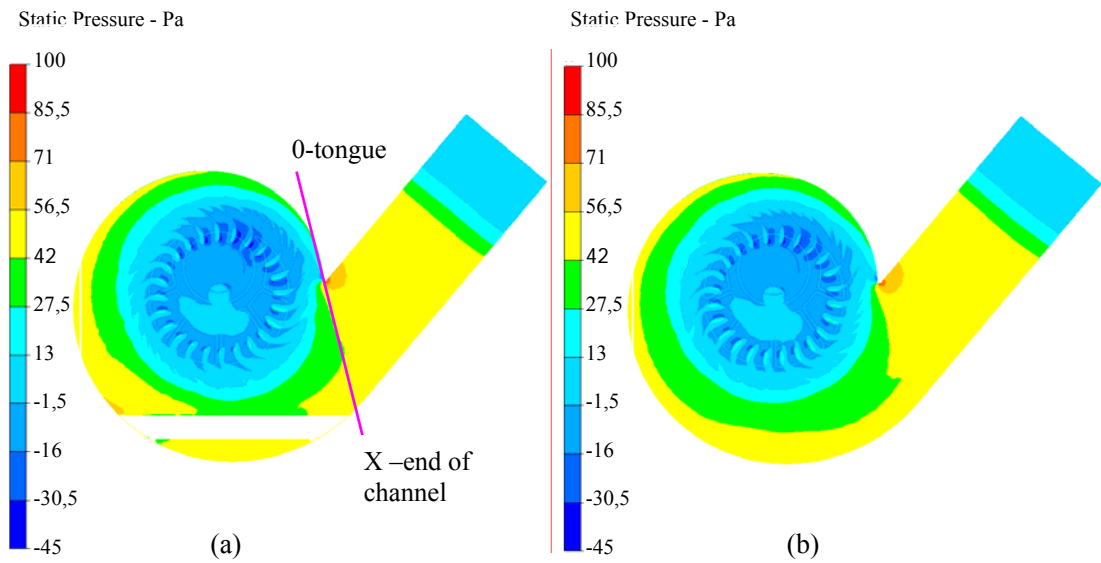


Figure 6.7 The pressure contours of (a) casing with channel, (b) casing without channel (at the mid height of the fan)

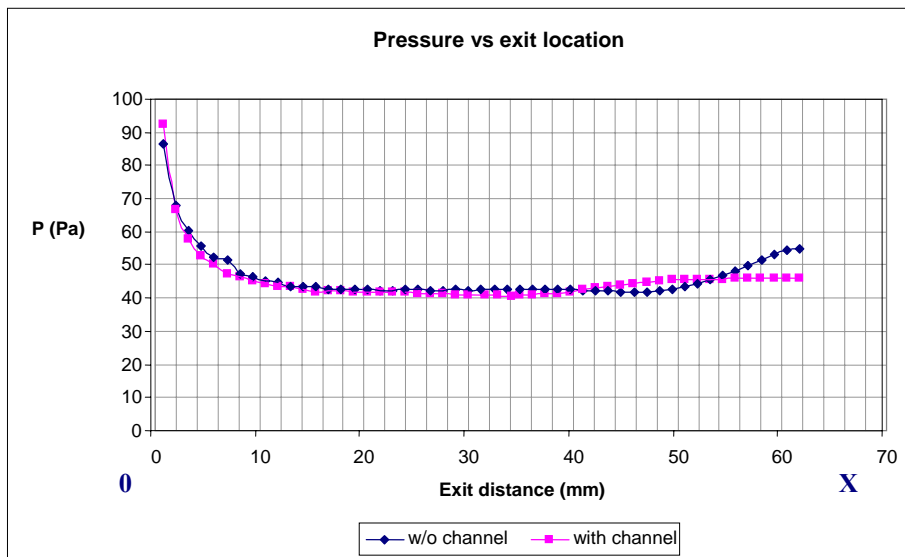


Figure 6.8 Pressure distributions along (0-X) section (between tongue and the end point of channel)

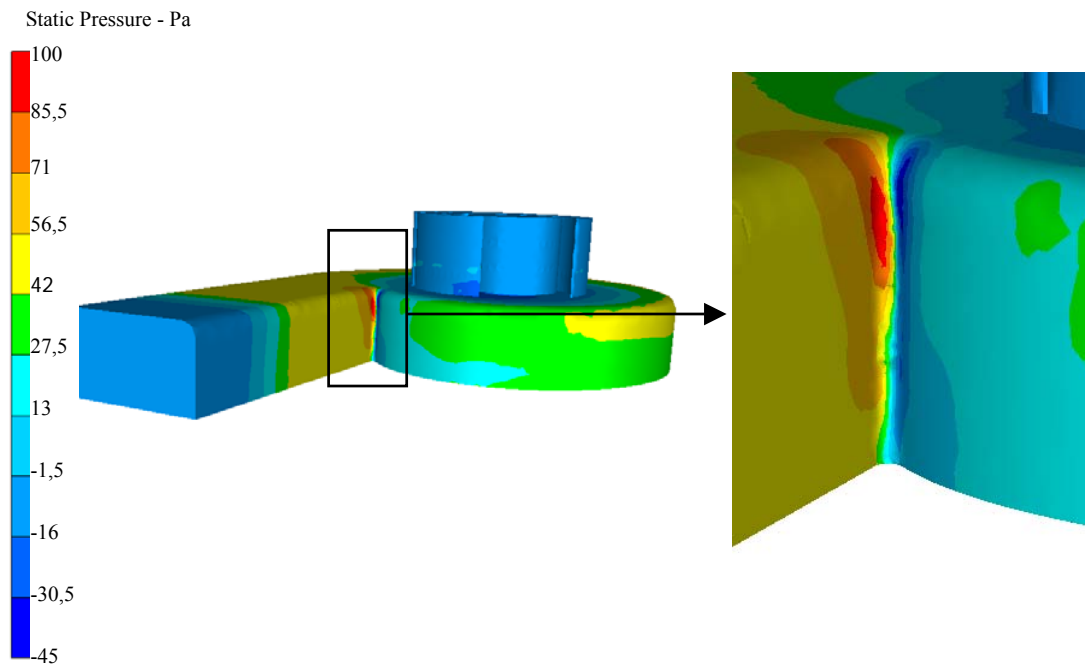


Figure 6.9 Pressure change at the tongue region

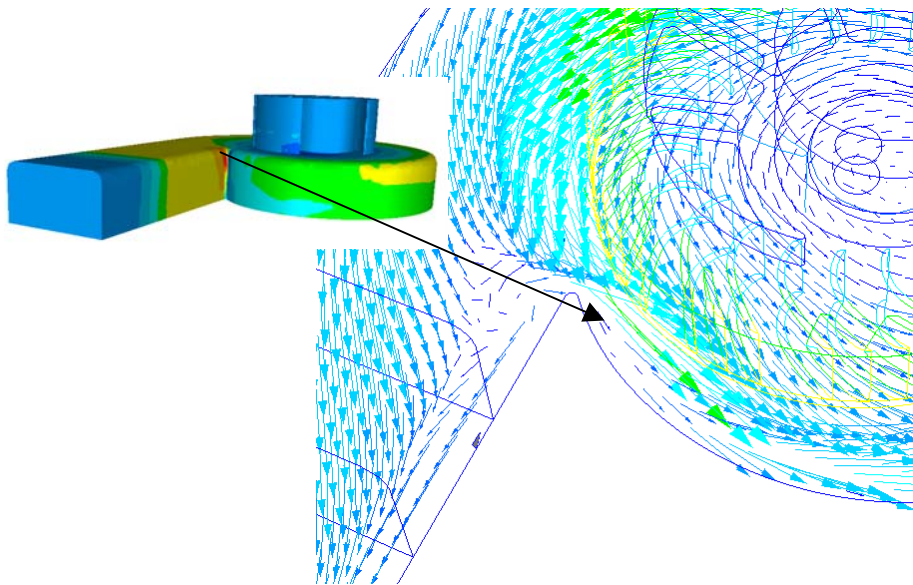


Figure 6.10 Velocity vectors showing the recirculation zone

### 6.1.3 Velocity and Pressure Contours for Case-C

The Case-C has an impeller without a splitter and the casing with a channel. This alternative is analyzed to investigate the effects of splitters on sound pressure level of the fan. Figure 6.11 and 6.12 depict the velocity and vorticity contours, respectively. Figure 6.13 shows the pressure contour of this case.

The velocity contours, Figure 6.11, shows that the velocities are decreasing towards the outlet and the pressure is increasing. There are vortices near the blades at the rotational region. These vortices can be better observed in Figure 6.12. There are separated vortices at the blade tips. The vorticity level is almost zero near the outlet region of the spiral, as it is seen from Figure 6.12, since the rotational effects are diminished.

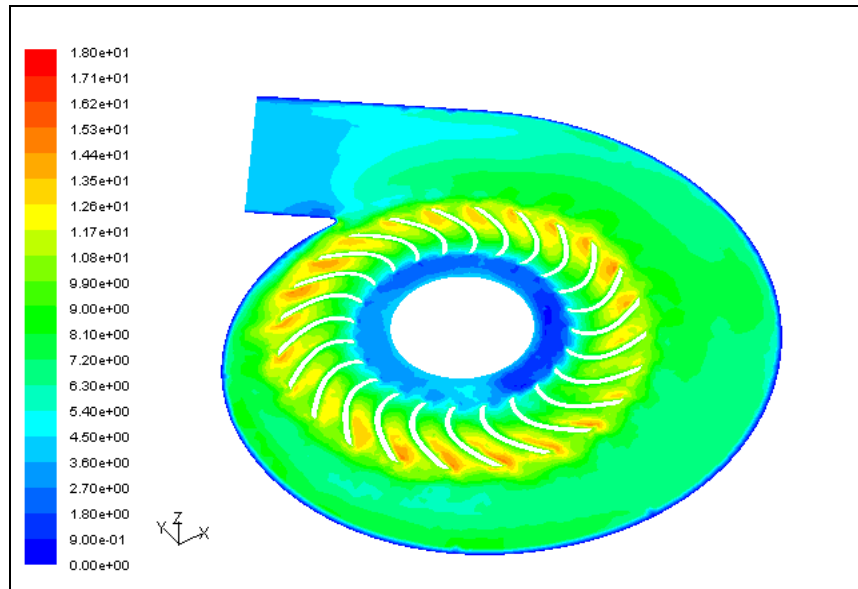


Figure 6.11 Velocity contours of the Case-C (at mid-height of the blades)

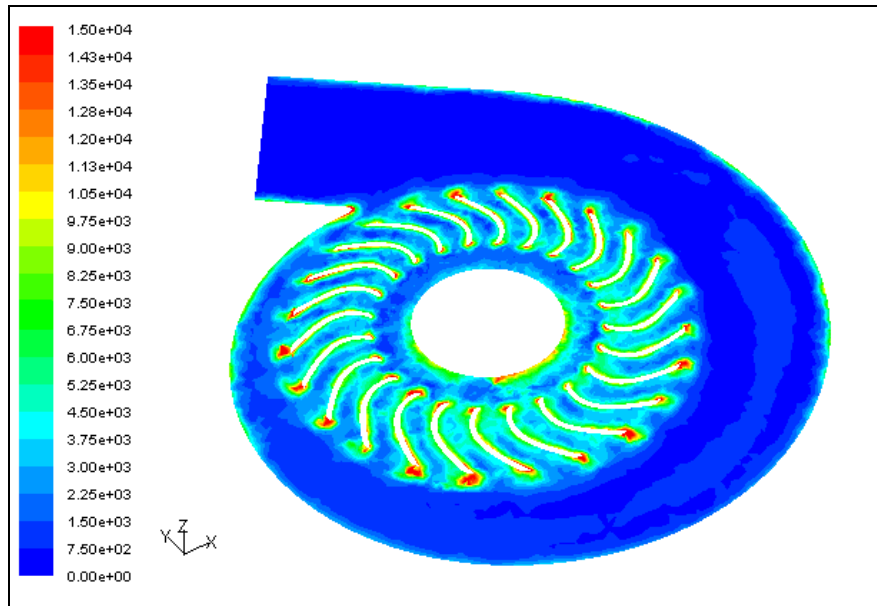


Figure 6.12 Vorticity levels of the flow region for the Case-C

Figure 6.13 demonstrates the pressure contours. Since the contours are disturbed little on the channel section of the volute, it is concluded that the channel has not significant effect on the flow.

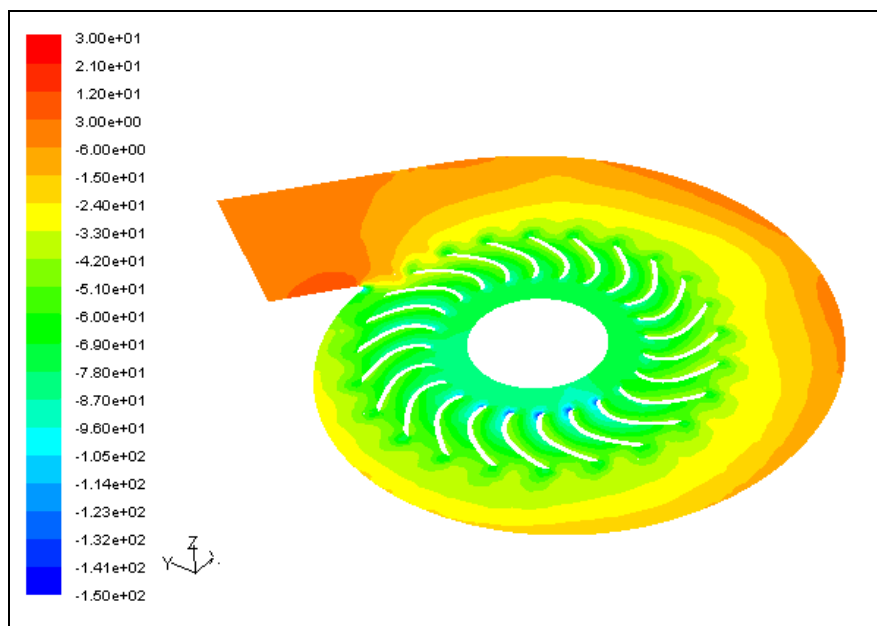


Figure 6.13 Pressure Contours for the Case-C



## 6.2 The Results of Acoustical Analysis

It is desired to investigate whether the coupling of flow solver and vibroacoustic solver could provide a useful technique so that the sound performance requirements of a fan can be included in the theoretical design stage at the beginning. For this purpose, Case-A and Case-C are selected as the example cases. The blades are unevenly distributed in the former, and evenly distributed in the latter.

The vibroacoustic solver has limitations about its memory size. The architecture of the software is suitable for making analysis with evenly distributed blade structures. Since in this case, only a single blade is introduced as a noise source and calculation matrices become smaller. The symmetrical geometry need of the solver creates problems during the acoustic modeling of the original fan design (Case-A) due to its uneven blade distribution. Making analysis with the quarter of the impeller may be an alternative solution because there is a  $90^{\circ}$  period that the blade distribution repeats itself as it is shown in Figure 6.14. But in this case, the total number of blades to be input is 4 and that causes incorrect calculation of BPF and its harmonics. However, this approach can give an idea about the location of highest sound pressures on the fan surface. This information is still valuable since the geometry can be improved to decrease sound pressures at these locations in design stage before making prototypes and tests. Therefore Case-A is used in the acoustic analysis to get this information.

Case-C is suitable for searching the capabilities of the vibroacoustic solver due to its symmetrical blade distribution. The cavity excitation modes and tonal noise characteristics are investigated. Sound pressure distribution is examined over the stationary surfaces where the dipoles are defined as acoustic sources.

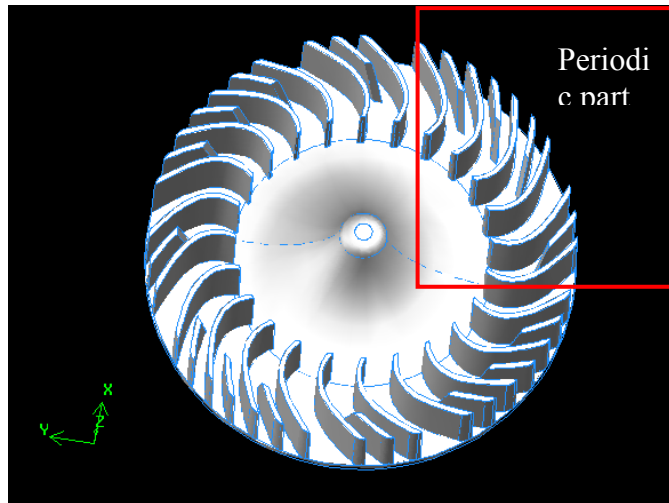


Figure 6.14 The blade distributions of Case-A

### 6.2.1 Cavity Excitation Modes

The cavity of the fan casing generates noise at some frequency values. These resonance frequencies of the cavity are called as excitation modes of the cavity. In order to determine the natural frequencies of the casing, a multi domain BEM model is set-up in the numerical model as described in Chapter 4. The strength of the monopole source is specified arbitrarily since the aim is to capture the excitation modes.

The sound pressures on the surfaces of the sphere, defined in numerical model, at 885 Hz, 900 Hz, 910 Hz and 915 Hz are shown in Figure 6.15, 6.16, 6.17 and 6.18 respectively. The level of sound pressures are increasing from 885 Hz to 910 Hz and then decreasing from 910 Hz to 915 Hz. That means there is a turning point between these frequencies, which represents the cavity mode of the structure. When this result is compared with the noise spectrum of the fan, it is seen that there is a peak pressure level at 912 Hz, which is shown in Figure 6.19. It is concluded that this peak comes from the cavity natural frequency of the casing. This result shows that there is a good agreement between the experimental data and numerical simulation. Also, the

numerical simulation gives evidence about the reasons of the peaks on the fan spectrum.

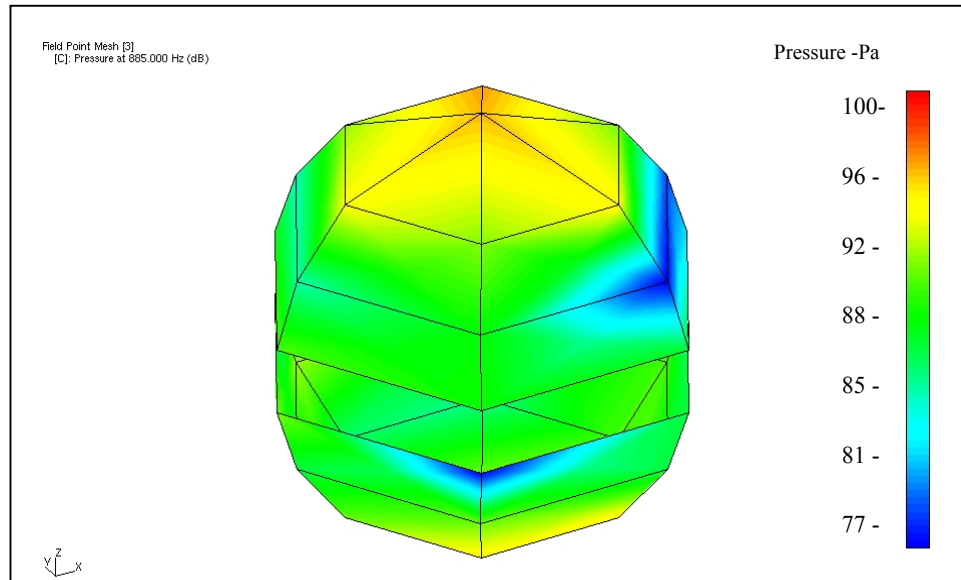


Figure 6.15 Sound Pressures at 885 Hz when the casing cavity is excited with monopole source

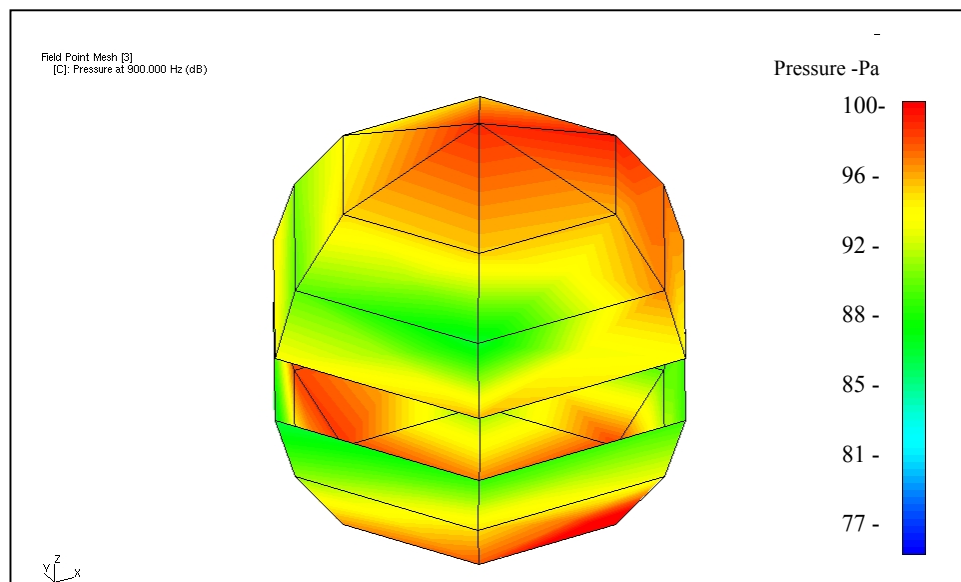


Figure 6.16 Sound Pressures at 900 Hz when the casing cavity is excited with monopole source

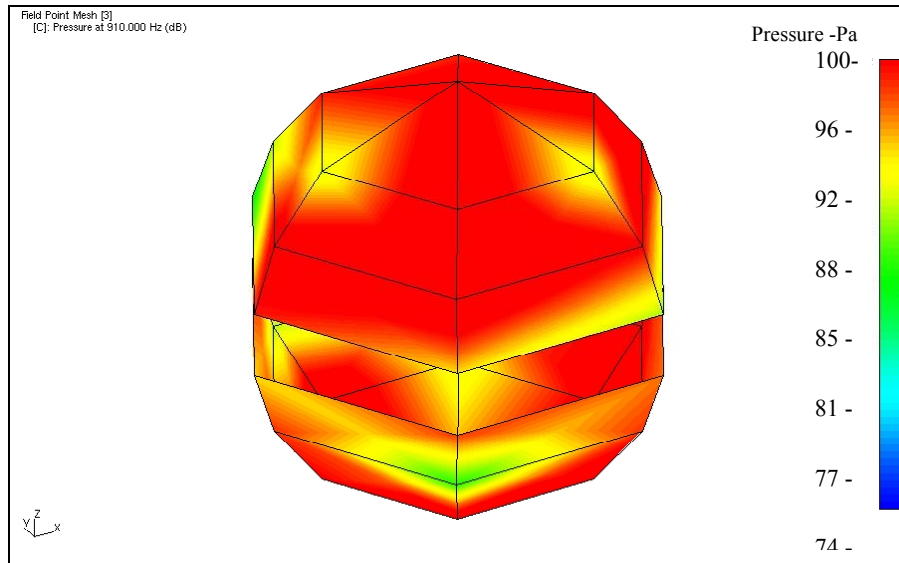


Figure 6.17 Sound Pressures at 910 Hz when the casing cavity is excited with monopole source

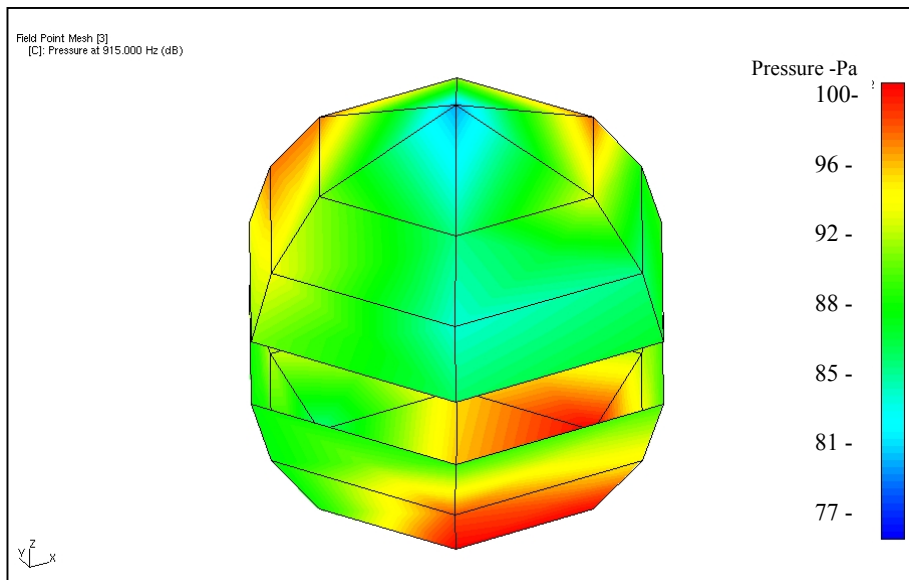


Figure 6.18 Sound Pressures at 915 Hz when the casing cavity is excited with monopole source

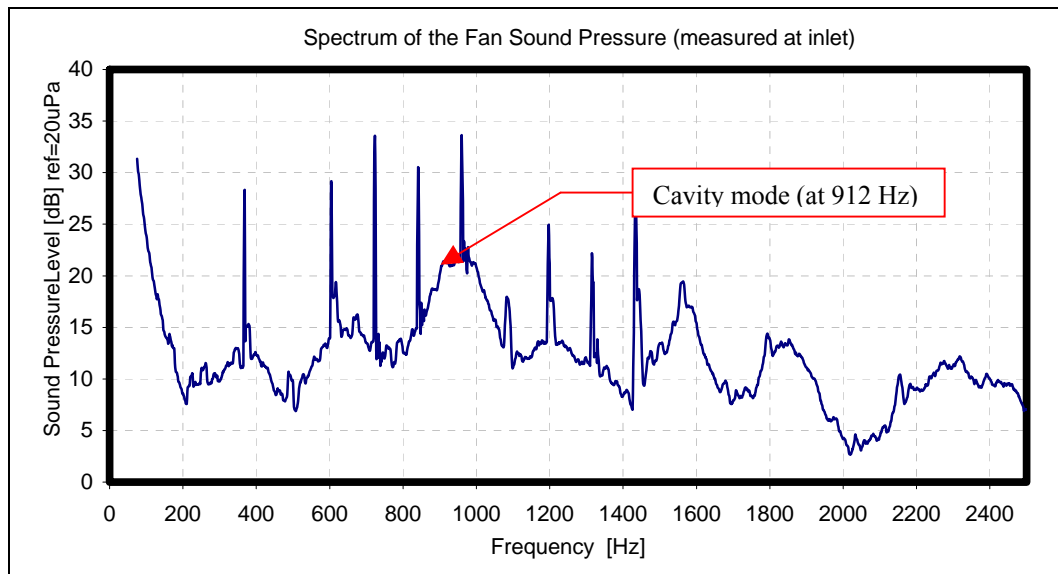


Figure 6.19 Spectrum of the fan sound pressures for Case-A (measured at fan inlet)

## 6.2.2 The Source Strength Distributions of Case-A

The numerical color maps of the sound pressure level distributions are presented in Figures 6.20 and 6.21. These figures designate the directivity of the sound.

Figure 6.20 denotes the sound pressure levels on the casing. Due to the uneven blade distributions, BPF of the model Case-A is not calculated correctly for the first harmonic. The periodic part of the impeller includes 6 long blades, 4 splitters and 1 space. That group is introduced as the noise source and since there are 4 of these, the number of blades is given as 4 in the vibroacoustic solver. As it is mentioned in Chapter 4 (page 43), the BPF of the Case-A is expected to be between 770 Hz and 1283 Hz. The frequency value in this range that can be simulated by the vibroacoustic solver is 1073 Hz. Therefore; the surface sound pressures are examined at this frequency level for the Case-A.

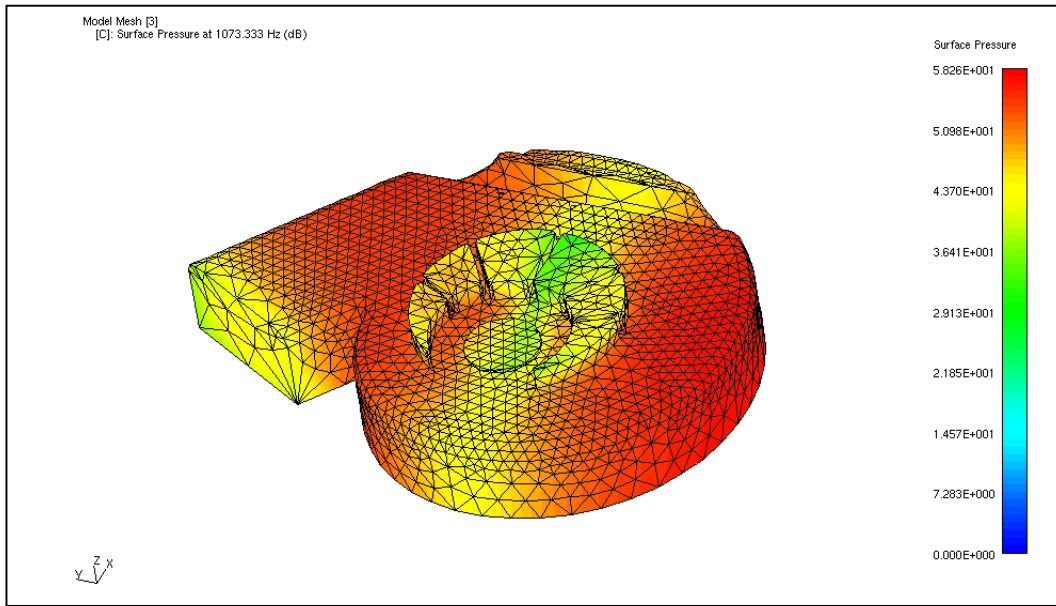


Figure 6.20 Case-A: The pressure distributions of sound at 1073 Hz

Figure 6.21 presents the sound pressures 0.5 m away from the surfaces. (The numerical set-up is described in Figure 4.16). The fan is in the center of the prism both horizontally and vertically. The orientation of the fan is such that the top surface of the prism represents the sound propagated from the fan inlet. The intersection of the right and left sides of the prism corresponds to the mid line of the fan exit.

Figure 6.21 imply that both the fan inlet and the fan exit have equal importance about the propagation of the sound. The radiated sound has nearly the same levels at the microphone positions of these two surfaces. This result is supported by the experimental measurements. As it is shown in Figure 6.22, the fan inlet and the exit have similar sound pressure contours. Both numerical and experimental results are agreed that the propagated sound decreases through the right side. However, the levels of numerical and experimental results are not the same. The regular blade distribution requirement of the vibro-acoustic solver is the reason of this difference. Since the periodic part of the blades are introduced as consolidated blade for this case, BPF and its harmonics cannot be calculated correctly.

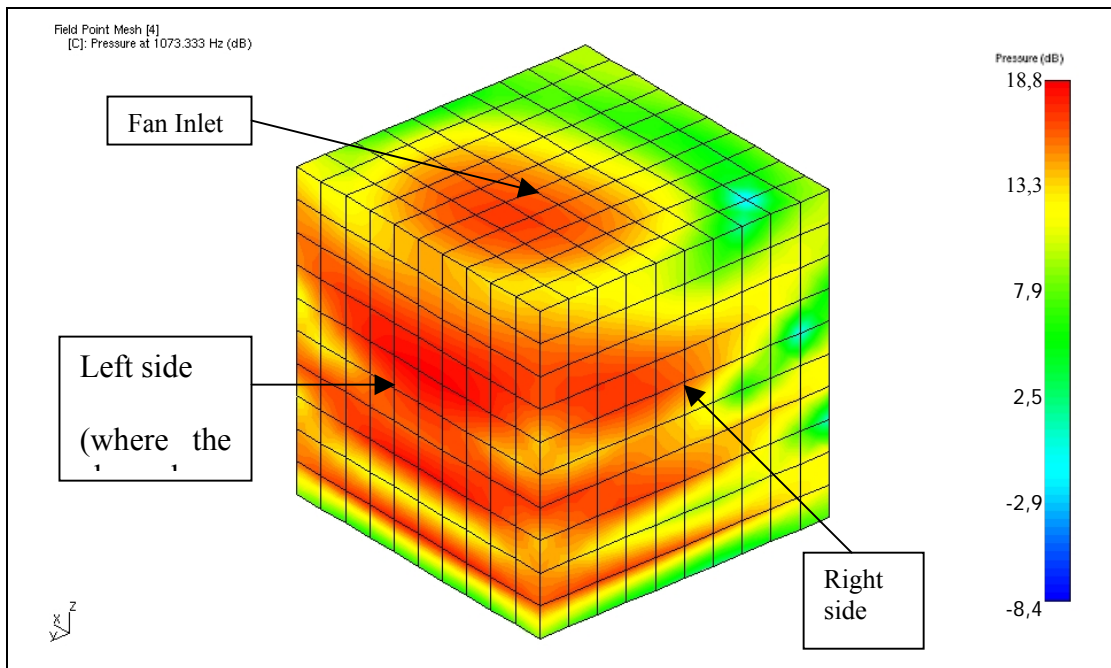


Figure 6.21 Numerical sound directivity map for Case-A at 1073 Hz

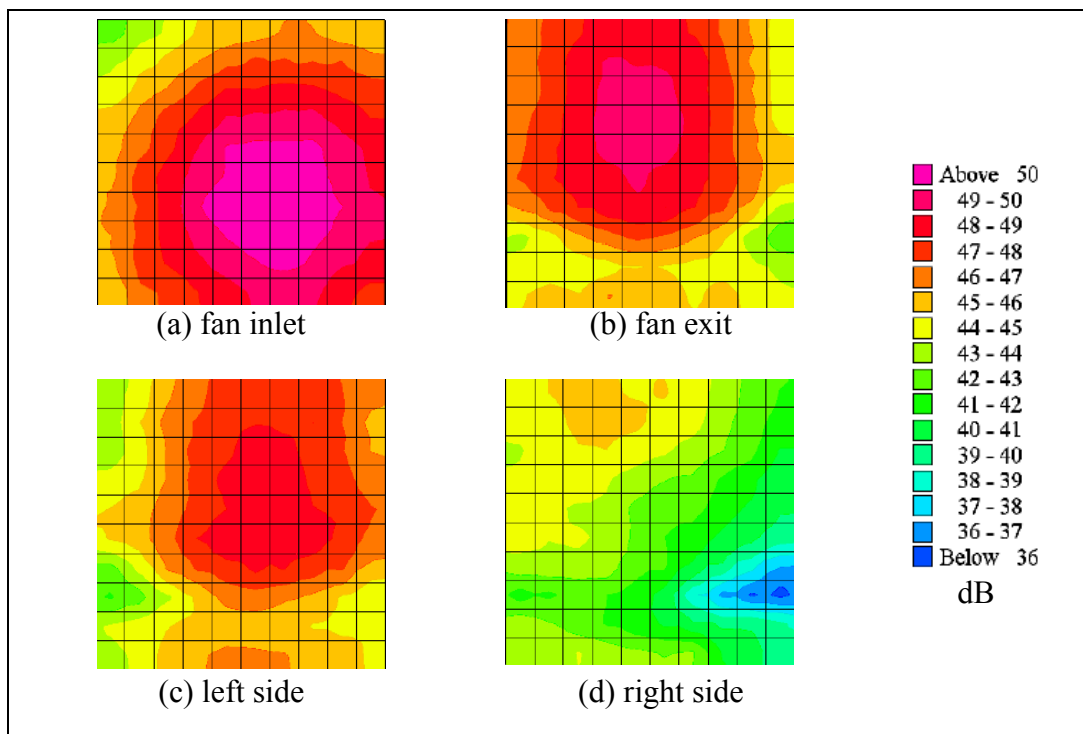


Figure 6.22 Experimental sound intensity levels (dB) at the surfaces 0.5m away from the fan surfaces.

### 6.2.3 The Source Strength Distributions of Case-C

The natural frequency investigation of the casing has shown that the frequency of 912 Hz is the cavity excitation mode of the fan casing. When the sound directivity map is examined at this frequency for the Case-C, it is observed that the sound is propagating through the inlet of the fan. That is, the inlet dominates the sound propagation and the noise level of the fan. The corresponding illustration is given in Figure 6.23. Other surfaces have lower levels and similar sound radiation characteristics.

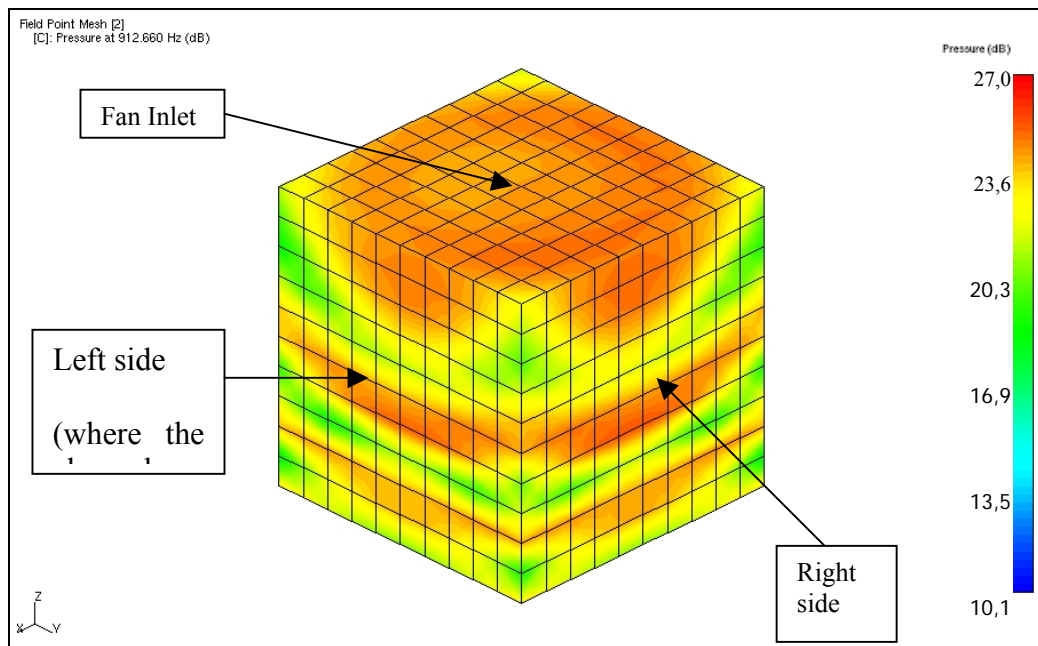


Figure 6.23 Sound directivity map at 912 Hz for the Case-C

The numerical results given in Figure 6.23 are supported by the experimental results. It is obvious from Figure 6.24 that the fan inlet is the dominant surface for sound propagation and other surfaces have lower levels and similar sound radiation characteristics.



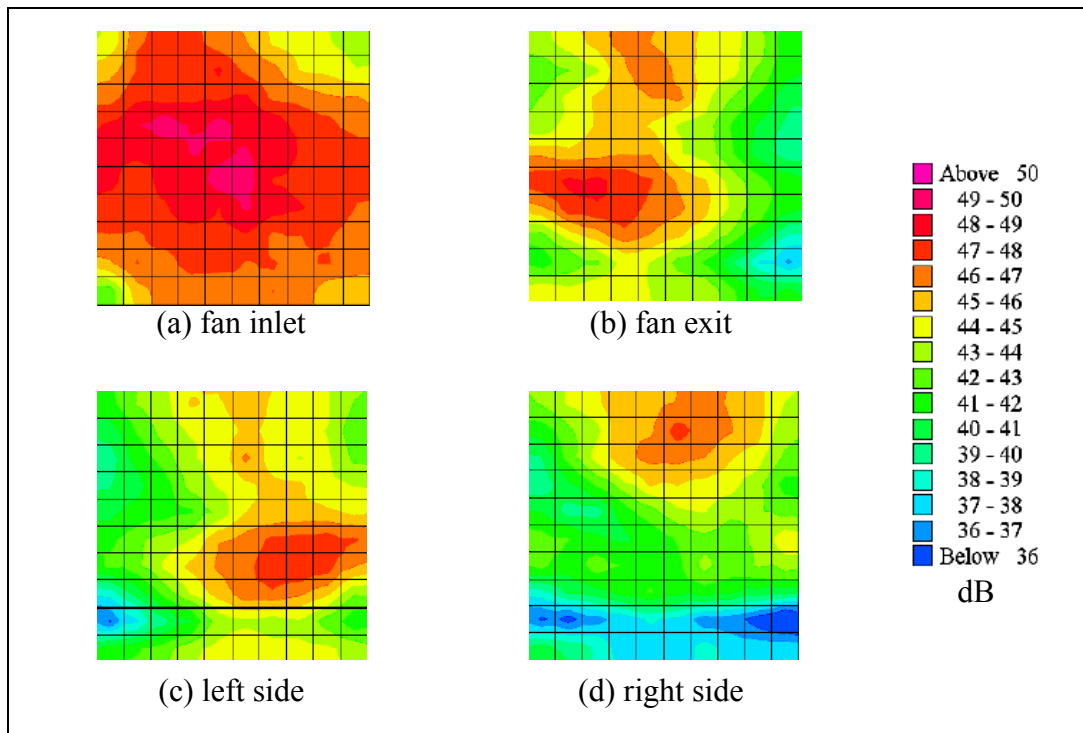


Figure 6.24 Experimental sound intensity levels (dB) of Case C at the surfaces 0.5m away from the fan surfaces.

Again in this case study, the numerical and experimental results are schematically similar but their levels are not the same. These results may become closer if the turbulence model is changed, i.e., if a high level of turbulence model and fine mesh are used, numerical results can be improved.

Although the numerical and experimental acoustic pressure levels are not exactly the same, Figure 6.23 is still very important from the designer's point of view. With this information, the fan design can be changed before making a prototype and testing in the laboratory since the numerical sound pressure map explains the sound radiation characteristics of each surface good enough.

The BPF of the Case-C is 770 Hz. Since it is focused on the tonal noise of the fan in this study, the sound pressure levels at 770 Hz are examined for the Case-C.

Figure 6.25 presents the sound pressure level of the tonal noise at the BPF. In this figure, the highest level of the sound pressure is illustrated as 40 dB for the fan inlet, outlet and side surfaces. The corresponding experimental data are 49 dB for the inlet and 41 dB for the outlet and side surfaces. Discrepancies between the numerical and experimental results can be attributed to the low resolution of the turbulent structures in the flow field. Since URANS models all the turbulence, the accuracy decreases. In addition, numerical model does not perfectly represent the experimental set-up.

The related graphical representations of the experimental data are given in Figure 6.26 for the inlet, Figure 6.27 for the outlet, Figure 6.28 and Figure 6.29 for the side surfaces.

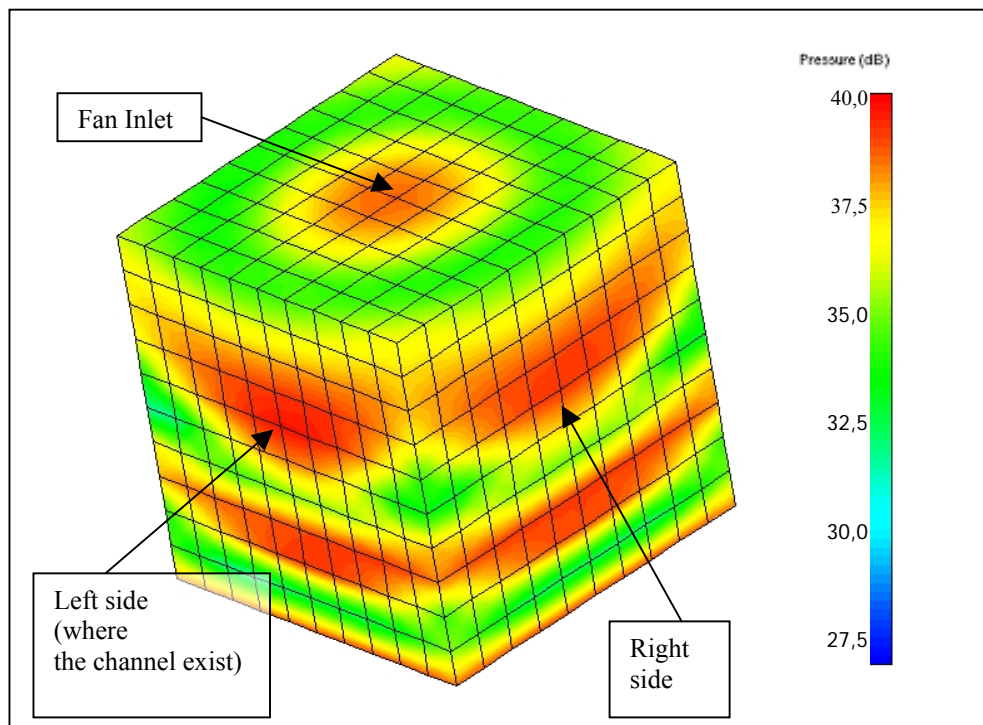


Figure 6.25 Sound directivity map at 770 Hz - 1<sup>st</sup> harmonic of BPF

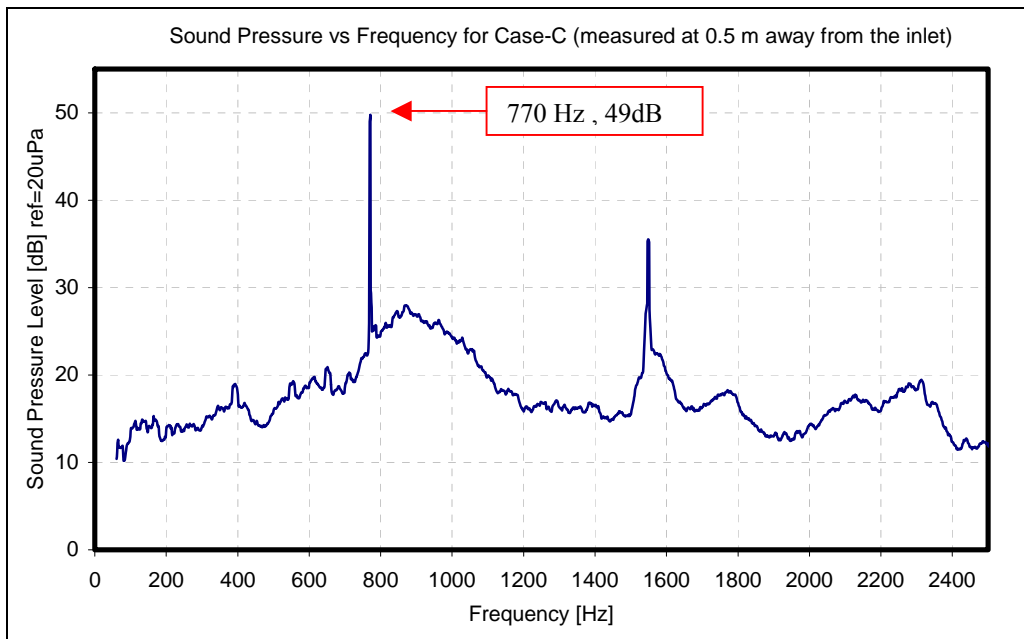


Figure 6.26 Experimental Sound Pressure Spectrum at 0.5 m away from the inlet

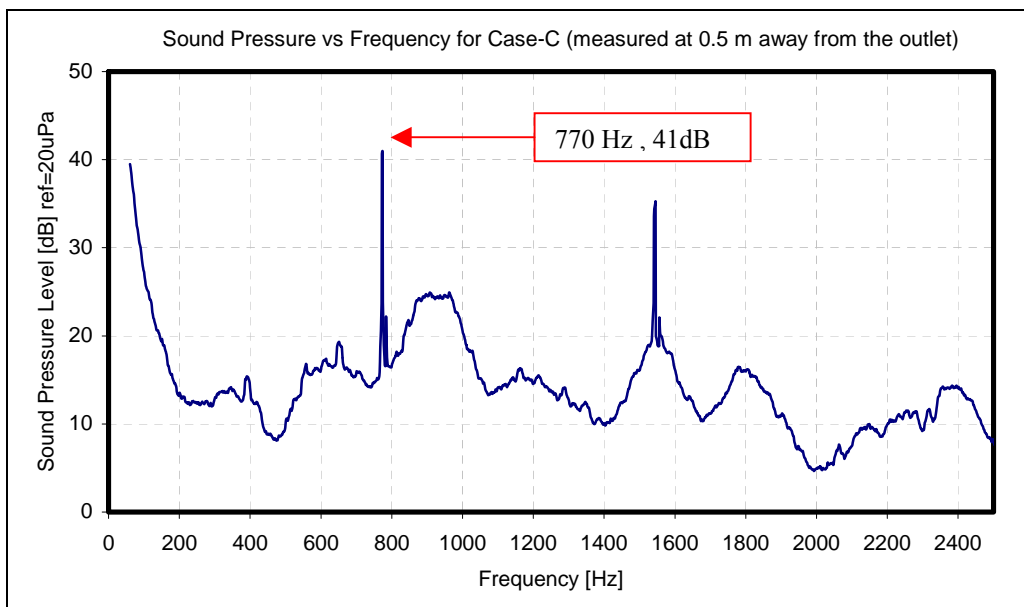


Figure 6.27 Experimental Sound Pressure Spectrum at 0.5 m away from the outlet

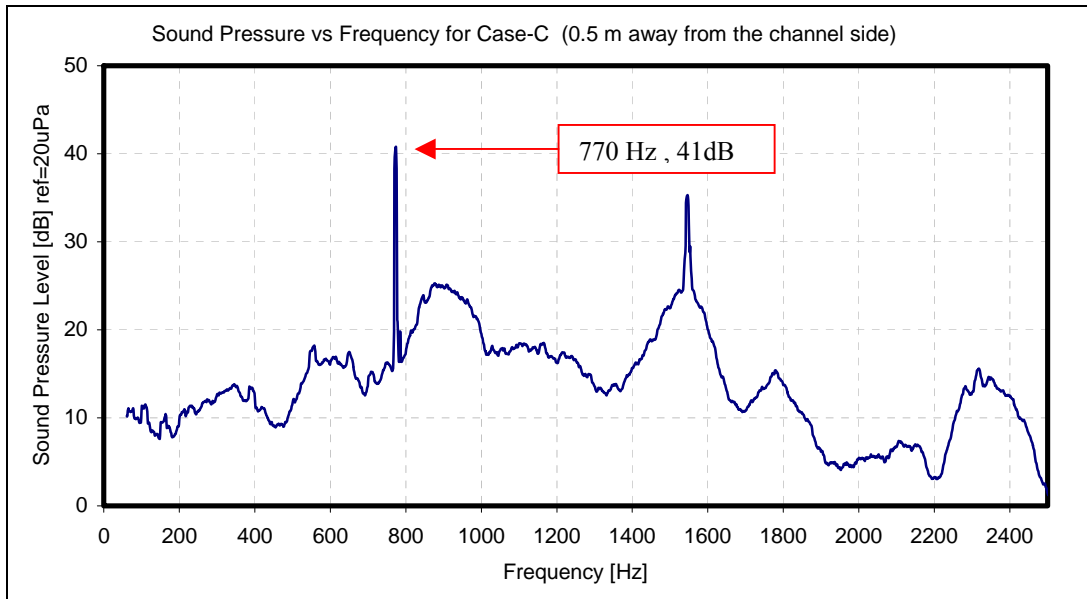


Figure 6.28 Experimental Sound Pressure Spectrum at 0.5 m away from the left side

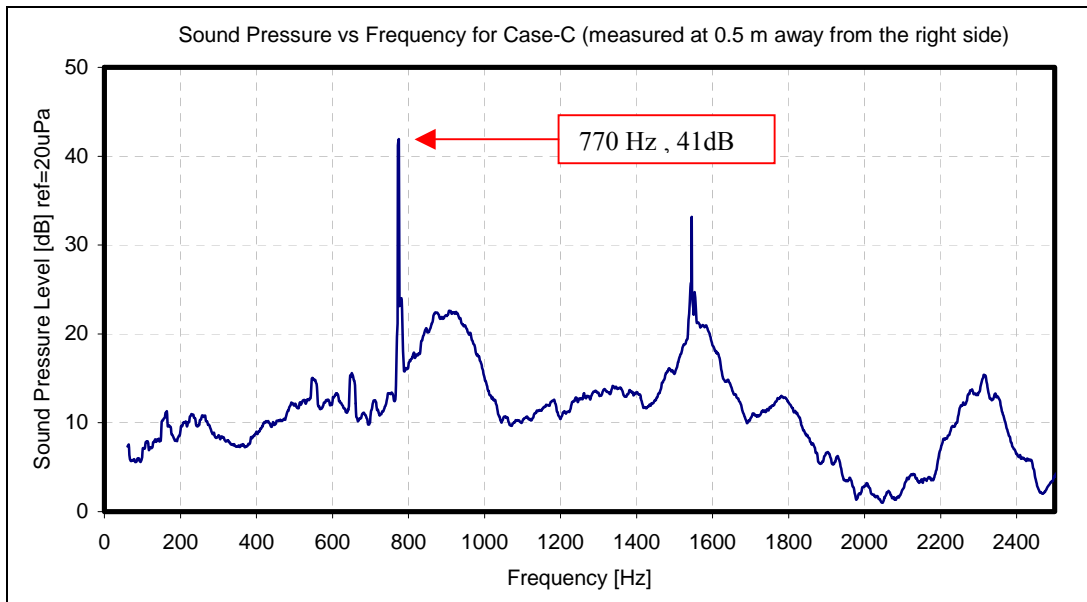


Figure 6.29 Experimental Sound Pressure Spectrum at 0.5 m away from the right side

To check how the numerical solution approaches the experimental results about sound intensities, the inlet surface intensity maps are compared. The reason for selecting the inlet surface is its dominant effect on the sound propagation.

Figure 6.29 (a) shows the numerical sound intensity simulation, and Figure 6.29 (b) gives the experimental results in 1/3 octave band. In both figures, intensity levels are decreasing while moving away from the center. The highest level is 46 dB for the numerical simulation and 50 dB for the experimental result. Considering the orders of the levels, results are close. Having this information at the theoretical design stage is very valuable for the designer.

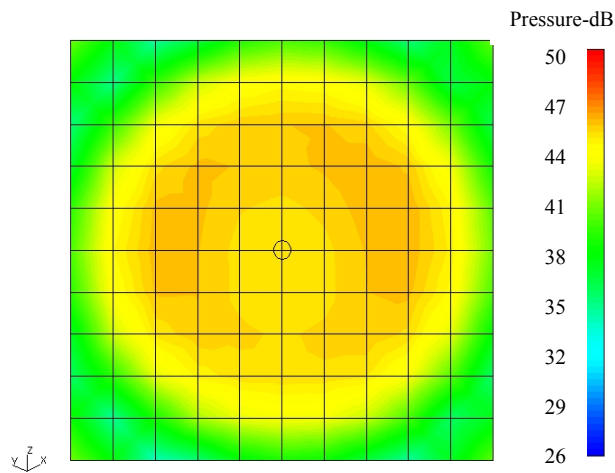


Figure 6.30 (a) Sound intensity maps for the inlet surface – Numerical Result

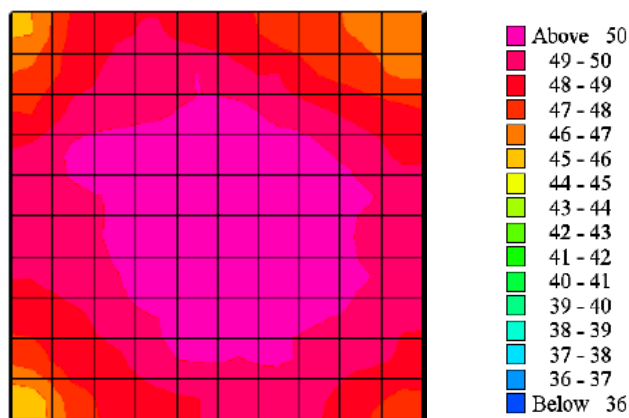


Figure 6.30 (b) Sound intensity maps for the inlet surface – Experimental Results

### 6.3 Experimental Investigations for Noise Reduction

The effect of geometrical differences on the fan noise level is investigated experimentally.

In this study, five different models are used as described in Chapter 5 in detail. The sound pressure levels are measured using an intensity microphone. Then A-weighted sound pressure level spectrum and sound intensities are plotted in 1/3 octave band for the cases given in Table 6.1. The orientation of the fan during intensity measurements is shown in Figure 6.31.

Table 6.1 The fan models used for the experimental study

| <b>Design Alternatives</b>    | <b>Number of blades</b> | <b>Channel on the volute</b> |
|-------------------------------|-------------------------|------------------------------|
| Original design (Case-A)      | 40                      | +                            |
| Channel eliminated (Case-B)   | 40                      | -                            |
| Splitters eliminated (Case-C) | 24                      | +                            |
| Inlet modified (Case-D)       | 40                      | +                            |
| Bitumen coated (Case-E)       | 40                      | +                            |

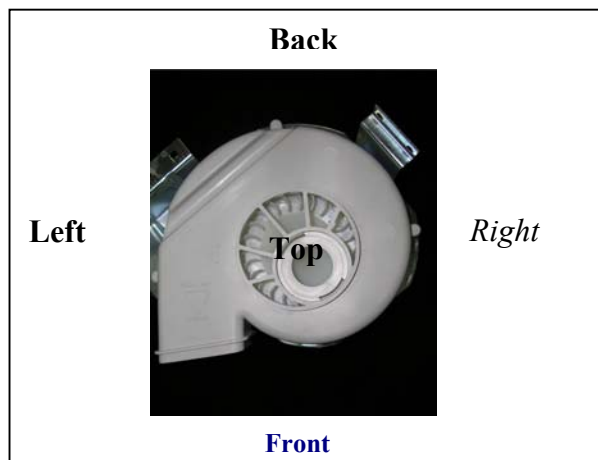


Figure 6.31 The orientation of the measurement surfaces for intensity mapping

Figure 6.32 a – e show the A-weighted sound pressure spectrum in 1/3 octave band for the Case A, B, C, D, E respectively. The details of these cases are listed in Table 6.1. The comments about the situations are given below.

If the Case-A (original design) and the Case-B (channel eliminated) are compared, it can be seen that the channel on the fan casing has almost no effect on the A-weighted 1/3 octave band sound pressure spectrum. There are little changes between Figure 6.32-a and 6.32-b. This result shows that the casing is big enough to compensate the flow area reduction due to channel.

Comparing the Figure 6.32-a and 6.32-c, it can be inferred that the splitters decrease the tonal noise and shift the peak level to the high frequency values where the sound isolation can be achieved better. When the splitters are eliminated, sound pressure level increases almost 6 dBA.

After changing the inlet design as in the Case-D, Figure 6.32-d, the peak pressure level is moved down to 630 Hz. Total pressure level is slightly decreased. However, this modification has a disadvantage about the noise isolation studies. As this modification is applied, the peak level approaches to the low frequency levels where the noise isolation becomes difficult and inefficient.

Figure 6.32-e indicates that there is no change on the sound pressure levels as compared to the Case-A after coating the casing with bitumen. There may be two reasons for this result. First, the inlet and the outlet openings of the fan dominate the sound propagated. Therefore, coating may have no influence on the resulting levels. Second, the bitumen is used as a vibration control material for the dishwasher tub but its effect is observed well as the temperature increases. That means it has good isolation performance at high temperatures. Since the sound pressure measurements are carried out in laboratory conditions, there is no improvement obtained due to the bitumen coating.

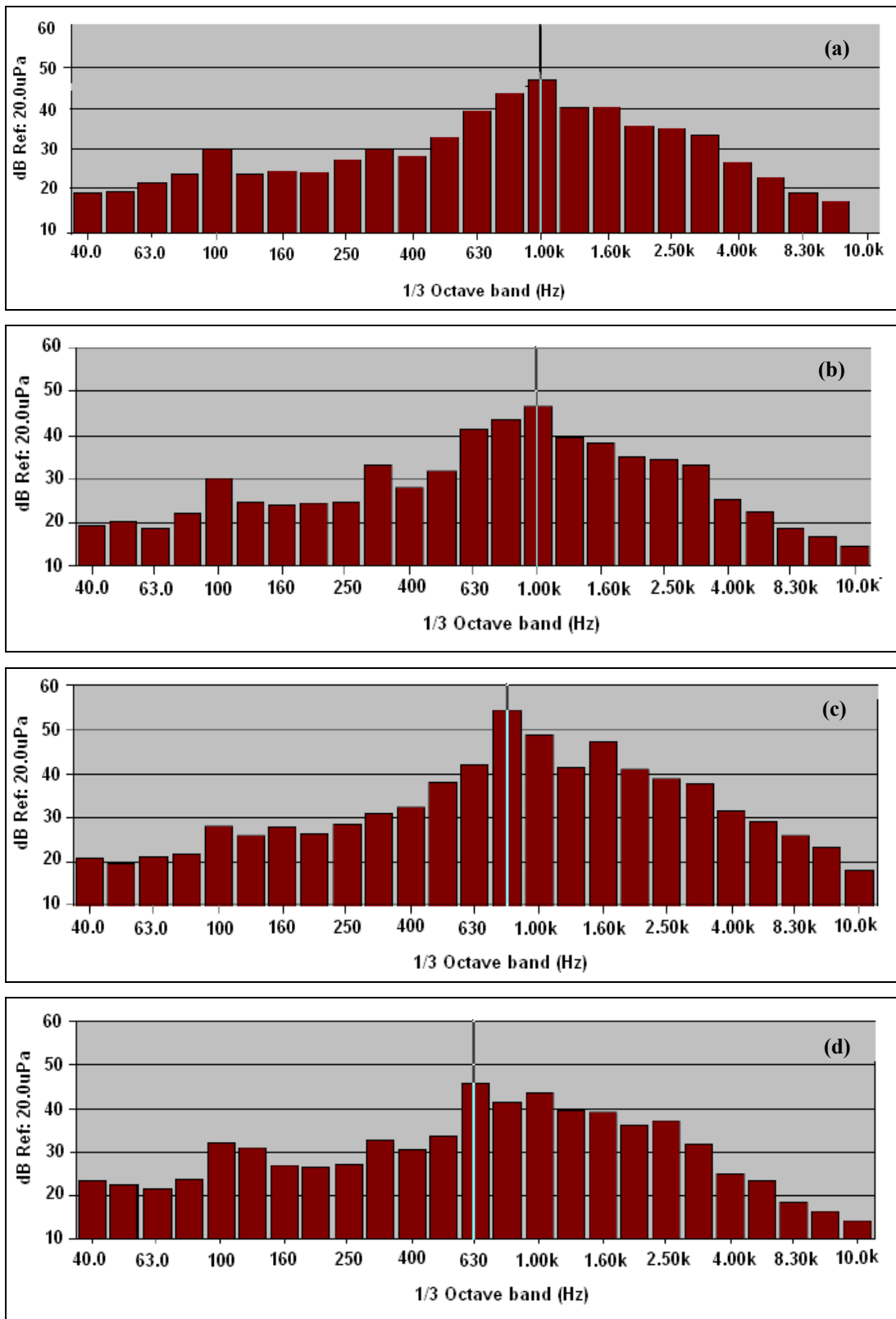


Figure 6.32 A-weighted Sound Pressure Spectrum measured at the center of top surface for (a) original design, (b) channel eliminated, (c) splitters eliminated, (d) inlet modified



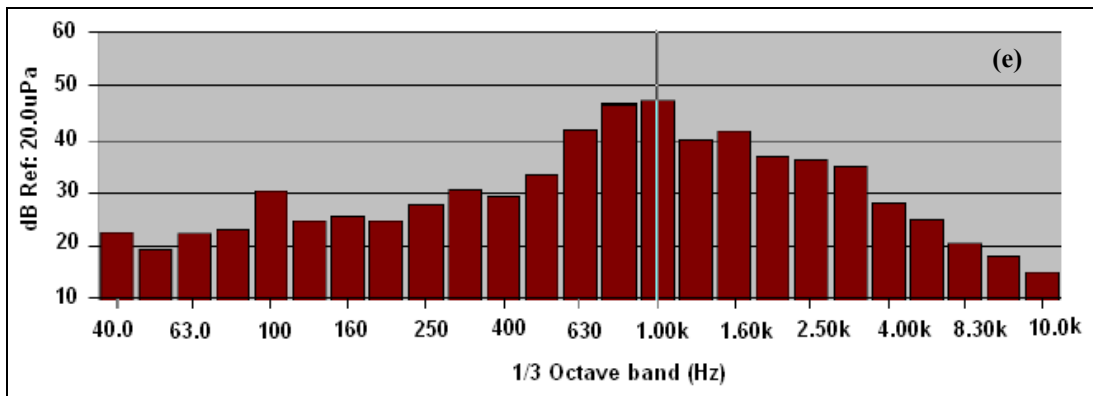


Figure 6.32 – cont. – A-weighted Sound Pressure Spectrum measured at the center of top surface for (e) bitumen-coated designs

Table 6.2 summarizes the frequency of highest sound pressure level and their corresponding levels. According to the table original design, channel eliminated case and bitumen coated alternatives have the highest level at 1000 Hz. Modifying the inlet and eliminating the splitters had move the highest level to lower frequencies.

Table 6.2 Peak Levels of the alternative cases

| <i>ALTERNATIVES</i>  | <b>Frequency Value where the peak sound pressure obtained (Hz)</b> | <b>Peak Sound Pressure Level (dBA)</b> |
|----------------------|--|--|
| Original design      | 1000   | 46,8                                   |
| Inlet modified       | 630  | 45,8                                   |
| Channel eliminated   | 1000   | 46,4                                   |
| Bitumen coated       | 1000   | 47,0                                   |
| Splitters eliminated | 800  | 54,3                                   |

The effect of the design changes can be summarized with the Figure 6.33 that demonstrates the highest-pressure levels obtained from the microphones placed each sides of the fan alternatives. The splitters eliminated case has the highest sound pressure levels at all sides as previously mentioned.

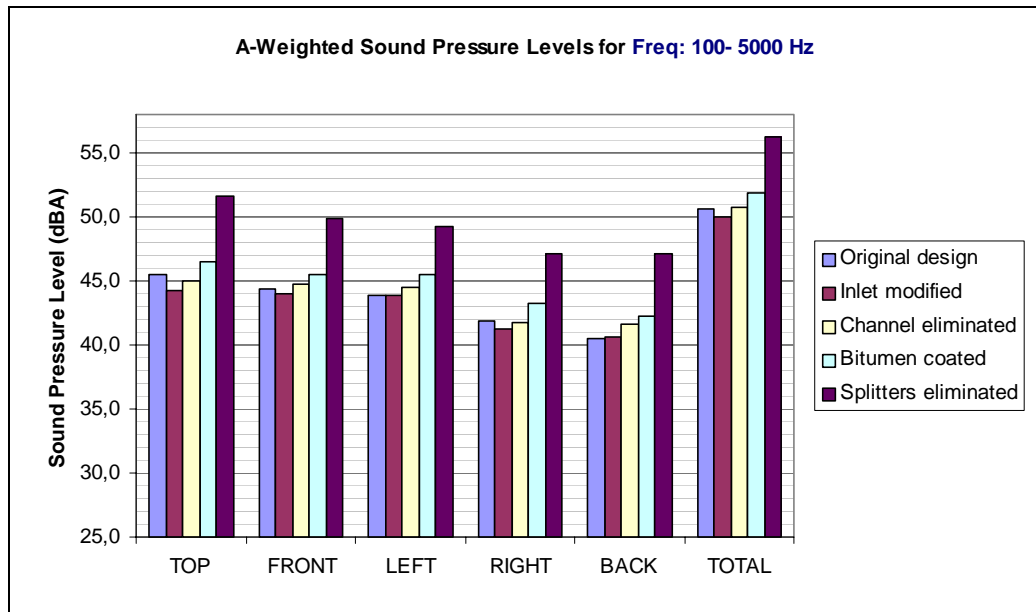


Figure 6.33 A-weighted Sound Pressure Levels in 1/3 Octave Band for the alternative cases (in the range of 100 – 5000 Hz)

Figures 6.34 – 6.38 give the comparison of sound intensity contours of each alternative for the frequency range of 100 – 5000 Hz.

The effect of inlet modification is better observed by comparing original design and inlet modified cases from Figure 6.35. The sound intensity levels are lower in the second case.

The effect of channel is very significant on the back surface as it can be seen from Figure 6.38. The sound propagated from the back surface increases considerably when the channel does not exist.

Coating the casing with bitumen increases the radiated sound compared to the original design unexpectedly. This result can be observed by comparing the original design with bitumen coated one through Figures 6.34 to 6.38. Bitumen is hard when it is cold. In this application since the air temperature is 22°C, it may lead to have more rigid surfaces so that the propagated sound is increased.

Experimental results proved that the splitters help to decrease to noise level of the fan. When the sound contours of original design is compared with the splitters-eliminated case from Figures 6.34 to 6.38, it can be seen that the latter case has higher levels in all sides. When splitters are removed, their flow blockage effect is eliminated. The flow area becomes wider. That increases the airflow in the fan but also increases secondary flows and recirculation.

Figures 6.39 – 6.43 give the comparison of sound intensity contours of each alternative at their peak pressure levels.

In all cases, it is obvious that the fan inlet, fan exit and the left surface (near tongue region) are dominant on the radiated sound.

The inlet modified and splitters eliminated cases are producing lower noise levels. When inlet ribs are removed, the disturbances of the airflow at the fan inlet improved. Inlet turbulences are decreased. This also decreases the turbulence level at the exit. Therefore radiated sound becomes lower at the fan inlet and the fan exit.

When the splitters are removed, the speed of the flow inside fan increases. At the same time flow area becomes wider, secondary flows increases. Therefore, the sound generation from the tongue region is decreased. That improves the sound radiated through the fan inlet and the fan exit.

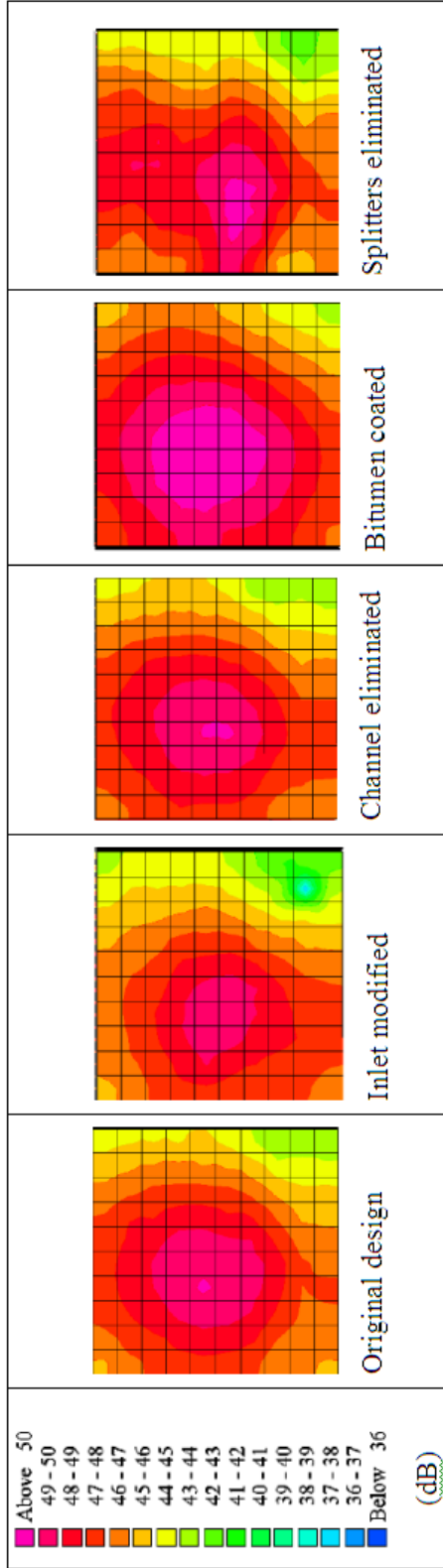


Figure 6.34 Intensity Map for the FRONT (Fan Exit) Surfaces (100-5000 Hz)

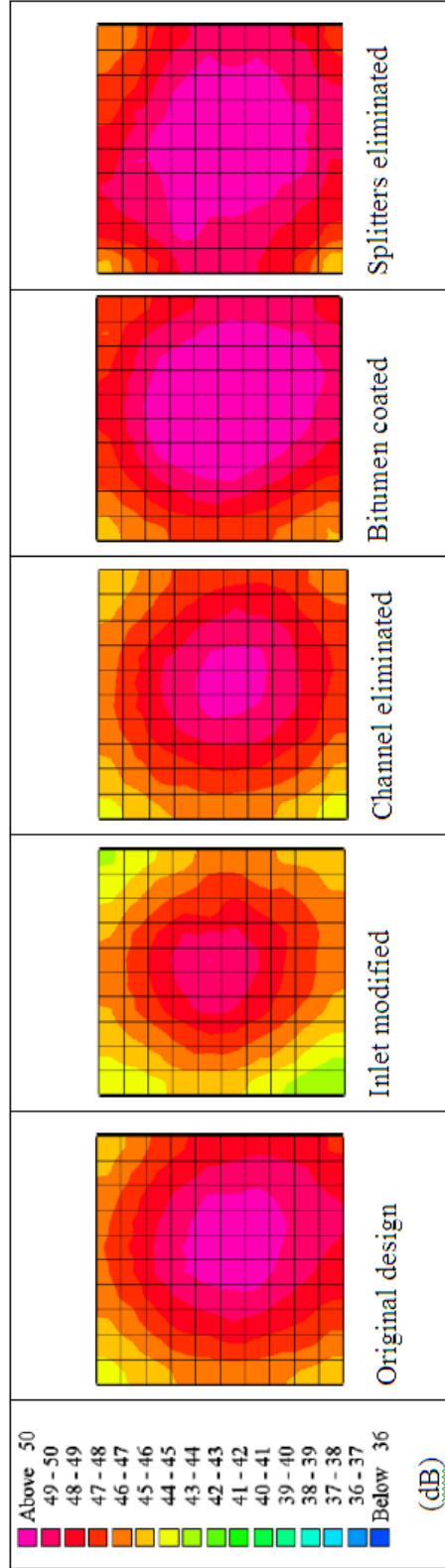


Figure 6.35 Intensity Map for the TOP (Fan Inlet) Surfaces (100-5000 Hz)

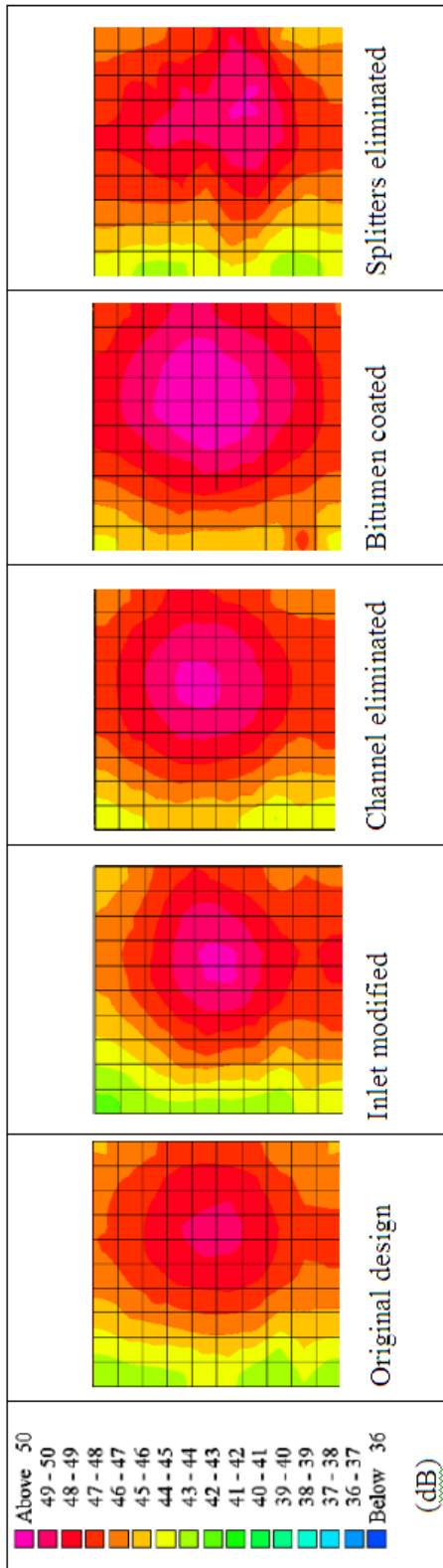


Figure 6.36 Intensity Map for the LEFT Surfaces (100-5000 Hz)

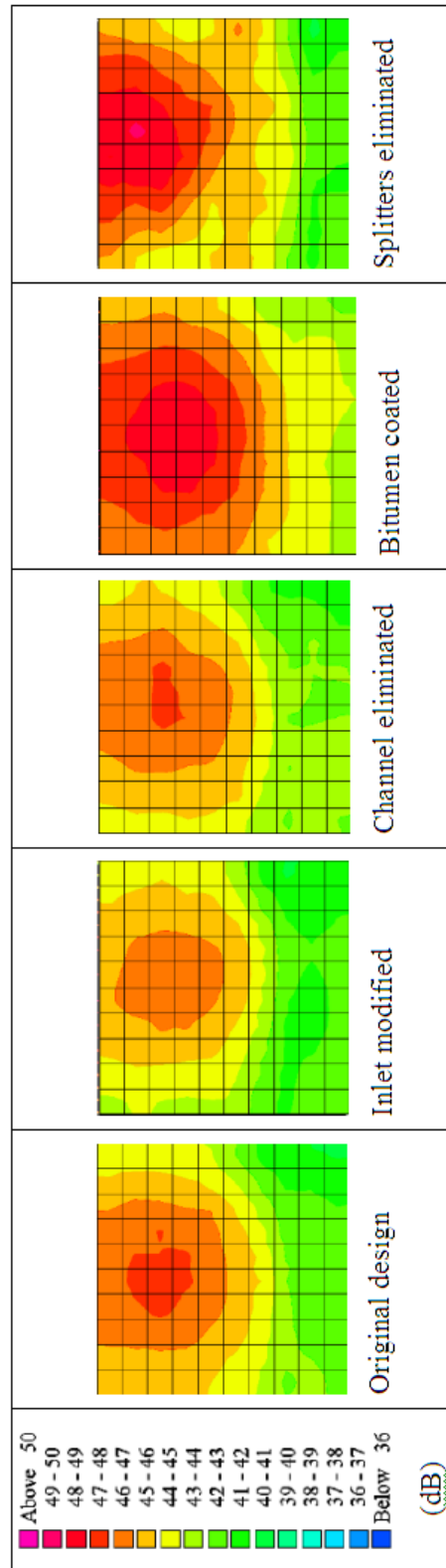


Figure 6.37 Intensity Map for the RIGHT Surfaces (100-5000 Hz)

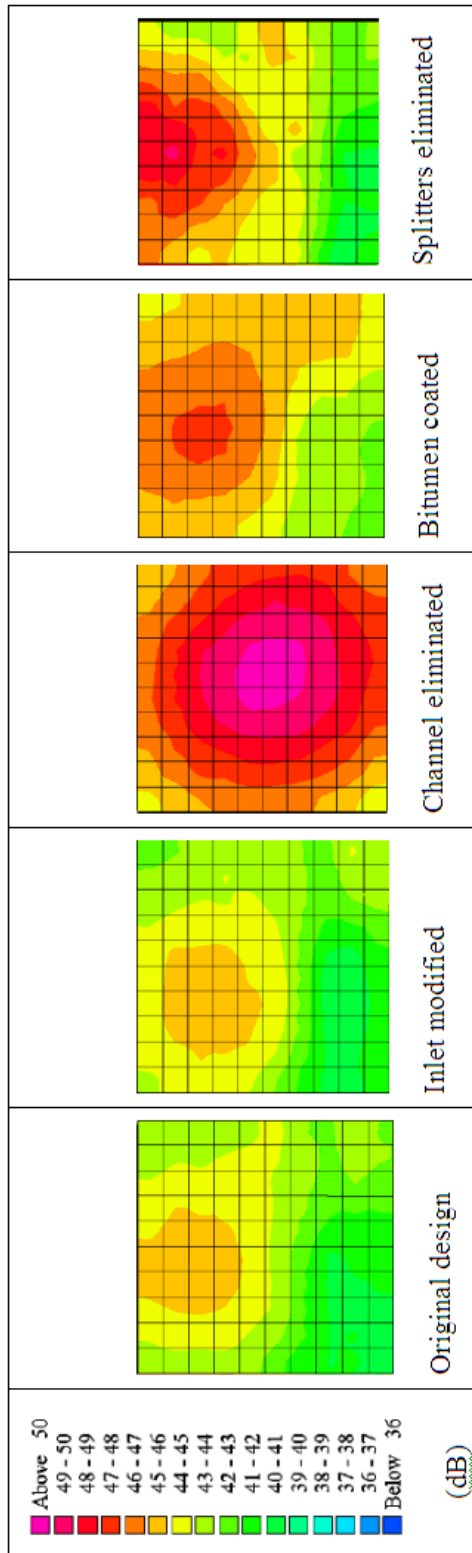


Figure 6.38 Intensity Map for the BACK Surfaces (100-5000 Hz)

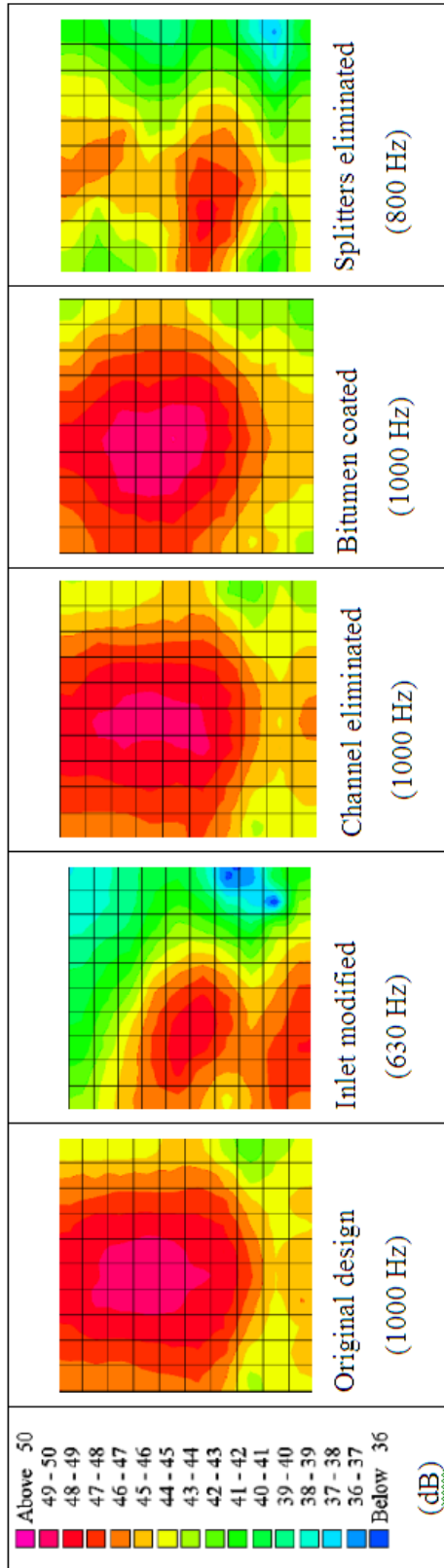


Figure 6.39 Intensity Map for the FRONT (Fan Exit) Surfaces at the Peak Frequency Values

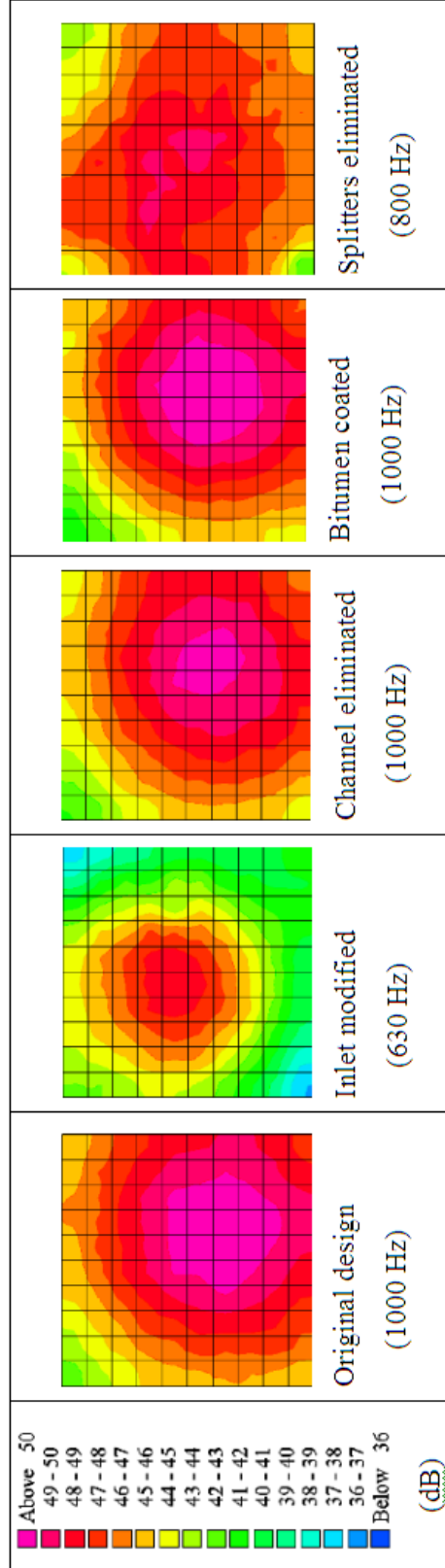


Figure 6.40 Intensity Map for the TOP (Fan Inlet) Surfaces at the Peak Frequency Values

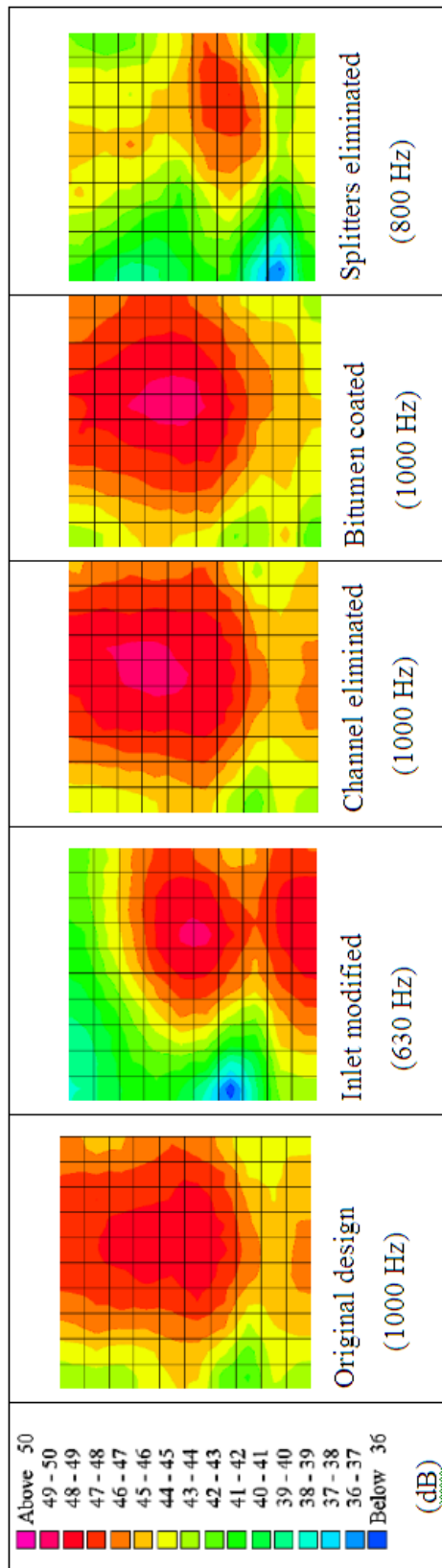


Figure 6.41 Intensity Map for the LEFT Surfaces at the Peak Frequency Values

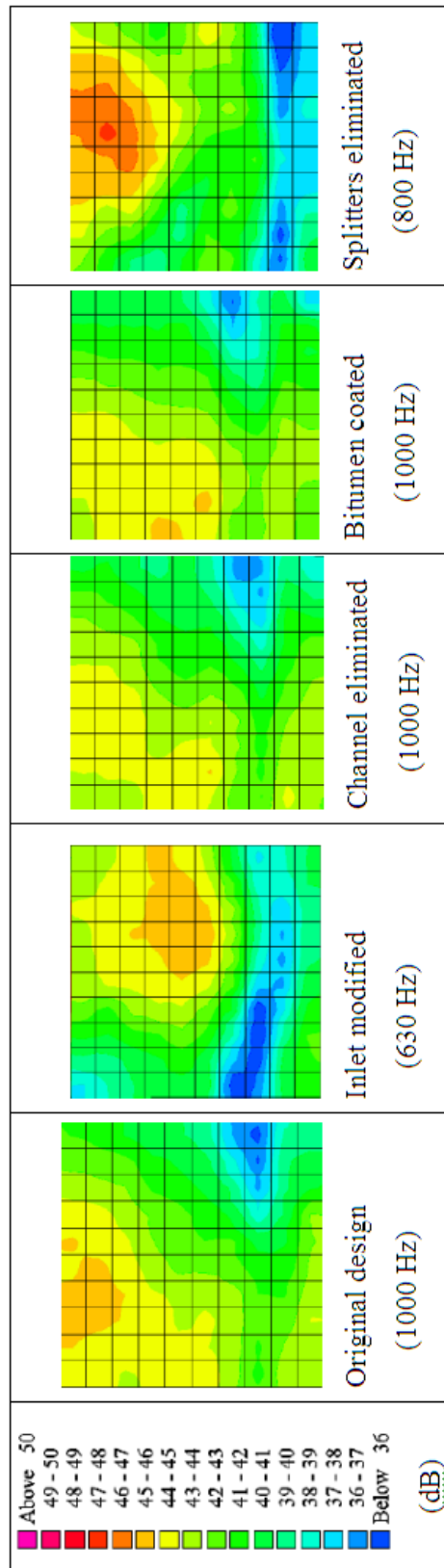


Figure 6.42 Intensity Map for the RIGHT Surfaces at the Peak Frequency Values



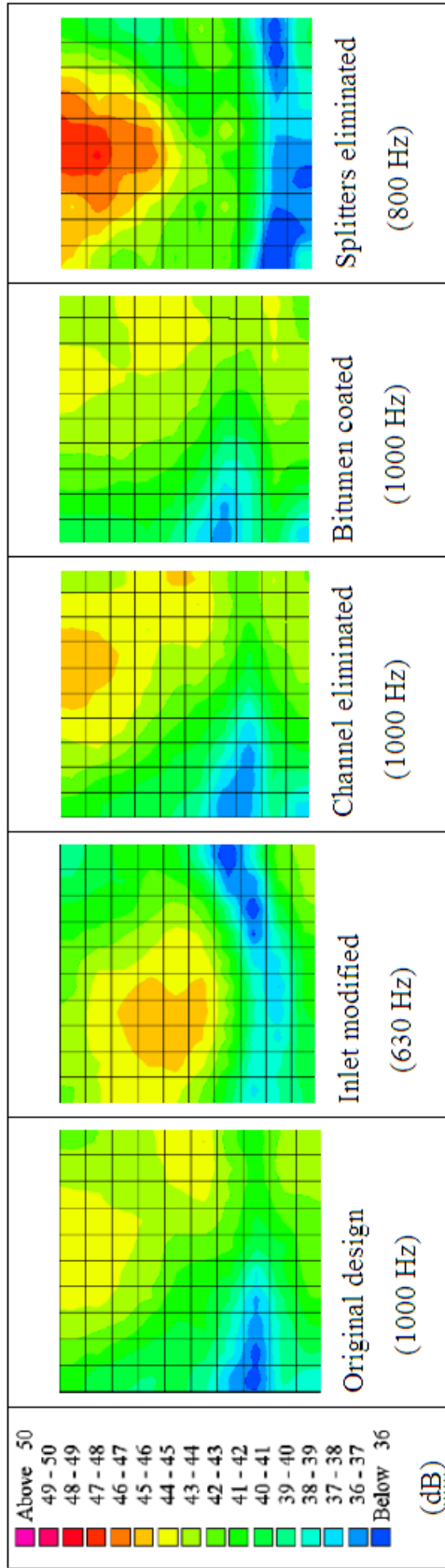


Figure 6.43 Intensity Map for the BACK Surfaces at the Peak Frequency Values

## CHAPTER 7

### DISCUSSION, CONCLUSIONS AND RECOMMENDATIONS FOR FUTURE WORK

#### 7.1 Summary

In this research study, flow-induced noise by a centrifugal fan has been investigated numerically and experimentally.

In the numerical analysis, a flow solver and a vibroacoustic solver are coupled. This approach consists of two main parts: a transient calculation of the flow field for the determination of sound sources, and the calculation of the sound propagation to obtain the resulting sound field. The time dependent turbulent flow is simulated with FLUENT and the aero acoustic field is computed with the LMS SYSNOISE. The viscous, incompressible, transient flow field solution is obtained by using URANS Spalart-Allmaras turbulence model. The time dependent flow data are fed into the aero acoustic module where the propagated noise is computed by solving the inhomogeneous wave equations with Boundary Element Method. The tonal noise radiation representing Blade Passing Frequency and the excitation at the cavity resonance frequencies are investigated. The sound pressure and intensity levels are predicted. The quality of the method is evaluated on the basis of two test cases.

The experimental studies are carried out in the ARÇELİK A.Ş, R-D Laboratories. Both the aerodynamic and aero acoustic results are validated with acceptable errors. The predicted and measured sound pressure levels compare well for the frequency ranges of interest. Different phenomena like acoustic modes, narrowband peaks are resolved qualitatively and quantitatively.

In addition, the contribution of the design changes on the fan sound pressure level is investigated and useful design informations are obtained. For this study, five

different cases are analyzed by measuring A-weighted, 1/3-octave band sound pressure levels and sound intensities.

Figure 7.1 shows the steps of Aero-acoustic Analysis. The procedure followed for Cavity Excitation Modes Analysis is given in Figure 7.2.

## **7.2 Discussion**

The design methodology of a turbomachinery has been defined since early 1960's. In this conventional procedure, the fundamental inputs are head, flowrate, speed and efficiency values. The geometrical details can be found by means of theoretical and empirical relations. However, in this design process, the noise is not considered and the acoustical performance of the turbomachinery cannot be predicted at the beginning. Development speed and a reliable development process are key success factors in the industry. Therefore a definition of a new methodology that decreases the design time and the design cost of a low noise fan is a necessity.

This methodology is established by coupling of flow solver and vibroacoustic solver such that the sound propagation of a fan can be investigated in the design phase theoretically. For this purpose, two example cases are investigated. In the first case, the impeller blades are unevenly distributed and in the second case study they are evenly distributed.

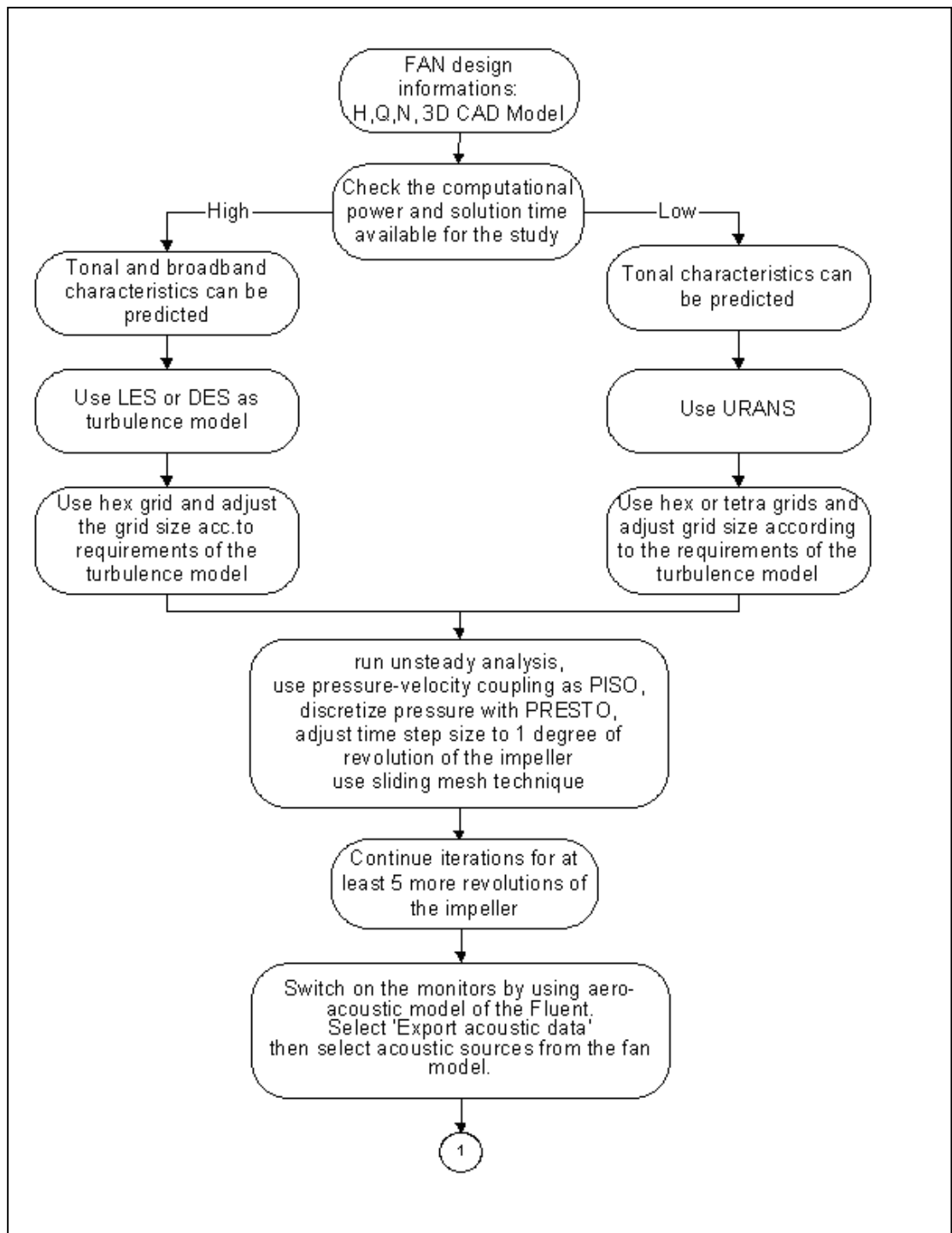


Figure 7.1 The steps of Aero-acoustic Analysis

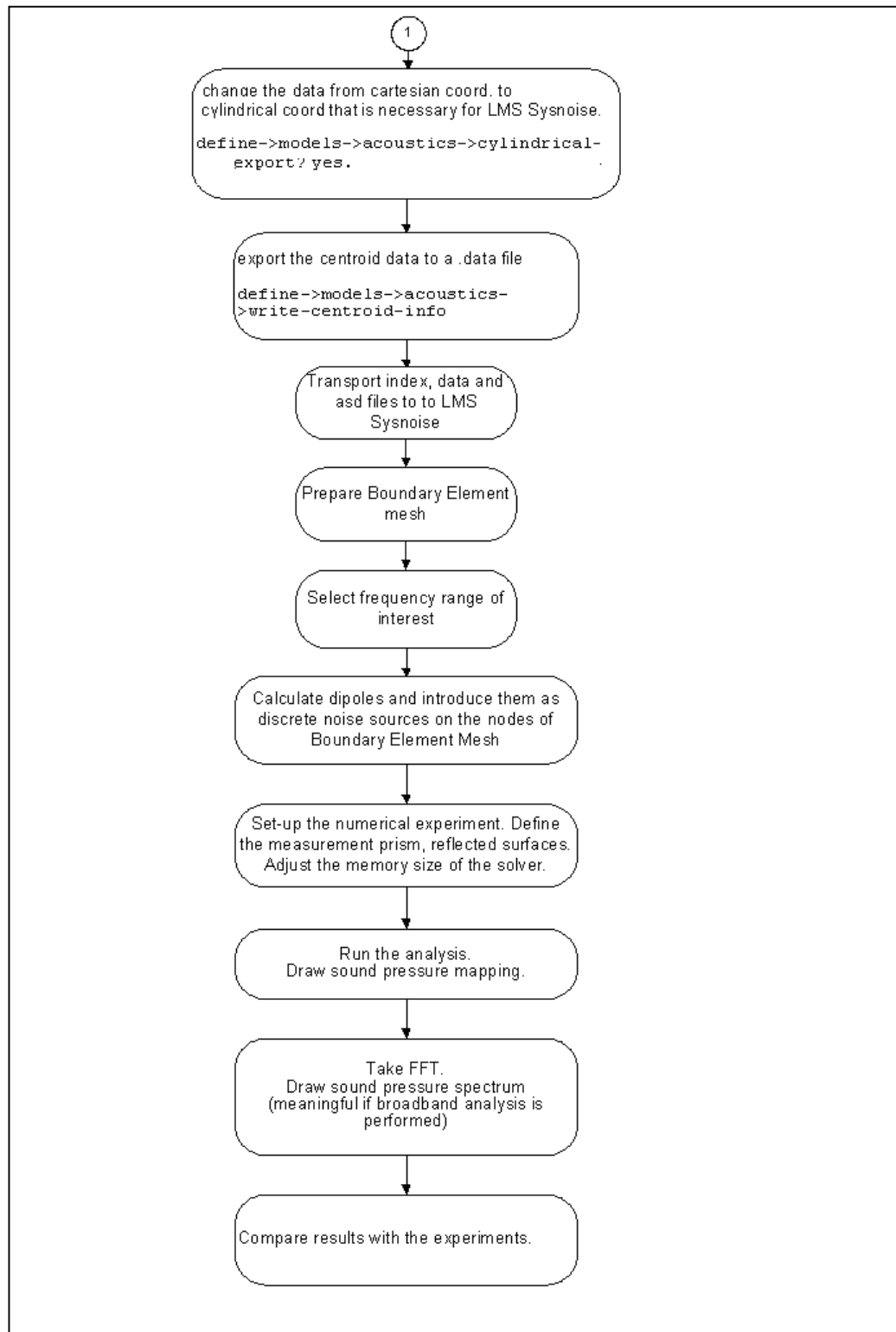


Figure 7.1 - cont. - The steps of Aero-acoustic Analysis

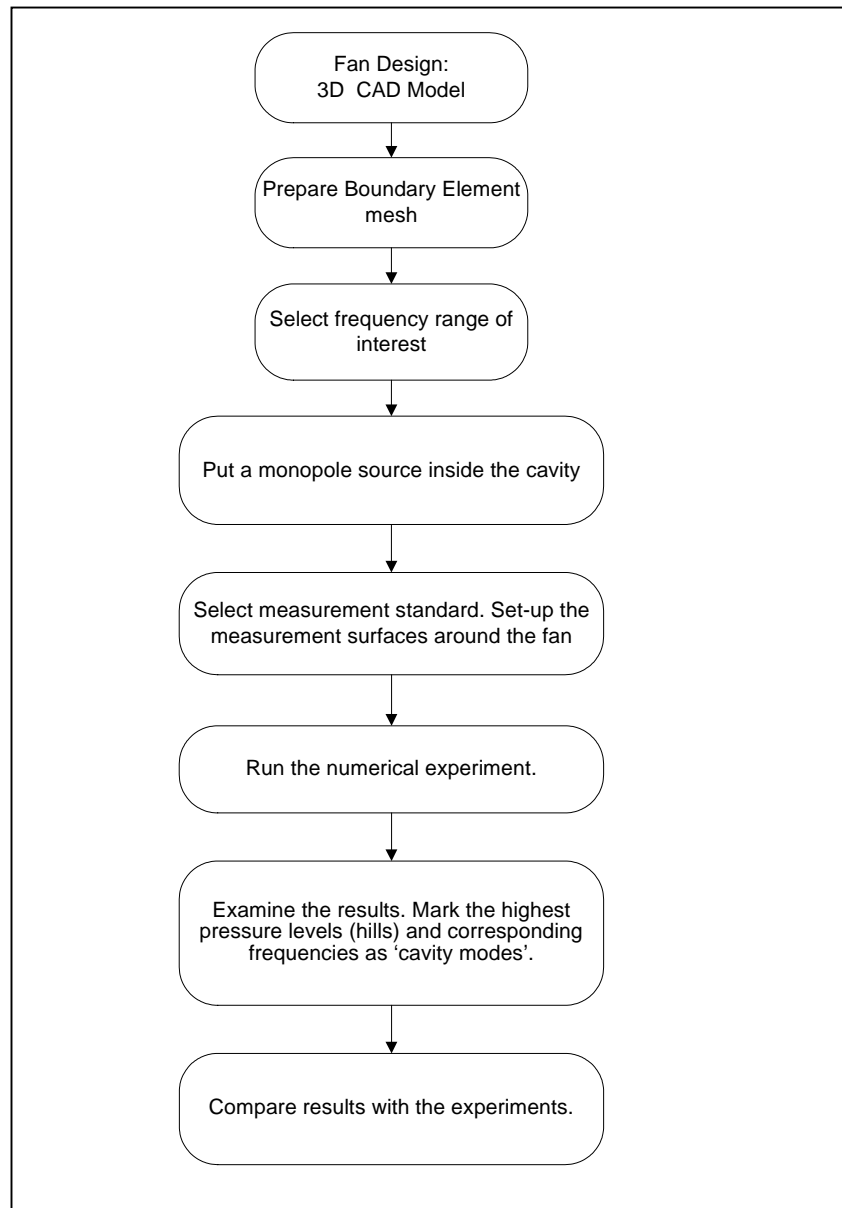


Figure 7.2 The steps of Cavity Excitation Modes Analysis

The numerical simulations start with the flow field solution. The turbulence model is very important for the level of accuracy. In this study URANS model is preferred. The need for URANS, LES or DES for fan noise depends on what really generates the noise. If the noise is due to wake interaction then URANS is able to get the tonal noise. But if the pure fan noise is mentioned, like a fan in free stream without shroud, then LES or DES is needed. Otherwise relevant unsteadiness cannot be caught. If it can be assumed that the impeller creates too much turbulent noise, i.e., there is little separation, then the URANS model may well produce the desired results, which comparatively means a faster solution. If it is known that the impeller is efficient and creates little turbulence then this approach is recommended.

The fan analyzed in this study has an operational speed of 1925 rpm. The tip Mach number is low. At this condition the tonal noise is expected to dominate. The Sound Pressure Spectrum of the fan also supports this information. Therefore URANS analysis is selected.

The aerodynamic results of the flow solver show a good agreement with the experimental data. There is 2% difference between its flowrate values at the operating point pressure.

At the beginning of the study it was planned to see the effect of the mesh size on the noise prediction analysis. This cannot be realized because both the flow solver and the vibroacoustic solver have limitations on the memory sizes. The flow solver cannot handle the data of the casing having finer mesh. The casing cannot be selected as a noise source. Also, the vibroacoustic solver cannot process the data.

It is experienced that the vibroacoustic solver can only make analysis with evenly distributed blade structures (same blade structure with same spacing between blades). Since in this case, only a single blade is introduced as a noise source and calculation matrices become smaller.

The symmetrical geometry need of the solver created problems during the acoustic modeling of the unevenly distributed blade case.

**For the analysis of unevenly (irregular) distributed blades**, the quarter of the impeller is introduced as a consolidated blade because there is a  $90^{\circ}$  period that the blade distribution repeats itself. In this case, the total number of consolidated blades is 4. This approach is valid for the investigations of the cavity excitation modes and tonal noise characteristics. But it creates problems when BPF and its harmonics are calculated. Since the solver accepts the number of blade as 4, BPF and its harmonics are located incorrectly and the spectrum cannot be predicted properly.

When the cavity resonance frequency obtained from numerical analysis is compared with the spectrum of the fan, it is seen that there is a peak pressure level at 912 Hz. It is concluded that this peak comes from the cavity resonance frequency of the casing. This result shows that the numerical simulation gives evidence about the reasons of the peaks on the fan spectrum.

The sound pressure levels on the casing show that the fan inlet and the fan exit have equal importance considering the propagated sound from these surfaces. The radiated sound has nearly same levels at the microphone positions of these two surfaces. This result is supported by the experimental measurements. It is experimentally proved that the fan inlet and the exit have similar sound pressure contours and nearly the same levels.

**As for the regularly distributed blades**, the cavity excitation modes and tonal noise characteristics are investigated. Sound pressure distributions are examined over the stationary surfaces where the dipoles are defined as acoustic sources. The sound pressure levels and intensities are predicted.

For this case, the numerical predictions indicate that the inlet dominates the sound propagation and the noise level of the fan. This information is important from the



designer's point of view since the designer may revise the inlet design of the model before making a prototype and testing in the laboratory.

The sound pressure level of the tonal noise at the BPF is numerically obtained as 40 dB for the fan inlet, outlet and side surfaces. The corresponding experimental data are 49 dB for the inlet and 41 dB for the outlet and side surfaces. When numerical and experimental sound intensity maps are compared, it is seen that the distributions in both numerical and experimental contours are similar. The highest level is 46 dB for the numerical simulation and 50 dB for the experimental result. Considering the orders of the levels, results are quite close.

The differences between the numerical and experimental results can be attributed to the low resolution of the turbulent structures in the flow field. Since URANS models all the turbulence, the accuracy decreases. In addition the reflection and the fan can not be exactly modeled to simulate the reflection and scattering characteristics. In the numerical analysis, only the fan is taken into account. The motor box, supporting circular duct are not taken into account in the computations. The reflections due to the box and supports are not considered. Some sources of errors may arise due to assumptions about material properties, geometrical approximations, boundary conditions and discretization of the acoustic field into elements.

The fan, which is subject of this study, has been in mass production for three years. At the beginning, its noise level was low enough compared to the noise level of the appliance in which it is used. However, its level is now significant because of the improvements on the sound power level of the appliance. Therefore, a noise level improvement is necessary on the current design of the fan. For this purpose, prototypes are prepared and tested in the laboratory for the effects of geometrical changes on the sound pressure levels produced.

The original design has a channel on the volute. This detail was added to the design due to some space problems where the fan is mounted. When the sound pressure level and intensity results are compared, it is observed that this channel has no

significant effect on the acoustical characteristics of the fan. This shows that the casing is big enough to compensate the flow area decrement due to the casing

There are 24 blades and 16 splitters in the original design. These splitters were added to the design to decrease the tonal noise at BPF and carrying the BPF to high frequencies. Although carrying BPF to high frequencies affects A-weighted levels and increases the sound pressure declaration levels, this condition is preferable from the designer's point of view because isolation of noise at high frequencies is easier than isolation of noise and vibration at low frequencies. If the sound pressures and intensity measurement results of the fan with no splitters and the original fan design are compared, it is understood that this aim has been achieved. The splitters decrease the tonal noise and shift the peak level to the high frequency values where the sound isolation can be realized better.

After cutting the ribs at the inlet, the peak pressure level is moved to lower frequency levels as compared to the original fan design. Total pressure level is slightly decreased. This modification has a disadvantage about the noise isolation studies because if the peak level approaches to the low frequency levels, the noise isolation becomes difficult and inefficient.

When the fan casing is coated with the bitumen, no change is obtained on the sound pressure levels as compared to the original design. The inlet and the outlet openings of the fan dominate the sound propagated. Therefore coating may have no influence on the resulting levels. Also, it is found that the bitumen has good sound isolation performance when it's heated. Since the sound pressure measurements are carried out in laboratory conditions, there is no improvement obtained due to the bitumen coating.

### 7.3 Conclusions

Flow induced noise generated by a centrifugal fan is examined numerically and experimentally. Results are satisfactory in terms of level and spatial distribution. The experimental investigations on the alternative fan design show that the highest sound pressure and intensity levels occur if the blades are regularly distributed.

In the noise reduction studies, the peak sound pressure values have much importance than the others since these levels are dominant on the perceived noise level. If the reasons of the peaks are known, the noise isolation study becomes easier. The methodology used in this study provides one of these hints by predicting the cavity excitation modes.

The tonal noise is the most annoying part of the noise created by machinery. In this study, the methodology is developed for the designer to investigate tonal part of the sound created by a centrifugal fan at the design stage.

The main objective of this study on the prediction of flow-induced noise is the integration of the presented methodology into product development process of a fan. It was considered that this approach could reduce design time of low noise fan by eliminating the trial-error design and testing process. Thus, it may decrease the prototype cost. This aim is achieved for the regularly spaced fan blades and using mesh sizes affordable by the computer memory available.

If the complete spectrum of the fan noise is to be obtained, it is necessary to use high-level turbulence models and very fine grids. However, in this case it is experienced that the flow solver has memory limitations. It cannot handle the acoustic data properly. It is concluded that the mesh sizes has to be selected carefully first considering this drawback, second the high computational power requirement of the high-level turbulence models.

Finally, it is experienced that the vibro-acoustic solver cannot process irregularly distributed blades. Therefore it is concluded that the proposed methodology still needs time before replacing the current methodology considering the unevenly distributed blades.

To sum up, this research study shows that the tonal noise prediction of a centrifugal fan is possible with the proposed methodology. This methodology can be used at design stage for preliminary check of sound propagation characteristics of the fan surfaces. Therefore design improvements can be initiated.

The followings are achieved with the numerical analysis study:

1. Uneven blade distribution:

- Cavity modes can be predicted.
- Sound Pressure levels are not same as the experimental data.
- BPF and its harmonics cannot be calculated correctly. However, the sound mapping (sound radiation characteristics) has good agreement with the experimental data.

2. Regularly spaced blade distribution:

- Cavity modes can be predicted.
- Tonal noise can be predicted with good accuracy.
- Sound intensity maps are close to the experimental data. Therefore, the relative effects of the surfaces on the propagated sound can be visualized before making prototypes and performing experiments.

After the comparison of the numerical results with the experimental data, it is concluded that;

- If flow induced noise at every frequency in the range of interest is investigated, a better turbulence model has to be used. Depending on the total number of mesh, LES can be preferred.

- As the mesh size increases, both flow solver and vibro-acoustic solver have problems. They cannot handle the data and analysis is interrupted frequently. This information should be taken into consideration while preparing the mesh and selecting the noise sources.
- As the size of the pressure data increase, vibro-acoustic solver cannot process the data due to its memory size limitations. The size of the data transferred from Fluent should be adjusted such that it will not make the resolution worse but also it will not cause overflow in LMS Sysnoise.
- Also, the algorithm of LMS Sysnoise is suitable for making analysis with the fan having regularly spaced blade distribution.

The experimental studies for investigating the geometrical differences on the fan noise show that:

- Splitters decrease the sound pressure levels.
- Removing the inlet ribs improves the total sound pressure level of the fan.
- The channel has no effect on the fan performance and total sound pressure level of the fan. But it decreases the radiated sound from the backside of the fan (where channel exist).

#### **7.4 Recommendations for Future Work**

In this study it is focused on the simulation of the tonal noise of a centrifugal fan. The broadband noise is not investigated. Since the tonal noise is dominant in the fan under consideration and it is a major concern due to annoyance produced on humans. The second reason is the high computational power requirement of the broadband noise analysis.

The recommendations for the future work are stated below:

If the fan to be analyzed has unevenly distributed blades, it is recommended to produce prototypes and perform laboratory experiments for the analysis of the radiated noise.

If the fan has regularly distributed blades, the acoustical characteristics of the fan can be simulated with the proposed method. But in this case, if the computational facilities are enough for making analysis with high level of turbulence models, such as LES or DES, then broadband characteristics of the fan can be simulated. Therefore whole spectrum of the fan sound pressure can be obtained.

In addition, the structural resonance frequencies can be analyzed for the fan casing. Finite Element Method can be used to obtain these modes. After FEM analysis, the contributions of BPF and its harmonics, and surface dipoles on the excitation of these structural modes can be predicted by using LMS Sysnoise. Therefore the noise generation due to the structural characteristics of the fan can be simulated. That information may be used to decide whether it is necessary to change the material properties of the casing in order to reduce the noise level of the fan.

## REFERENCES

1. Tyler, J., M., Sofrin, T., G., "Axial Flow Compressor Noise Studies", SAE Transactions, Vol.70, pp.309-332, 1962.
2. Bommers, L., Grundmann, R., Klaes, K., Kramer, C., "Effects of Blade Design on Centrifugal Fan Noise and Performance", Noise Control Engineering Journal, Vol.43 (4), pp.91-101, 1995.
3. Fehse, K.R., Neise, W., "Generation Mechanism of Low Frequency Centrifugal Fan Noise", AIAA – 98– 2370, 1998.
4. Konieczny, P., Bolton, J., S., "Design of Low-Noise Centrifugal Blowers – Part 1: Measurement and Analysis Procedures", Noise Control Engineering Journal, Vol.43, pp.103-116, 1995.
5. Boltezar, M., Mesaric, M., Kuhelj, A., "The Influence of Uneven Blade Spacing on the SPL and Noise Spectra Radiated from Radial Fans", Journal of Sound and Vibration, Vol.270(4), pp.697-711, 1998.
6. Sentek, J., "Influence of Geometrical Parameters upon the Sound Power Level of Centrifugal Fans", Journal of Sound and Vibration, Vol.61(3), pp.383-389, 1978.
7. Trunzo, R., Lakshminarayana, B., Thompson, D., E., "Nature of Inlet Turbulence and Strut Flow Disturbances and Their Effect on Turbomachinery Rotor Noise", Journal of Sound and Vibration, Vol.76(2), pp.233-259, 1981.
8. Yeager., D.M., "An Investigation of the Noise Related by Centrifugal Blowers", Internoise 88, pp.789 – 792, 1988.
9. Yeager., D.M., Lauchle, G.C., 1990, " Flow in Centrifugal Fan of the Squirrel-Cage Type", ASME Journal of Turbomachinery, vol.112, pp.84-90.
10. Marcinowski, H., "Motortechnische Zeitschrift (MTZ)", Einfluss des Lautfradspaltes und der Luftführung bei einem Kühlgeblase axialer Bauart, 14, 259-262, 1953.
11. Neise, W., Hoppe, G., "Effect of Inflow Conditions on Centrifugal Fan Noise", Proceedings of the First European Symposium on Air Conditioning and Refrigeration, pp. 165 – 172, Brussels, 1986.
12. Morunishi, K., "The Influence of Geometric Parameters on FC Centrifugal Fan Noise", ASME Journal of Vibrations, Acoustics, Stress and Reliability in Design, vol. 109, pp. 227 – 234, 1987.
13. Krishnappa, G., "Effect of Modulated Blade Spacing on Centrifugal Fan Noise", Internoise 80, pp. 215 – 218, 1980.

14. Cremer, L., The second annual Fairey lecture: The treatment of fans as black boxes, *Journal of Sound and Vibration*, 16, 1-15, 1971.
15. Terao, M., Sekine, H., "Fan acoustic characteristics required for reliable HVAC duct sound prediction", *Proceedings of Fan Noise Symposium, CETIM, France*, 342-350, 1992.
16. Abom, M., Boden, H., 1995, "A Note on the Aeroacoustic Source Character of In-Ducer Axial Fans", *Journal of Sound and Vibration*, Vol.186 (4), pp.589-598.
17. Baade, R.K., Ray W. Herrick Laboratories Report HL 85-3, Purdue University, Mathematical models of fan sound generation, 1983.
18. Margetts, E., J., "A Demonstration That an Axial Fan in a Ducted Inlet Ducted Outlet Configuration Generates Predominantly Dipole Noise", *Journal of Sound and Vibration*, Vol.117 (2), pp.399-406, 1987.
19. Clark, P., J., F., Ribiner, H., S., "Direct Correlation of Fluctuating Lift with Radiated Sound for an Airfoil in Turbulent Flow", *Journal of Acoustic Society of America*, Vol.46, pp.802-805, 1969.
20. Hersh, A., S., Meecham, W., C., Bies, D., A., "Investigation of Aerodynamic Sound Radiation from Small Airfoils", *Journal of Acoustic Society of America*, Vol.50, 121 (A), 1971.
21. Chanaud, R. C., "Aerodynamic Sound from Centrifugal-Fan Rotors," *Journal of the Aeroacoustical Society of America*, Vol. 37, pp.969-974, 1965.
22. Write, S., E., "Sound Radiation from a Lifting Rotor Genrated by Asymmetric Disc Loading", *Journal of Sound and Vibration*, Vol.9, pp.223-240, 1969.
23. Wright, S., E., "Discrete Radiation from Rotating Periodic Sources", *Journal of Sound and Vibration*, Vol.17, pp.437-498, 1971.
24. Mugridge, B., D., "The Noise of Cooling Fans Used in Heavy Automotive Vehicles", *Journal of Sound and Vibration*, Vol.44(3), pp.349-367, 1976.
25. Jeon W., Baek S., Kim C., "Analysis of unsteady flow field and aeroacoustic noise of an air-conditioner including cross flow fan", *Fan Noise Symposium, Senlis France*, 2003.
26. Longhouse, R., E., "Control of Tip Vortex Noise of Axial Flow Fans by Rotating Shrouds", *Journal of Sound and Vibration*, Vol.58(2), pp.201-214, 1978.
27. Longhouse, R., E., "Control Noise Mechanism Separation and Design Considerations for Low Tip-Speed, Axial Flow Fans", *Journal of Sound and Vibration*, Vol.48 (4), pp.461-474, 1976.



28. Gutin, L., "On the Sound Field of a Rotating Propeller", NACA TM No.1195, 1942.
29. Neise, W., "Noise Reduction in Centrifugal Fans: A Literature Survey", *Journal of Sound and Vibration*, Vol.45 (3), pp.375-403, 1976.
30. Chanaud R.C., "Aerodynamic sound from centrifugal fan rotors", *Journal of the Aeroacoustic Society of America*, 37, 969 –974, 1965.
31. Neise W., "Application of similarity laws to the blade passage sound of centrifugal fans", *Journal of Sound and Vibration*, 43, pp. 61-75, 1975.
32. Mongeau L, Thompson D.E, McLaughlin D.K., "Sound generated by rotating stall in centrifugal turbomachines", *Journal of Sound and Vibration*, 163 (1), pp. 1-30, 1993.
33. Neise W., "Review of fan noise generation mechanisms and control methods", *An International INCE Symposium, Senlis France*, pp. 45 – 56, 1992.
34. Write, T., "The Search for Simple Models to Predict Fan Performance and Noise", *Noise Control Engineering Journal*, Vol.43 (4), pp.85-89, 1995.
35. Maling, G.C., "Dimensional Analysis of Blower Noise", *Journal of the Aeroacoustical Society of America*, Vol.35, pp.1556-1564, 1963.
36. Weidemann J., "Analysis of relation between acoustic and aerodynamic parameters for a series of dimensionally similar centrifugal fan rotors", *NASA TT F- 13*, p. 798, 1971.
37. Roger, M., "The Acoustic Analogy Some Theoretical Background", *VKI LS 2000-02*, 2000.
38. Rumsey, C., L., Biedron, R., T., Farassat, F., Spence, P., L., "Ducted Fan Engine Acoustic Predictions Using a Navier Stokes Code", *Journal of Sound and Vibration*, Vol.213 (4), pp.643-664, 1998.
39. Dunn, M., H., Tweed, J., Farassat, F., "The Application of a Boundary Integral Equation Method to the Prediction of Ducted Fan Engine Noise", *Journal of Sound and Vibration*, Vol.227 (5), pp.1019-1048s, 1999.
40. Wu, S., F., Su, S., G., Shah, H., S., "Modelling of the Noise Spectra of Axial Flow Fans in a Free Field", *Journal of Sound and Vibration*, Vol.200 (4), pp.379-399, 1997.
41. Farassat, F., "Acoustic Radiation from Rotating Blades – The Kirchhoff Method in Aeroacoustics", *NASA Langley Research Center*, 2000.

42. Fukano, T., Takamatsu, Y., “Noise Generated by Low Pressure Axial Flow Fans, III: Effects of Rotational Frequency, Blade Thickness and Outer Blade Profile”, *Journal of Sound and Vibration*, Vol.56 (2), pp.261-277, 1978.
43. Kiya M., “Discrete vortex simulation of separated unsteady flow in a centrifugal impeller”, *Journal of Computational Fluid Dynamics*, pp.1-7, 1988.
44. Lawson, M.V., “The sound field for singularities in motion”, *Proceedings of Royal Society London Series*, A286, pp. 559 – 572, 1965.
45. Lee D.J., Chung K.H., Choi H.L., Jeon W., Prediction of noise radiation from a fan system: Connection between generation and propagation, *Fan Noise Symposium Senlis France*, 2003.
46. Tournour M., El Hachemi Z., Read A., Mendonca F., Barone F., Durello P., “Investigation of the tonal noise radiated by subsonic fans using the aero-acoustical analogy”, *Fan Noise Symposium Senlis France*, 2003.
47. Jeon W.H., “Overview of numerical analysis of fan noise, *Fan Noise Symposium Senlis France*, 2003.
48. Jeon W.H, Lee D.J., “A numerical study on the flow and sound fields of centrifugal impeller located near a wedge”, *Journal of Sound and Vibration*, 266, pp. 785-804, 2003.
49. Neise, W., “An Analysis of the Flow and Aero-Acoustic Sources of a Centrifugal Impeller”, *Journal of Sound and Vibration*, Vol.22(3), pp.505-511, 1999.
50. Holste, F., Neise, W., “Experimental Comparison of Standardized Sound Power Measurement Procedures for Fans”, *Journal of Sound and Vibration*, Vol.152 (1), pp.1-26, 1992.
51. Suzuki, S., “Study on the Noise Reduction in a Centrifugal Fan”, *Internoise-91*, pp.71-74, 1991.
52. Neise W., Koopmann G.H., “Reduction of centrifugal fan noise by using resonators”, *Journal of Sound and Vibration* 73 (1980), pp. 297-308, 1980.
53. Moreland, J.B., “Housing Effects on Centrifugal Blower Noise”, *Journal of Sound and Vibration*, v.43, pp.61-75, 1975.
54. Bartenwerfer, M., Gikadi, T., Neise, W., and Agnon, R., “Noise Reduction in Centrifugal Fans by Means of an Acoustically Lined Casing”, *Noise Control Engineering*, vol. 8(3), pp.100-107, 1977.
55. J. E. Ffowcs-Williams and D. L. Hawkings, “Sound Generation by Turbulence and Surfaces in Arbitrary Motion.”, *Proc. Roy. Soc. London*, A264:321-342, 1969.

56. M. J. Lighthill. "On Sound Generated Aerodynamically", *Proc. Roy. Soc. London*, A211:564-587, 1952.
57. Curle, N., "The Influence of Solid Boundaries on Aerodynamic Sound", *Proceedings of the Royal Society of London, Serial A*, 231 A, pp.505-514, 1955.
58. Brentner, K. S., Farassat, F., "Modeling Aerodynamically Generated Sound of Helicopter Rotors", *Progress in Aerospace Sciences* 39, pp.83-120, 2003.
59. Wagner, S., Barei, R., Guidati, G., "Wind Turbine Noise", Springer-Verlag Berlin Heidelberg, ISBN 3-540-60592-4, 1996.
60. Kohonen, R., "Low-Noise Design in Air Handling: Challenges for Industry and Research Society", *Industrial Presentation*, 2001.
61. Lyrantzis, A., "Surface Integral Methods in Computational Aeroacoustics – From the (CFD) Near-field to the (Acoustic) Far-field", *Journal of Aeroacoustics*, vol. 2 (2), pp.95-128, 2003.
62. Di Francescantonio, P., "A New Boundary Integral Formulation for the Prediction of Sound Radiation," *Journal of Sound and Vibration* Vol. 202, No. 4, pp. 491–509, 1997.
63. Brentner, K. S., and Farassat, F., "An Analytical Comparison of the Acoustic Analogy and Kirchhoff Formulations for Moving Surfaces," *AIAA Journal*, Vol.36, No. 8, pp. 1379–1386, 1998.
64. Fluent 6.2, User's Guide, FLUENT Inc., 2004.
65. Sysnoise Rev 5.6: Computational Vibroacoustics, User Manual, LMS International, 2004.
66. Brüel & Kjaer : Sound and Vibration Measurement Lecture Notes, BA 7669-11, 1998.
67. Ali, A., Rajakumar, C., "The Boundary Element Method- Applications in Sound and Vibration", A.A Belema Publishers, 2002.
68. Chandler-Wilde, S., Langdon, S., "Boundary Element Methods for Acoustics", Lecture Notes, Department of Mathematics of the University of Reading, UK, 2005.
69. ISO 3745 Acoustics - Determination of sound power levels of noise sources using sound pressure - Precision methods for anechoic and hemi-anechoic rooms, 2003
70. Neise, W., 1975, "Application of Similarity Laws to the Blade Passage Sound of Centrifugal Fans," *Journal of Sound and Vibration*, Vol. 43, No. 1, pp.61-75.

71. Weidemann, J., 1971, "Analysis of the relations between acoustic and aerodynamic parameters for a series of dimensionally similar centrifugal fan rotors," NASA TT F-13, 798.
72. Neise, W., and Barsikow, B., 1982, "Acoustic Similarity Laws for Fans," Trans. of the ASME, Vol. 104, pp.162-168.
73. ESDU DataItem 79037, 1979, "A guide for Fan Selection and Performance".
74. Lee, C., Chung, M., K., Kim, Y., H., 1993, "A Prediction Model for the Vortex Shedding Noise from the Wake of an Airfoil or Axial Flow Fan Blades", Journal of Sound and Vibration, Vol.164 (2), pp.327-336.
75. Quinlan, D., A., Bent, P., H., 1998, "High Frequency Noise Generation in Small Axial Flow Fans", Journal of Sound and Vibration, Vol.218 (2), pp.177-204.
76. Kameirer, F., Neise, W., 1997, Journal of Sound and Vibration, 203 (5), 833-853, Rotating blade flow instability as a source of noise in axial turbomachines.
77. Marcinowski, H., 1953, Motortechnische Zeitschrift (MTZ) 14, 259-262, Einfluss des Laufradspaltes und der Luftführung bei einem Kühlgeblase axialer Bauart.
78. Mugridge, B.D., Morfey, C.L., 1972, Journal of the Acoustical society of America 51, 1411-1426, Sources of Noise in axial flow fans.
79. Longhouse, R.E, 1978, Journal of Sound and Vibration. 58, 201-214, Control of tip vortex noise of axial flow fans by rotating shrouds.
80. Fukano, T., Takamatsu, Y., Kodama, Y., 1986, "The Effects of Tip Clearance on the Noise of Low Pressure Axial and Mixed Flow Fans", Journal of Sound and Vibration, Vol.105, pp.291-308.

## CURRICULUM VITAE

### PERSONAL INFORMATION

Surname, Name: Bayraktar, Songül  
Nationality: Turkish (TC)  
Date and Place of Birth: 10 August 1975, Ankara  
Marital Status: Single  
Phone: +90 312 5892132  
Fax: +90 312 589 2121  
Email: [songul.bayraktar@arcelik.com](mailto:songul.bayraktar@arcelik.com)

### EDUCATION

| Degree      | Institution                  | Year of Graduation |
|-------------|------------------------------|--------------------|
| MS          | METU, Mechanical Engineering | 1999               |
| BS          | METU, Mechanical Engineering | 1996               |
| High School | Ayrancı Lisesi, Ankara       | 1991               |

### WORK EXPERIENCE

| Year           | Place                                | Enrollment                 |
|----------------|--------------------------------------|----------------------------|
| 1998 - Present | Arçelik A.Ş, Dishwasher Plant        | Product Development Eng.   |
| 1996 - 1998    | METU Dept. of Mechanical Engineering | Research Assistant         |
| 1995 July      | Doğa HVAC Sist. Tic. A.Ş, İstanbul   | Intern Engineering Student |
| 1994 July      | ERDEMİR, Zonguldak                   | Intern Engineering Student |

### FOREIGN LANGUAGES

Advanced English

### PUBLICATIONS

1. Bayraktar, S., Eralp, C. 'Santrifüj Pompaların Bilgisayar Destekli Tasarımı', 4. Pompa Kongresi ve Sergisi Yayınları, 2001.
2. Bayraktar, S., Diril, O. 'Dishwasher with Variable Speed Drive System', IATC Conference Proceedings, Chicago USA, 2005.

### HOBBIES

Movies, Traveling, Tennis.